Status of the Compressed Baryonic Matter (CBM) experiment at FAIR

N. Herrmann[1], for the CBM collaboration

[1]Physikalisches Institut, Univ. Heidelberg, Heidelberg, Germany

The exploration of the QCD phase diagram in the region of high baryon densities is the primary goal of the physics program of the Compressed Baryonic Matter (CBM) experiment at FAIR.

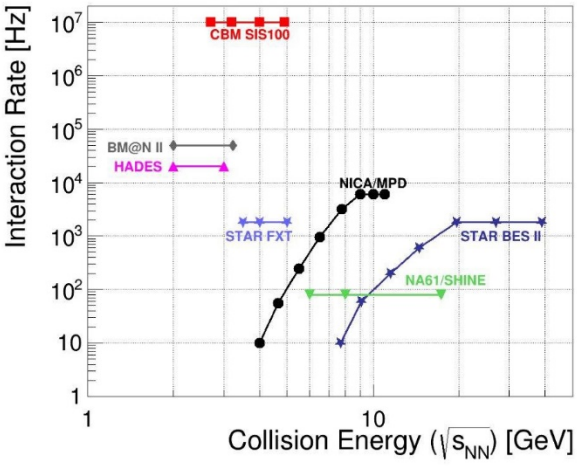

Figure 1: Rate capabilities as function of collision energy of existing experiments and experiments under construction.

In order to make substantial progress beyond existing data and currently running experiments the CBM experiment is designed to be operated at extremely high reaction rates of up to 10 MHz. This unprecedented rate capability allows to perform unique systematic measurements of multi-differential observables and at the same time the measurement of rare diagnostic probes. Figure 1 depicts a comparison of the interaction rates of existing and future heavy-ion experiments as function of collision energy.

The planned experimental setup shown in Fig. 2 is designed to address all observables that are currently employed in our research field to quantify QCD matter properties. Towards that goal CBM can be operated in various configurations, most notably two different base configurations are being prepared: i) the electron - hadron setup that allows the simultaneous measurement of electrons, positrons and charged hadrons, including all mother particles that have decay branches into these particles, and ii) the muon setup that focusses on the measurement of dimuon pairs originating from vector mesons including charmonium and the continuum exhibiting the same quantum numbers.

The key for high-rate operation are fast and radiation hard detectors, and a data acquisition and analysis concept that allows to enhance the rare probes to the level of significant results while keeping and characterising the accompanying features of the surrounding bulk matter. This will be achieved by a system without a traditional hardware based trigger system. All data items from the sensors will receive a time stamp and will be forwarded by the DAQ system in the so-called free streaming mode to a high performance computing cluster where event building and event selection occurs in real time.

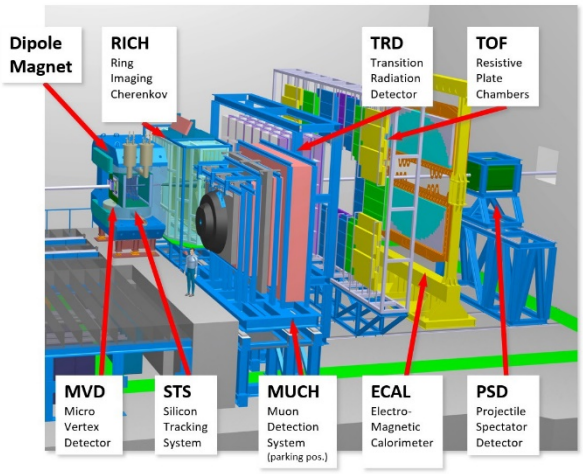

Figure 2: Overview of the CBM experimental setup. The experiment comprises high precision tracking by the MVD and STS detector systems in the magnetic field of a superconducting dipole magnet, event characterisation by a projectile spectator calorimeter (PSD) combined with two different detector arrangements for particle identification. Shown is the electron hadron setup in measuring and the muon setup in waiting position. For further details, see text.

The overall timeline for the construction and installation of the CBM experiment was adapted to the new FAIR baseline planning with the major milestones:

Dec 2021 - CBM building ready for infrastructural installations

Dec 2022 - CBM building ready for installation of components

Jun 2024 - First commissioning beam from SIS100 In the following recent developments of the overall CBM concept and its realisation are highlighted.

Detectors

On the detector side the Technical Design Report (TDR) for the last missing major component with large production time demands, the Transition Radiation Detector (TRD) was completed in 2017 and submitted to the FAIR ECE. A system of 4 layers of TRD chambers is

proposed that was shown to be efficient for achieving the physics goals:

i) electron - pion separation with a pion suppression factor of 20 at 90% electron efficiency in the momentum range beyond 5 GeV/c and ii) separation of nuclear charges e.g. for distinguishing deuterons from α - particles.

All other detector systems are as well on track to meet the FAIR timeline presented above.

Data Processing System

CBM is developing a high throughput data acquisition system that is based on the GBTx frontend ASIC developed at CERN. During the past year this system got further refined by shifting the long distance data transport task to commercial (Infiniband) components. Thus the former data processing board (DPB) and the FLES interface board are merged into a new component, the Common Readout Interface (CRI). The layout of the data processing system is shown in Fig.3.

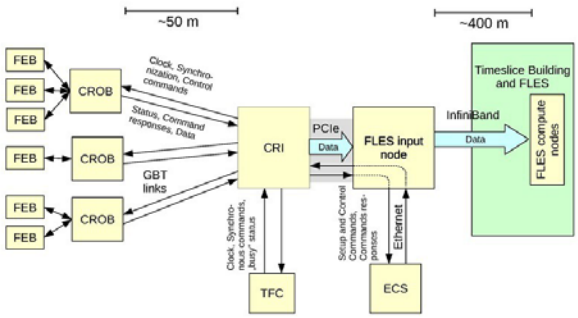

Figure 3: Schematics of the CBM data acquisition and pro- cessing system. Acronyms: FEB - Front End Board, CROB

- Common Readout Board, CRI - Common Readout Interface, TFC - Timing & Fast Control, ECS - Experiment Control System, FLES - First Level Event Selector

The CRIs will be placed into FLES input nodes that are part of the CBM experimental setup and are located in the counting house of CBM. The interface to the Online compute farm housed in the GreenCube of GSI/FAIR will be provided by a high performance Infiniband switch.

Computing

The execution of a high rate experiment like CBM that implements all data selection steps in software requires a software framework that is flexible, scalable and makes use of the latest hardware development. In order to accommodate the various tasks the computing effort within CBM was restructured and a Computing Board (COB) was installed.

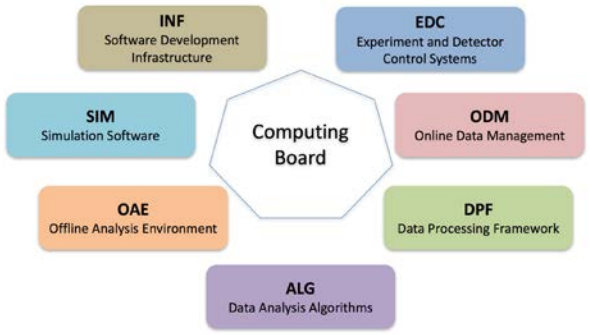

Further details can be found in the corresponding chapter of this report.

Physics Performance

The physics goals of CBM encompass all relevant observables for studying the QCD equation of state, the signals for a possible phase transition, investigation of a possible critical point, chiral symmetry restoration at large baryon chemical potential and the search for rare (quasi) bound states of QCD. These observables are described in detail in the recent CBM publication [1].

The evaluation of the physics capabilities of the CBM experiment is being continued and extended e.g. with detailed studies of the reconstruction of neutral pions, weak decays with neutral daughter particles and evaluation of the accuracy of directed flow measurements.

FAIR Phase-0 Program

Due to the delay of the overall FAIR completion FAIR council has endorsed the usage of CBM detector components and the participation in running experiments, especially at the GSI site making use of the beams available from the SIS18 synchrotron.

Currently CBM groups are pursuing the following projects within the framework of FAIR phase-0:

1) Participate in the HADES experiment at SIS18 by providing an enhanced performance of the HADES RICH detector by employing a readout with CBM owned MAPMT photo sensors.

2) Participate in the Beam Energy Scan II (BES-II) campaign of the STAR experiment at the RHIC at BNL, USA by installing 10% of the final CBM - TOF modules as endcap time-of-flight system, significantly extending the phase space coverage of the experiment. [2]. In addition, CBM high performance tracking software will be used for elaborating efficient data processing.

3) Participate in the BM@N experiment at the Nuclotron accelerator of JINR with the installation of 4 STS tracking

DOI:10.15120/GR-2018-1

stations in order to enhance the momentum resolution of the setup and with the PSD detector for better event characterization.

4) Install and operate a CBM test facility (mCBM) at the SIS18 accelerator of GSI in order to develop and verify the full data acquisition and analysis chain of the CBM experiment (see next section).

The FAIR phase-0 programs will be terminated at latest in 2023, afterwards shifting the core activities to the preparation of running at SIS100. The experience gained during the phase-0 program will certainly help to minimize the commissioning time needed to get full CBM online.

mCBM

mCBM is a test installation of CBM in order to evaluate the performance of detector and data acquisition and analysis components for their full functionality under realistic load conditions at the SIS18 accelerator of GSI [3]. The conceptual design of the experiment is shown in Fig.5.

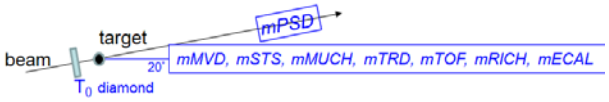

Figure 5: Conceptual layout of the mCBM experiment

mCBM is designed to explore the rate capability of all detector components arranged in a telescope like. Prototype and preproduction modules of MVD, STS, MUCH, TRD, TOF, RICH and ECAL will be placed under a scattering angle of about 20◦ with respect to the beam direction. In addition, one module of the PSD will be placed under the primary beam pipe at an angle of 5 degrees with respect to the beam direction. All detectors will be read out by a common triggerless data acquisition system. A dedicated link into the GreenIT cube to a mFLES cluster will be provided to exercise data transport and analysis.

The experiment is being prepared in the HTD area of the SIS18 experimental hall. No magnetic field will be available at the target spot.

One of the goals of mCBM is the validation of the CBM analysis concept that has to perform under real time conditions. The performance can and will be evaluated ma- king use of (sub)threshold Λ - baryon production in Ni + Ni (1.93A GeV) and Au + Au (1.24A GeV) collisions with cross sections available in literature. However, the unique and distinguishing feature of CBM, that has been worked out in the context of the proposal [3], is that spectra like the ones shown in Fig.7 have to be accumulated within 10s beam on target.

This report is also part of the CBM Progress Report 2017 (doi:10.15120/GSI-2018-00485)

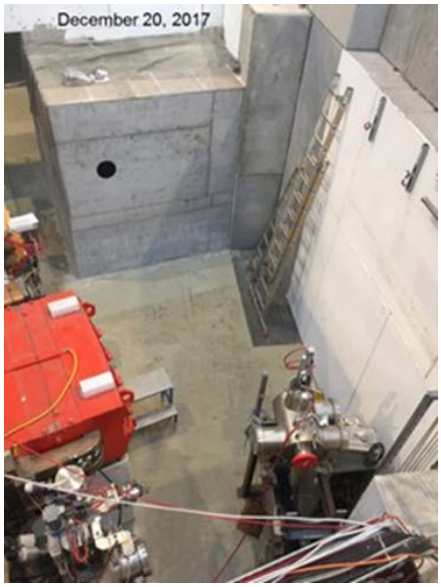

Figure 6: Cave of the mCBM experiment. A new beam dump surrounding the nominal beam position visible as a black circle had to be designed and constructed to enable the planned beam particle flux of 108 Au - ions per second at the highest SIS18 energy.

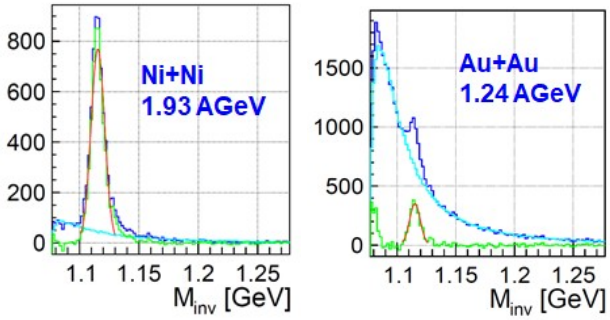

Figure 7: Benchmark observables for the mCBM experiment.

References

[1] T. Ablyazimov et al. (CBM Collaboration), “Challenges in QCD matter physics - The scientific programme of the Compressed Baryonic Matter experiment at FAIR”, Eur.Phys.J. A53 (2017) 60

[2] STAR and CBM - eTOF collaboration, “Physics Program for the STAR/CBM eTOF Upgrade”, arXiv:1609.05102v1 [nucl- ex]

[3] https://cbm-wiki.gsi.de/foswiki/bin/view/Public/Documents#mcbm 45proposal2GPAC 45fullVersion.pdf

Experiment beamline: SIS18-CaveC
Experiment collaboration: CBM
Experiment proposal: S471
Accelerator infrastructure: SIS18 / SIS100 / RHIC / Nuclotron
PSP codes: 1.1.1

Grants: see individual contributions
Strategic university co-operation with: Darmstadt / Frankfurt-M / Gießen / Heidelberg

 DOI:10.15120/GR-2018-1

The superconducting dipole magnet of the CBM experiment

P. Senger and the CBM collaboration

GSI, Darmstadt, Germany;

Magnet parameters

The magnet has a free aperture of 1.44 m vertically and 3.0 m horizontally in order to accommodate the STS detector system with a polar angle acceptance of 25 degrees and a horizontal acceptance of 30 degrees. The total length of the magnet is 1.5 m. The maximum magnetic field in the center of the magnet is 1.08 T, and the field integral within STS detector is BxL = 1.004 Tm. The fringe field downstream the magnet has values of the order of 50 to 100 Gauss at a distance of 1.6 m from the target at the position of the first RICH detector box. The field clamps are dismountable for the MUCH. The magnet can be operated as both polarities. The magnet is of the H-type with a warm iron yoke/pole and cylindrical superconducting coils. The wire has Nb-Ti filaments embedded into a copper matrix with a total Cu/SC ratio of about 7.1. The operating current and the maximal magnetic field in the coils are 686 A and 3.9 T, respectively. The coil case is made of stainless steel. The vertical force in the coils is about 250 tons. The cold mass is suspended from the room temperature vacuum vessel by six suspension links. Six cylindrical support struts compensate the vertical forces. The energy stored in the magnet is about 5 MJ.

Magnet design

The 3D magnetic field calculations were made with the Mermaid code, whereas the forces on the coils and the poles were calculated with the ANSYS 2D model. It was found that the calculated stresses in the coil structure and inside the windings are found to be well below acceptable stresses in stainless steel, copper, and the NbTi superconductor. The cross section of the iron yoke is shown in figure 1. The iron yoke serves as a construction frame for the magnet and systems of the detector. The total mass of the iron yoke is about 140 tons. It has special tools for adjusting its position in all directions. The yoke is assembled of iron blocks having masses in the range between 3 and 13.6 tons. The magnet comprises two separated superconducting coils symmetrically placed close at the top and bottom blocks of the iron yoke. The coils are placed around the cylindrical pole shoes of the magnet.

The lower coil is shown in figure 2. The main components of the coils are superconducting cables, the copper and the stainless steel cases. The copper case has a U-shape profile, and will serve as a bobbin during a winding procedure of the coil. The stainless steel case will be assembled around the copper case after finishing of the winding procedure. The parts of the stainless steel case will be bolted together. Each coil will be made of two pieces of superconducting cable each with a length of about 4.5 km. The splicing will be made during a winding procedure of one coil using soft soldering on a base of Sn-Ag alloy. The coils will cooled indirectly by a flow of liquid helium at 4.5 K through a tube which has an internal diameter 16 mm and wall thickness 2 mm. These tubes will be imbedded in the copper case such that the exit end of the tube is placed at a higher position than the inlet end of the tube (see figure 2). In this case the helium bubbles will accelerate the total helium flow along the tubes. If necessary, this thermosyphon cooling concept can be improved by additional heaters at the outlet of the tubes. The design includes the complete cryogenic system including the branch box, helium transfer line, the cryostat and the feed boxes, as well as the power supply and the quench detection and protection system. The magnet will be built by the Budker-Institute for Nuclear Physics (BINP) in Novosibirsk.

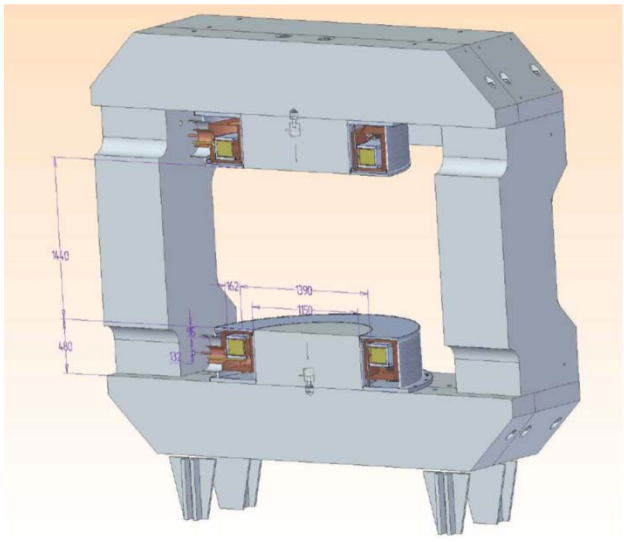

Figure 1: Cross section of the CBM superconducting dipole magnet.

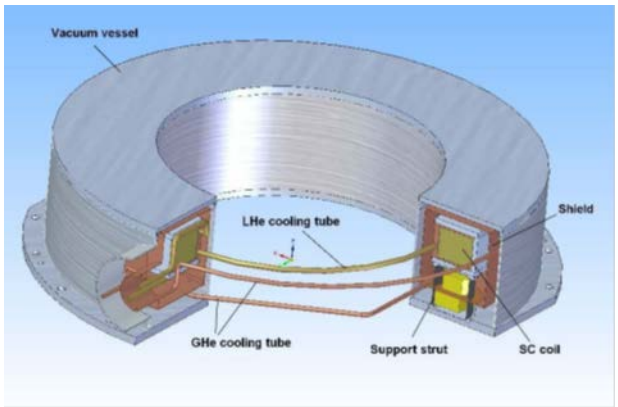

Figure 2: Total view of the lower coil of the CBM magnet (for explanation see text).

DOI:10.15120/GR-2018-1

CBM Micro Vertex Detector - Summary

C. Müntz, J. Stroth, and the CBM MVD working group

Goethe University Frankfurt, Germany; GSI, Darmstadt, Germany

The R&D carried out by the MVD team in 2017 focused on the design of the next generation pixel sensor MIMO- SIS and a review of the detector geometry. Moreover, the detector integration and slow control was studied in a dedicated research program. Radiation tolerance studies aimed to enable MAPS to resist the excessive radiation levels considered for a future MVD detector upgrade.

Sensor R&D and detector geometry review

Given the progress in sensor technology, is has recently decided to abandon the rolling shutter readout and to equip the MAPS sensors for CBM with the faster priority encoder readout, which was previously developed for the ALICE APIDE sensor. Among the benefits of the technology choice is an acceleration of the time resolution of the sensor by one order of magnitude, which turns into a proportional decrease of the detector occupancy and easier event reconstruction. Despite of this benefit, ALPIDE does not reach the radiation tolerance and data bandwidth needed for CBM. Therefore, a dedicated CBM sensor named MI- MOSIS is being developed. A first small size detector prototype MIMOSIS-0, which integrates updated pixel cells and priority encoders was designed at the IPHC Strasbourg and fabricated in 2017. Moreover, a dedicated test bench has been build. The necessary sensor tests will be carried out at the Goethe University Frankfurt and the IPHC Strasbourg in 2018.

The novel MIMOSIS sensor is projected to show different dimensions than the previously considered design. Therefore, an update of the MVD geometry and of the related simulation model was required. The updated model was build based on new scripting tools for CbmRoot. Two geometries, one optimized for vertexing and one optimized for low momentum tracking, were generated and their tracking performance was simulated. Preliminary results suggest that the tracking geometry provides indeed an improved tracking performance, namely in case the field of the CBM dipole magnet is reduced below its maximum intensity.

Sensor Integration and slow control

The integration of sensor into a full detector station was studied with the ”PRESTO” (PRototype of thE Second sTatiOn) prototype. The assembling of the prototype, which is formed from a TPG support holding two layers of MIMOSA-26 sensor, dedicated flex print cables and a TRBv3-based readout, has been completed.

The resulting sensor integration yield after sensor assembly is, though based on very limited statistics, not yet satisfactory. The wire bonding quality was excluded to cause the observed yield. Instead, ESD issues due to possibly low relative humidity during assembly in our laboratory are considered as origin of the observed sensor malfunction. At present, corrective measures are being implemented. Here- after, a second PRESTO module will be assembled in the hope to obtain a significantly improved integration yield.

The existing prototype is now being used as a test system for validating thermal management concept and the vacuum compatibility of the device. Doing long term in-vacuum tests requires to equip the prototype with robust slow control and protection system. A suited system based on EPICS was designed, implemented and commissioned.

Radiation Hardness

While the tolerance of present MAPS to non-ionizing radiation is sufficient to match the requirements of the CBM MVD, only few safety margin is remaining. Therefore, and in the prospective of a future MVD upgrade, options for a further improvement of this radiation tolerance was studied. The strategy consisted in fully depleting the active volume of the sensor, which was previously shown to improve the charge collection efficiency of the damaged device decisively. However, intense cooling was required to operate the irradiated sensors, which was initially not understood. Studies carried out in 2017 revealed that in- creasing the depleted zone of the photo diodes of the sensors comes with draw backs in terms of increased leakage currents, which were compensated by the cooling. An alternative solution to handle this issue suggests employing a faster shaping/readout mechanism, which is in any case required for a potential detector upgrade. Studying this effect more quantitatively is considered to provide valuable guidance for the next steps of sensor R&D.

This report is also part of the CBM Progress Report 2017 (doi:10.15120/GSI-2018-00485)

Experiment beamline: mCBM@SIS18
Experiment collaboration: CBM
Experiment proposal: S471
Accelerator infrastructure: SIS18 / SIS100
PSP codes: 1.1.1
Grants: BMBF 05P16VTFC1
Strategic university co-operation with: Frankfurt-M

Status of the Silicon Tracking System

H. R. Schmidt[1,2], J. M. Heuser[2], K. Agarwal[1], O. Bertini[2], A. Chaus[3], S. Das[1], M. Dogan[2,4], U. Frankenfeld[2], E. Friske[1], J. Hoffmann[2], M. Kis[2], K. Koch[2], P. Koczon[2], E. Lavrik[1], J. Lehnert[2], A. Lymanets[2], H. Malygina[2,6], O. Maragoto Rodriguez[2,6], S. Mehta[1,2], I. Momot[2,6], I. Panasenko[1,3], V. Pugatch[3], A. Rodriguez Rodriguez[2,6], Ch. Schmidt[2], C. Simons[2], M. Teklishyn[5], R. Visinka[2], O. Vasylyev[2], A. Weis[2], A. Wilms[2] for the CBM Collaboration

[1]Universität Tübingen, Germany, [2]GSI, Darmstadt, Germany, [3]KINR, Kiev, Ukraine, [4]Istanbul University, Turkey, [5]FAIR, Darmstadt, Germany, [6]Universität Frankfurt, IKF, Germany

The Silicon Tracking System (STS) of the CBM experiment will provide standalone charged-particle trajectory measurement and associated momentum determination, thus being the key detector in any phase of the CBM physics program, from the beginning of operation.

In this chapter of the Scientific Report, the STS work group teams from Germany, Poland, Russia and Ukraine give a cross section of the achievements made in the last year in the various fields of activities. On the chapter's title page, the depicted "mini STS" set-up for operation in the precurser project mCBM@SIS18 illustrates that the finalizing developments move from the component level to prototyping composite structures and their application in demonstration systems, prior to the start of series production of the CBM-STS parts after a number of readiness reviews in 2018.

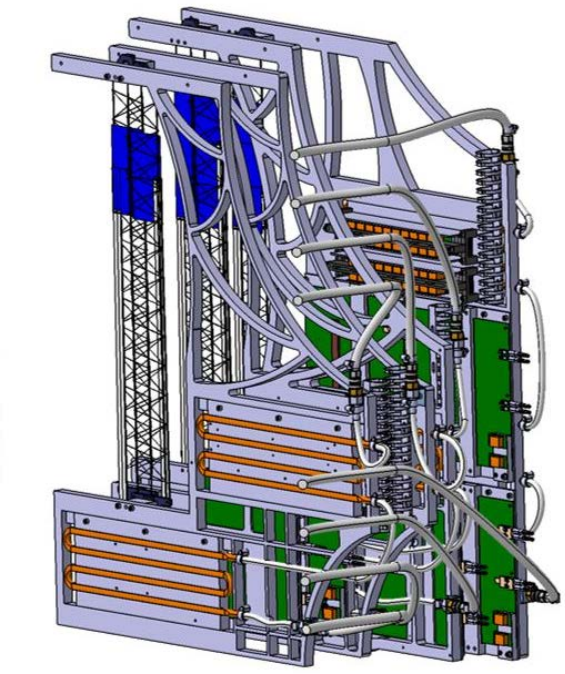

Figure 1: Sketch of the mSTS set-up planned for operation in the pre-curser project mCBM@SIS18.

The CBM Silicon Tracking System

The STS detector has been laid out to achieve the track reconstruction task (beam-target interaction rates up to 10 MHz, charged track multiplicities up to 700 per central Au+Au collision, momentum resolution of $dp/p \approx 1.8\%$, detection of strangeness by in-flight decays) with eight low-mass tracking layers in a 1 Tm dipole magnetic field covering the CBM aperture of $2.5^\circ < \theta < 25^\circ$, corresponding to rapidities ranging from mid rapidity to close to beam rapidity. The sensor technology is based on double-sided silicon wafers with microstrip segmentation. The readout strip pitch of 58 μm under 7.5° stereo angle realizes single-hit resolution of about 25 μm. The read-out is based on self-triggering front-end electronics streaming time-stamped data to a computing farm for on-line hit sorting, track identification, event forming and analysis. To minimize material budget in the acceptance region, the STS has been designed such that front-end read-out electronics, cooling and mechanical infrastructure are located outside of the physics acceptance. The detector modules employ ultra-thin microcables for separating those from the sensors. Four sensor variants (6.2 cm wide, 1024 strips per side, and 2.2/4.2/6.2/12.4 cm long, with the corresponding strip lengths matched to the hit densities at their respective positions) and different microcables up to 50 cm lengths result in 18 module variants to be constructed, 896 modules total. Eight or ten modules are integrated onto a detector ladder. The STS will comprise 106 detector ladders that are mounted on 18 mechanical units within the STS space frame, forming the tracking stations. The modules and ladders for the 4 upstream tracking stations are to be assembled at JINR VB-LEHP, those for the 4 downstream stations at GSI, where also the system assembly will be done. The detector's front-end and powering electronics will dissipate about 40 kW of power. Efficient heat removal through cooling plates circulating bi-phase CO_2 will be applied. The sensors will be operated at up to 500 V bias, at a temperature of around -5 °C to limit radiation damage induced leakage currents from the integrated lifetime fluence of up to 1×10^{14} cm^{-2} 1-MeV neutron equivalent in the regions close to the beam axis. The STS will thus be housed in a thermally insulating enclosure, incorporating feed-throughs for low and high voltage supply, optical and control links. A section of the vacuum beam pipe will cross the detector, made from 0.5 mm thick carbon fiber/foil layers, attaching to the target vacuum box on the beam upstream side and to

the downstream STS wall with further connection towards the RICH or MUCH detectors.

Progress with silicon microstrip sensor

The final prototypes of the STS silicon microstrip sensors have been developed. The four main variants with strip lengths matched to particle densities in the STS and the layout optimized for module assembly have been produced in small series with two vendors (CiS, Erfurt, Germany; Hamamatsu, Japan). The technical specifications and quality criteria are fixed. Radiation tolerance has been demonstrated in various tests on specimen irradiated up to twice the lifetime fluence. An internal sensor review was held in March, 2017, covering all aspects of required specifications, their realization, performance, quality assurance, capabilities of vendors. One open work item was identified: the demonstration of sensor performance (charge collection, signal-to-noise ratio, efficiency for track finding) in a realistic prototype module structure with the sensor tab-bonded to microcables and STS-XYTERv2.0 ASIC. This test took place in the in-beam test at COSY in February 2018. The production readiness review is planned for April 2018 and the call for tender in the second quarter of 2018

Progress with module assembly

The assembly of sensors, microcables and front-end electronics boards into the basic building block of the STS, the detector module, has been developed. The workflow for the double-sided handling has been established, assembly tools have been designed and manufactured, last improvements are being made for the modules to be assembled for the mSTS in 2018. The production site at GSI is equipped and ready for production. Likewise, at JINR where the module assembly with two daisy-chained sensors replacing the largest prototype has been studied. The specifications for the microcables with aluminum traces are almost fixed. Microcables with Copper traces have been ordered in industry and will be tested as an alternative. An internal production review is planned for July 2018.

Progress with ladder assembly

Ladders are the mechanical assemblies of detector modules onto carbon fiber support structures that will be attached to the mechanical units. Carbon fiber prototype structures with varying specifications have been produced with two companies in Germany and Switzerland; a third producer is to be tried. A work flow for ladder assembly has been established at GSI and the required module placement precision ± 35 μm demonstrated, using an optical survey machine installed there. The next iteration of the tools will address the ladders to be produced for mSTS. An internal review on ladder assembly will be held jointly with the module assembly review in July 2018.

Progress with front-end and read-out electronics

In preparation of the final STS front-end chip, STS-XYTERv2.1, detailed studies of the prototype v2.0 have been carried out. For the first time, hundreds of ASICs have been screened and the high production yield determined. Detailed insight into the performance of the analog and digital building blocks has been gained through dedicated measurements. Particular focus has been put on understanding the different loads and their influence on noise. Several substantial modifications to the analog front-end and to the digital back-end will be implemented for the submission in 2018. A first prototype of the front-end board holding 8 ASICs has been designed and produced at GSI. In a module, a left and a right-handed version are required. The prototypes are required for the mSTS modules in 2018. For the read-out of the FEB-8, the GBT protocol has to be used. A first prototype of the read-out board ("Common ReadOut Board", CROB) with GBTX ASICs and VersatileLink optical modules is under test. A prototype link cable for the transmission of data from the front-end to the read-out board has been produced and tested.

Progress with system integration and mSTS demonstrator

The system integration team has addressed various aspects of this wide topic. The STS CAD model is already quite detailed. Its finalization is ongoing, starting with a final confirmation of the sensor positions in a physics performance simulation study and subsequent freezing of all details of the module and ladder variants as well as the detailed dimensions of the mechanical units. A mechanical demonstrator of a quarter C-frame has been finished, allowing decisions regarding ladder mounting technology, mechanical precision, ladder installation, cabling in the detector. The routing of cables from the detector to the supplies in the CBM cave has been addressed. A cooling demonstrator under study addresses the feed-through panels in the thermal wall for HV/LV/data/control links, thermal interfaces for efficient cooling of the electronics, and cooling of the sensors. A first prototype of the STS beam pipe section has been produced and awaits vacuum stability tests. Simulation studies address detector alignment based on tracks to achieve higher-than-intrinsic mechanical precision of sensor positioning for physics measurements. Several aspects of system integration, as well as detector module operation and read-out ASIC performance, are to be demonstrated before production readiness with the "mini STS" (mSTS) in the "mini CBM" (mCBM) set-up. The primary purpose of mCBM is to prove data transport/event building in technical runs in 2018/2019, with potentially further physics runs in 2020/2021. As this requires realistic input from prototype CBM detector systems ("sectors"), the mSTS has been conceived, implementing two small tracking stations with two and three ladders (four and nine modules), on a somewhat simplified mechanical structure. Electronics cooling will be implemented and tested but the sensors will be operated non-cooled at ambient temperature as the radiation load will be non-critical. The mSTS specifications have been frozen and the design is close

 DOI:10.15120/GR-2018-1

to full detailing. Production of the components will start in March 2018

STS project plan

A detailed STS project plan has been established from the current pre-production phase, over test-experiments, production readiness reviews in 2018, the construction phase from 2019 to 2022 and readiness for STS installation into the CBM cave in 2023. It comprises milestones and is an official planning document within the FAIR project. The planning has been matched with a detailed cost assessment and spending profile, backed up by contracts between the participating project partners.

This report is also part of the CBM Progress Report 2017 (doi:10.15120/GSI-2018-00485)

Experiment beamline: mCBM@SIS18
Experiment collaboration: CBM
Experiment proposal: S471
Accelerator infrastructure: SIS18 / SIS100
PSP codes: 1.1.1
Grants: BMBF 05P16VTFC1
Strategic university co-operation with: Frankfurt-M

stsDPB firmware development - preparations for CRI

W.Zabołotny[1], A.Byszuk[1], M.Gumiński[1], G.Kasprowicz[1], K.Poźniak[1], R.Romaniuk[1]

[1]Institute of Electronic Systems, Warsaw University of Technology, Warszawa, Poland

New functionalities in the tester firmware

The firmware for the tester of MUCH-STS-XYTER 2 (SMX2) ASIC was further developed.

The implementation of the GBTX-based access to the SMX2 chip required serious rework of the SMX2 controller core. The GBT-IC/EC controller was delivered by the CERN GBT team and was integrated with the tester firmware. That allowed control of the phase of downlink clocks and delay of the uplink data via the optical link. Successful synchronization of e-Links and transmission of data was achieved. However, the I2C access to the GBTX chip is still needed for its initial configuration[1].

The support of ``time deterministic'' commands, needed for proper synchronization of the front-end ASICS has been added to the tester firmware and successfully tested.

Development of the stsDPB firmware

Even though the final solution for the CBM readout will be the Common Readout Interface (CRI) board, the Data Processing Boards (DPBs) are needed for development and test purposes. Therefore, the functionalities tested in the tester firmware were integrated into the stsDPB firmware initially developed by Junfeng Yang. Additionally, some new functionalities have been implemented directly in that firmware.

The tester firmware supports only a single SMX2. In the stsDPB, it was required to add support for multiple SMX2 chips.

That resulted in the reorganization of the firmware, modification of the block used to generate the phase-shifted downlink clocks, and modification of the Python procedures so that adjustment of one downlink does not corrupt state of the SMX2 ASICs connected to other downlinks. In particular, the downlink transmitter had to be completely stopped when the clock phase was adjusted. The Python procedures have also been refactored and supplemented with extensive logging functionalities.

Another task was the integration of the FLIM module with the stsDPB firmware. New functions for sorting and splitting the received data into microslices were added. A dedicated sorting system [1], shown in figure 1, was developed to merge multiple streams of sorted 32-bit data into a sorted output stream of 32-bit data at 320 MHz, without a necessity to operate complex sorters at so high clock frequency. The final sorter-merger performs the

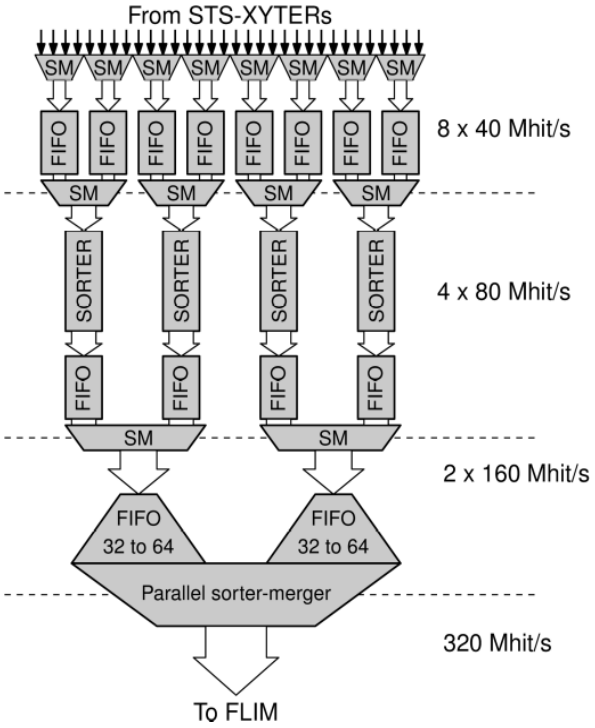

Figure 1: Structure of the data concentration system developed for stsDPB (SM - simple mergers).

comparison of 4 data words in parallel, selecting two oldest in a single 160 MHz clock cycle, producing the sorted stream of 32-bits words at 320 MHz.

The sorted data stream is split into Micro Slices and send via FLIM module to FLES.

Preparation for CRI

As a preparatory step for the development of the CRI boards, a review of available hardware solutions for the PCIe-based readout system was performed [2]. The results of this review allowed defining the viable configurations of the CRI boards and contributed to selection of the HTG-Z920 board as the first prototype of the CRI board.

1 The initial configuration of the GBTX provides settings needed to establish the connection via the optical GBT link. In the final setup the initial configuration will be read from e-Fuses. Because programming of e-Fuses is an irreversible operation, they could not be used at the development stage.

 DOI:10.15120/GR-2018-1

References

[1] M. Gumiński, “High-speed concentration of sorted data streams for HEP experiments”, presentation at Nica Days 2017

[2] W.M. Zabolotny et al., “Selection of hardware platform for CBM Common Readout Interface”, Proc. SPIE 10445 (2017) 1044549, doi:10.1117/12.2280938

Experiment beamline: none
Experiment collaboration: CBM
Experiment proposal: none
Accelerator infrastructure: none
PSP codes: none
Grants: Agreement between GSI and WUT “Development and implementation of a readout and control protocol between STS-XYTER and further data processing FPGA-based electronics for FAIR”
Strategic university co-operation with: none

Data transmission line for STS detector readout system

P.Koczon, J.Hoffmann[1], M.Kis, K.Koch[1], C.J.Schmidt, A.Weis

for the CBM collaboration FAIR@GSI and RBDL

[1] EEL GSI, Darmstadt, Germany

The silicon tracking detector STS for the CBM experiment @ FAIR/GSI in Darmstadt will consist of 900 double sided strip sensors and will register up to 10^7 events/sec of average multiplicity of 350. It will produce about 1 TB/s of data which has to be collected from 14000 front end ASICs (CBMxyter [1]) by a readout system based on the GBTx chip set [2]. The chips' specifications impose certain requirements on the quality of the data link between CBMxyter and GBTx which is proven for the concrete hardware realization in this work.

Test system for the link cable

The cable projected for the data transfer (Sumimoto Electric Interconnect) consists of 20 pairs of LVDS links and is 800 mm long and 20.5 mm wide. It has a strip pitch of 0.5 mm. These parameters were chosen to fulfil the STS@CBM specifications. Links are placed on one surface of a polyester supporting tape and shielded with aluminium foil along the entire length. The shielding can be grounded via extra pads at the cable ends. The cable ends are equipped with stiffening SUMI-CARDS fitting into 0.5 mm pitch horizontal ZIF FH41-40S-0.5SH(05) receptacle of Hirose. For the necessary data rate performance tests an adapter PCB with SMA connectors was constructed which allows to use high frequency LVDS signals produced by CLOSY2 [3]. Signals are fed via SMA- and ZIF [4]-connectors into the flat band cable of 20 LVDS link pairs. To avoid reflections 100 Ohm terminators were used on the end of the cable.

Test results

The signal propagation properties and the link quality of the link cable was proven through noise eye diagram measurement (Fig.1) and the cross talk measurements on side links (Fig.2). The horizontal opening of 1.25 ns of the very clean eye diagram obviously proves high quality of the cable under test to at least 800Mbit/s.

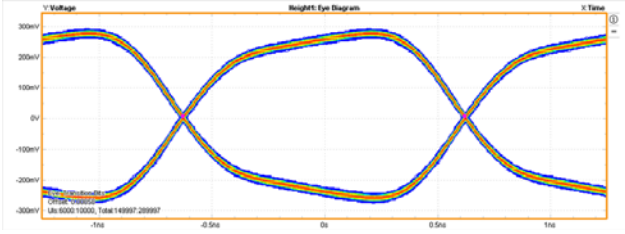

Figure 1. An eye diagram measured with DPO71254C Tektronix Oscilloscope at 400 MHz.

Fig. 2 shows very low cross talk between neighbouring links. Single ended signals are recorded on the end of the closest and second closest neighbour of an active LVDS link. The cross talk does not exceed 1% of the test signal height.

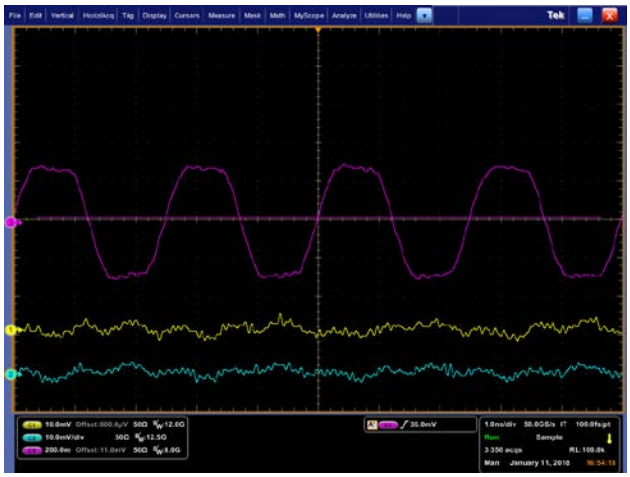

Figure 1. Crosstalk between one link carrying a *400 MHz LVDS signal and the neighbour*ing traces.

Conclusions

The symmetry of the eye diagram as well as the small RMS jitter of transitions together with very little crosstalk is a proof of high electrical quality of the tested LVDS cable. It seems that the cable can be used at still higher clock frequencies e.g. up to 800MHz and corresponding DDR rates of 1,6 Gbit/s, whereas 160 MHz (clk) and 320 Mbit/s is necessary for CBM.

References

[1] stacks.iop.org/1748-0221/11/i=11/a=C11018
[2] indico.gsi.de/event/3446/session/3/contribution/13/material/slides/0.pdf
[3] Helmholtz-berlin.de/media/media/spezial/events/sei/Desy10/koch_desy10_01.pdf
[4] hirose.com/product/en/products/FH41/FH41-40S-0.5SH%2805%29/

 DOI:10.15120/GR-2018-1

Summary Report of CBM RICH developments

J. Adamczewski-Musch[a], K.-H. Becker[b], S. Belogurov[c,f], J. Bendarouach[d], N. Boldyreva[e], C. Deveaux[d], V. Dobyrn[e], M. Dürr[d], J. Eschke[a], J. Förtsch[b], J. Heep[d], C. Höhne[d], K.-H. Kampert[b], L. Kochenda[e,f], P. Kravtsov[e,f], I. Kres[b], S. Lebedev[d], E. Lebedeva[d], E. Leonova[e], S. Linev[a], T. Mahmoud[d], J. Michel[g], N. Miftakhov[e], W. Niebur[a], J. Otto[d], E. Ovcharenko[c], V. Patel[b], C. Pauly[b], D. Pfeifer[b], G. Pitsch[d], S. Querchfeld[b], J. Rautenberg[b], S. Reinecke[b], Y. Riabov[e], E. Roshchin[e], V. Samsonov[e,f,h,] V. Schetinin[c], O. Tarasenkova[e], M. Traxler[a], C. Ugur[a], E. Vznuzdaev[e], M. Vznuzdaev[e], and A.A. Weber[d]

[a]GSI Helmholtzzentrum für Schwerionenforschung GmbH, Darmstadt, Germany;
[b]Department of Physics, University Wuppertal, Wuppertal, Germany;
[c]LIT JINR, Dubna, Russia;
[d]Institute of Physics II and Institute of Applied Physics, Justus Liebig University Giessen, Giessen, Germany;
[e]National Research Centre "Kurchatov Institute" B.P.Konstantinov PNPI, Gatchina, Russia;
[f]National Research Nuclear University MEPhI (Moscow Engineering Physics Institute), Moscow, Russia;
[g]Institut für Kernphysik, Goethe University Frankfurt, Frankfurt am Main, Germany;
[h]St. Petersburg State Polytechnic University (SPbSPU)

The CBM RICH project has made substantial progress in various fields in 2017 as will be presented in this report. First prototypes testing critical mechanical design issues of the RICH detector have been built. The RICH mirror wall is a sensitive part for the RICH detector as it has to combine high stability with low material budget. After discussing several conceptual ideas in 2015, an optimized design has been worked out in 2016 in which one pillar can support two rows of mirrors. In order to evaluate this design, a prototype pillar has been constructed in 2017 with 2 mm thick aluminum profile and successfully been tested for six months up to now with 150% of the expected load. The material budget of the small frames holding two mirrors each has been reduced by further 15-20% material budget. In parallel to ensuring highest stability from the mechanical part, software routines are in preparation in order to correct for any misalignment offline, should it happen to occur. In 2017 the full correction cycle was finally established showing that with software corrections remnant misalignments are on the level of 1 mrad which just fits to the specifications. Another critical design issue is the photodetector camera. A prototype ensuring a convenient construction of the cylindrical photodetector plane has been built and will be tested for stability, light and gas tightness in 2018. Unfortunately the shielding box of the photocamera remains to be an open design issue: The existing design could be adopted to the cylindrical photodetector plane, however partially blocks the acceptance of Cherenkov photons. In addition the redesign of the CBM magnet was not finished in 2017, the whole box has therefore to undergo a further iteration in 2018. The design of the RICH gas system was finalized and awaits the final approval. End of 2017 the last batch of the MAPMTs has been delivered by Hamamatsu. Within the first quarter of 2018 all 1100 MAPMTs will have been characterized. The RICH software underwent numerous changes to improve the realistic description, in particular quantum efficiency and sensitive area are now fully adopted to the chosen H12700 MAPMT. An important step forward was the implementation of an intermediate version of time-base RICH simulations. Within the next months this will be improved and tested 2019 with the participation of a mRICH detector in mCBM. A design of a mRICH prototype was developed and simulated reusing the testbox of the recent testbeam measurements at COSY. As radiator an aerogel tile will be used in order to enhance the pion-proton separation of mCBM.

The HADES RICH upgrade is running very well and driving the development of the RICH readout electronics. The first prototype of the RICH readout chain was available mid 2016, in 2017 an improved version was produced. This was tested in detail in the lab and could finally be fully verified in a testbeam experiment with proton beam at COSY. After initial problems with stability, the whole system was stable in the end and providing data with very low noise level. Automatic routines for threshold settings are available. First analysis of the data reveals that efficiencies are as expected from simulations, the time-over-threshold cut for noise suppression works successfully, and timing precision is on the order of 260 ps. Some MAPMTs were covered with WLS coating (p-terphenyl) in particular in order to measure timing properties. Results show a decay constant of 2.4 ns in agreement with time resolved fluorescence measurements. The previously increase of hit multiplicity of about 20 % was confirmed. Given these successful tests, the readout electronics was approved for mass production for the installation in HADES. The inner part of the photondetector will be coated with WLS films. Full installation is expected until the end of May 2018. The HADES RICH detector will then participate in the Ag+Ag beamtime of HADES in summer 2018 (FAIR phase 0) substantially enhancing the electron identification in HADES.

This report is also part of the CBM Progress Report 2017 (doi:10.15120/GSI-2018-00485).

Experiment beamline: mCBM@SIS18
Experiment collaboration: CBM
Experiment proposal: S471

Accelerator infrastructure: SIS18 / SIS100
PSP codes: 1.1.1
Grants: BMBF 05P15PXFCA, 05P15RGFCA, GSI
Strategic university co-operation with: Gießen

Summary on the CBM-TRD project

C. Blume[4,5], E. Bechtel[5], J. Beckhoff[8], A. Bercuci[1], N. Bialas[5], J. Book[5], V. Cătănescu[1], F. Fidorra[8], C. de J. García Chávez[8], S. Gläßel[5], M. Petrovivi[1], C. Şchiaua[1], S. Schreiber[5], H. Schuldes[5], D. Spicker[5], P. Kähler[8], L. Karalius[1,2], U. Kebschull[6], C. Klein-Bösing[8], M. Kohn[8], M. Krieger[7], A. Meyer-Ahrens[8], P. Munkes[8], I. Ouatu[1,3], F. Roether[5], R. Weihrich[5], the CBM collaboration, and the FAIR@GSI division

[1]National Institute for Physics and Nuclear Engineering (IFIN-HH), Bucharest, Romania; [2]Birmingham University, UK; [3]Oxford University, UK; [4]GSI, Darmstadt, Germany; [5]Institut für Kernphysik, Frankfurt am Main, Germany; [6]Infrastructure and Computer Systems for Data Processing (IRI), Frankfurt am Main, Germany; [7]ZITI, University of Heidelberg, Germany; [8]Institut für Kernphysik, Münster, Germany.

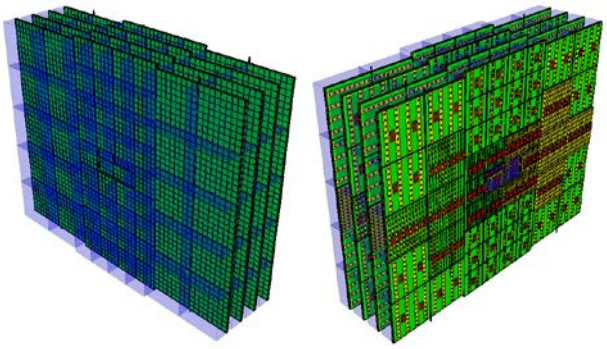

Figure 1: CBM-TRD geometry for SIS100, consisting of one station with four layers of detectors. Shown here is the implementation of the TRD geometry in the simulation framework. Visible are the ROCs with the radiator boxes in the front view (left), while the rear view (right) shows the backpanels of the ROCs together with the front-end electronics.

Introduction

The main task of the Transition Radiation Detector (TRD) is to identify electrons above momenta of 1 GeV/*c* and thus to extend the electron identification capabilities of the Ring Imaging CHerenkov (RICH) detector above momenta of $p \sim 5$ GeV/*c*. In this region the TRD should provide a pion suppression factor in the range of 10 – 20 at an electron efficiency of 90 %, in order to allow for a high quality measurement of dielectrons in the mass range from below the ρ and ω masses to beyond the J/ψ mass. Due to its capability to identify charged particles via their specific energy loss, the TRD in addition will provide valuable information for the measurement of fragments.

These requirements can be fulfilled with a Xe/CO_2 based Multi-Wire Proportional Counter (MWPC) detector in combination with an adequate radiator. The default MWPC design is composed of a symmetric amplification area of 3.5 + 3.5 mm thickness, complemented by a 5 mm drift region to enhance the TR-photon absorption probability in the active gas volume. This geometry provides also efficient and fast signal creation, as well as readout, with timescales below 200 µs per charged particle track. The performance of the detector is maximized by reducing the material budget between radiator and gas volume to a minimum.

The baseline design for the TRD at SIS100 will consist of one station, composed of four detector layers (see Fig. 1). It will be positioned between the RICH and the Time-Of-Flight (TOF) detector and thus will help to reduce the background in the TOF resulting from track mismatches by providing additional position information between RICH and TOF. The TRD will also be used as tracking station behind the last absorber of the MUCH detector in the muon configuration of CBM.

Technical design report

A first version of the Technical Design Report (TDR) for the TRD has been completed early in 2017. It was then scrutinized in an internal review in March 2017, which was performed by a committee of international experts on the various aspects of TRDs, electronics and the related physics topics. Based on the recommendations of the expert committee an extensive revision of the TDR and project was performed.

One major aspect of this process was the redesign of the TRD geometry with the aim of achieving an overall simplification. The new design, as shown in Fig. 1, now consists of only four (before six) different module types, two small ones (type 1 and 3, size 57cm × 57cm) and two large ones (type 5 and 7, size 99cm × 99cm). This facilitates the module production significantly and also allows for a simpler routing of service lines. Furthermore, many complications in the design of the readout system can now be avoided. E.g. only one type of Common ReadOut Board, namely C-ROB3, will now be required.

It was also decided to remove the chapter on alternative options from the TDR, such that the new version consistently describes a baseline solution for the whole TRD system. The innermost modules of the TRD, situated in the region of the highest hit rates, can still employ a different technology (i.e. pad planes with triangular pads and FASP readout), as being developed by the Bucharest group. This design will be described in an addendum to the existing TDR, which is currently under preparation.

The revised TDR has officially been submitted in Dec. 2017 to the ECE for the final approval.

Physics performance

The main physics cases for the TRD are the measurement of dielectrons in the intermediate mass range (i.e. between ϕ- and J/ψ-mass) and the identification of light nuclei. As a consequence of the TDR revision the corresponding physics performance studies had to be repeated with the

 DOI:10.15120/GR-2018-1

new TRD geometry and to be extended in order to address the referee comments. The results of the revised simulation studies are summarized in [7] (intermediate mass dielectrons) and [2] (identification of light nuclei). Both analyses were now done with three, four and five TRD layers in order to determine the optimal geometry for these physics observables. The results show that three layers would be insufficient, while an additional fifth layer is not needed to achieve the desired performance.

Front-end electronics

A test batch of the SPADIC 2.1 ASIC has been submitted. This version includes features suggested by the TDR referees, such as, e.g., an overload recovery and a running averaging for the baseline determination. It will have a BGA packaging in order to reduce the real estate occupied by the chip on the Front-End Boards (FEBs). This will allow to design FEBs which are small enough to fit flatly onto the backpanel of the TRD chambers, even for module type-1 which has the highest channel density.
The development of multi-ASIC FEBs is progressing well [3]. A first version of a quad-FEB, to be equipped with the SPADIC 2.0, is available and is intended to be used for mCBM.

Readout and feature extraction

The TRD readout has been upgraded for the connection of multiple SPADICS to a given AFCK board [4]. This implementation has been successfully tested at DESY and CERN-GIF and will be further extended for the quad-FEBs to be used for mCBM and for the GBTx-based C-ROBs.
An important part of the readout chain is the feature extraction stage, which will deliver event-filtered and bandwidth reduced data to the FLES. First performance studies on the online cluster reconstruction in terms of total cluster charge and position have been performed [5].

Laboratory and beam tests

Also in 2017 extensive test have been performed, both in the laboratory and at accelerators. The Bucharest group has set up a test stand equipped with a high intensity x-ray source, which allows to investigate the performance of prototypes under high counting rate conditions [6].
In Münster an automated calibration setup for the readout chambers using a Fe-source was build [7], which can be used for a quality assessment of newly produced readout chambers. This setup is currently also been used to study the multi-hit performance of the SPADIC [8].
A systematic test of four large prototypes with radiators was performed with electron beams at DESY [9]. These data allow for a detailed characterization of the radiators and will serve as a reference for the fine-tuning of the detector simulation.
In order to investigate the stability of the readout chambers and front-end electronics in a high rate environment a first test at the Gamma Irradiation Facility (GIF) at CERN was done [10].
The analysis of the test beam data of 2017 is currently still on-going. Several software developments on the software framework for the analysis of test beam data have been done [11], which now provide a unified environment for these studies.

Summary and outlook

With the finalization of the TDR the research and development phase for the TRD can almost be concluded. Ongoing activities mainly concern topics such as services, cooling and the gas system, while the design of the readout chambers themselves is essentially final. Four large chamber prototypes, which are already very close to this design and have already been operated at the CERN-SPS and DESY, will be available for mCBM. Also the development of the front-end electronics is progressing and final FEBs should be available by the end of 2018. Therefore, it is planned to start the production readiness review by the end of 2018 and to start mass production soon after that.

This report is also part of the CBM Progress Report 2017 (doi:10.15120/GSI-2018-00485).

References

[1] E. Bechtel et al., “Performance study on dielectron measurements in Au+Au collisions with the CBM-TRD”, CBM Progress Report 2017, p. 155.
[2] S. Gläßel et al., “Hadron identification via energy loss measurements with the TRD”, CBM Progress Report 2017, p. 156.
[3] F. Roether et al., “Front end board development for the CBM-TRD”, CBM Progress Report 2017, p. 86.
[4] C. de J. Garcia Chávez et al., “Status update of the TRD data acquisition chain during 2017”, CBM Progress Report 2017, p. 87.
[5] C. de J. Garcia Chávez et al., “Performance study of the feature extraction”, CBM Progress Report 2017, p. 88.
[6] A. Bercuci et al., “Laboratory tests of the TRD Bucharest prototype in close to realistic high counting rates (HCR) environment”, CBM Progress Report 2017, p. 89.
[7] J. Beckhoff et al., “Automated gain-table measurements for the CBM-TRD”, CBM Progress Report 2017, p. 91.
[8] M. Kohn et al., “Analysis of the SPADIC Multi-Hit feature”, CBM Progress Report 2017, p. 92.
[9] F. Roether et al., “Electron test beam campaign of the CBM-TRD at DESY”, CBM Progress Report 2017, p. 93.
[10] P. Kähler et al., “High-rate test of a CBM-TRD module at the CERN-GIF”, CBM Progress Report 2017, p. 94.

[11] P. Munkes et al., “A new in-beam-test data analysis framework for the CBM-TRD”, CBM Progress Report 2017, p. 95.

Experiment beamline: mCBM@SIS18
Experiment collaboration: CBM
Experiment proposal: S471
Accelerator infrastructure: SIS18 / SIS100
PSP codes: 1.1.1
Grants: BMBF-grants 05P15RFFC1 and 05P16PMF1, Romanian ANCSI/CAPACITATI Modul III Contract F04 and NUCLEU Project Contract PN 2018, Helmholtz-Alliance EMMI, HGS-HiRe.
Strategic university co-operation with: Frankfurt-M

Status on the CBM Time Of Flight system

I. Deppner[1], N. Herrmann[1], the CBM_TOF working group

[1]University of Heidelberg

We can look back, again, on a very successful year 2017. For the first time a trigger less readout system using close to final electronic components was operated successfully in the beamtime at SPS as well as in the cosmic setup in Heidelberg. Results concerning efficiency, time resolution and cluster size obtained in many beamtimes demonstrate that the counter development is far progressed and therefore in a very satisfactory situation. Along this line the mass production for the MRPC3a and MRPC3b counters [1] (foreseen for the FAIR phase 0 project at STAR and mCBM) started after the review readiness report in March 2017.

The main tasks for TOF in the last year were the following:

1) analysis of the data taken during the beamtime at ELBE in 2017 and at SPS in Nov. 2016,
2) operation of a free streaming cosmic stand in Heidelberg,
3) mass production of MRPC3a and MRPC3b counters for the FAIR Phase 0 projects at STAR and mCBM,
4) installation and conditioning of one eTOF sector in the STAR experiment at BNL.

Beamtimes are essential for testing high rate counters. At ELBE a mono-energetic single electrons beam of 30 MeV with pulse duration of 5 ps and a flux of $\leq$ 500 kHz/cm^2 is well suited to test the rate capability of single cell counters like the BFTC prototypes (active area is 4 cm^2) with ceramic resistive electrodes. However, since the beam has a diameter of only about 10 cm^2 only the spot response of counters larger than a few cm^2 can be tested. During the last year a beamtime at ELBE was carried out with the BFTC prototypes and results are reported in [2]. In order to achieve a full illumination on counters bigger than a few cm^2, beams with heavy ions impinging on lead targets like executed at CERN SPS is mandatory. The beamtime setup in Nov. 2016 (conf. Fig. 1), described in [3], consisted of about 500 read out channels distributed over 10 timing counters (including 2 layers of ceramic MRPCs) and one Bakelite resistive plate counter for the MUCH system from our Indian colleagues. For the first time a free streaming readout system was operated successfully and even synchronization with 2 GEM detectors (for the MUCH-subsystem) using FEBs with nXYTER (Rev-F) [4] could be demonstrated. During this campaign a Pb beam with an momentum of 156 AGeV/c was impinging on a 4 mm Pb target leading to high multiplicity events which are substantial to test the detector response under load. Occupancies higher than 50 % were reached. However, particle fluxes (measured by a plastic scintillator) above 1.5 kHz/cm^2 could not be reached even after adding 10 cm of iron to the target. As in the SPS beamtime in Nov. 2015 the radiation protection alarm was triggered and a reduction of beam intensity

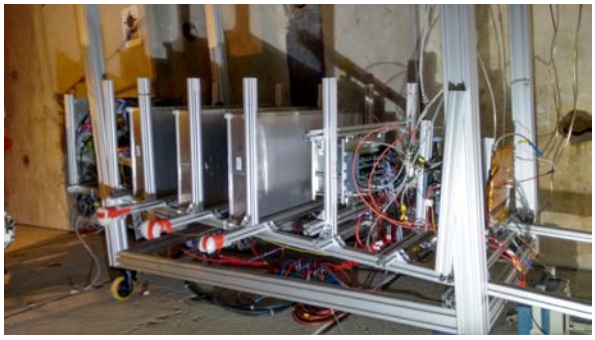

Figure 1: Photography of the CERN November 2016 setup. The beam enters the setup from the right side. The counters are arranged below the beam with an angle of 7◦.

was needed in order to continue the measurements. In conclusion the H4 beam line at SPS is not suited to deliver the anticipated rates for the inner part of the CBM TOF wall. Currently such high rates will only become accessible at the upcoming mCBM beamtimes at SIS 18 which shows the immense importance of this FAIR Phase 0 project not only in terms of DAQ integration tests but also as a test facility for high rate detectors. Nevertheless, during the beamtime at SPS more than 100 useful runs were taken which are right now still being analysed. First results for the MRPC1/2 prototypes [1] are presented in [5]. In order to adapt the MRPC1/2 prototypes to the front-end electronic and to minimize channel costs a redesign in the readout electrodes is currently ongoing where the number of channels is reduced from 40 to 32. The mechanical design for the inner TOF wall where these counters will be located is ongoing as well [6].

Equally important are counter tests with cosmic particles that have the advantage of being constantly available. A test stand for cosmics (see Fig. 2) was operated at Heidelberg during almost the full year. Per day about 100000 good tracks (in the acceptance of all counters) can be recorded and multi-dimensional analysis can be performed. On the left side of figure 3 an event with 2 tracks is shown that had hits in all 6 stations. Comparing 5 hit and 6 hit tracks, the efficiency as function of position in X and Y can be measured (see right plot in Fig. 3). Similar figures can be obtained for time resolution, cluster size, position resolution, time over threshold distributions and so on. In the cosmic setup counter time resolution of about 55 ps, X position resolution (across the strip) of about 2.5 mm and Y position resolution (along the strip) of about 5.5 mm was obtained. Beside resolution studies, the cosmic stand data also offer the opportunity to develop the software for calibration and reconstruction under clean conditions. In addition simulation with the same geometry can be performed and the counter response from realistic digitizer [7] as well as the analysis framework can be tested and compared to real data. However, this is not restricted only to cosmic data as shown in [8].

In the context of the CBM FAIR phase 0 programs for TOF the mass production of the MRPC3a and MRPC3b counter started in 2017. 73 MRPC3a counter with low

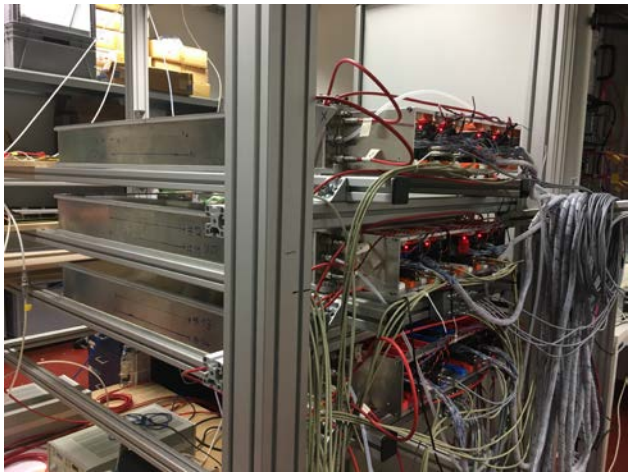

Figure 2: Photography of the Heidelberg cosmic setup. Three modules containing 2 counters each are placed on top of each other so that in total 6 counters can be tested simultaneously.

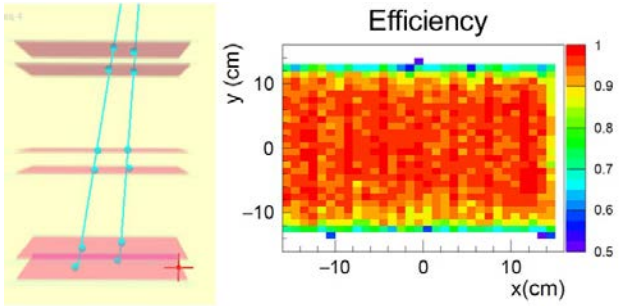

Figure 3: Left: cosmic setup with 6 MRPC stations. An event with 2 tracks with 6 hits each was found. Right: Efficiency of one MRPC as function of the X and Y coordinate.

resistive glass are produced at Nuctech in Beijing and most of them are tested and delivered to Heidelberg. The counter specs, the progress of the production, the test results as well as the QA procedure are described in [9]. It turned out that a conditioning time of about 120 hours is necessary in order to achieve stable operating conditions. 80 MRPC3b counter (float glass) are currently produced at USTC/Hefei. A short overview of the status and the QA procedure is given in [10]. The integration of the MRPC3a/b counters in modules will take place in Heidelberg. Currently 36 gas tight boxes for STAR and 5 boxes for mCBM are under construction in the mechanical workshop in Heidelberg. The module production for mCBM will be finished end of April while for STAR end of August. The plan is to test all modules extensively in the Heidelberg cosmic setup before the modules are delivered to GSI and to BNL.

Three modules for eTOF at STAR (see FAIR phase 0 program for TOF in [11] were produced last year, tested and shipped to Brookhaven National Laboratory. Figure 4 shows the three modules, forming one sector, mounted in the 6 o'clock position of the east-side end-cap of the magnet. The chambers are controlled remotely from Germany. Be- fore the RUN18 starts, cosmic data with the full STAR apparatus are taken and the data from eTOF are integrated in the data stream of STAR.

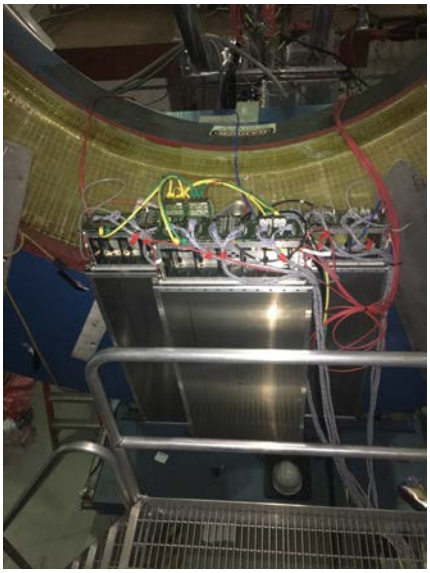

Figure 4: Sector consisting of 3 CBM-TOF modules moun- ted on the east pole tip of the STAR experiment.

This report is also part of the CBM Progress Report 2017 (doi:10.15120/GSI-2018-00485)

References

[1] N. Herrmann et al. "CBM-TOF Technical Design Report", http://repository.gsi.de/record/109024/files/, October 2014
[2] R. Sultanov et al., CBM Progress Report 2017 (2018)
[3] I. Deppner and N. Herrmann, CBM Progress Report 2016 (2017), S 124
[4] A. Kumar, CBM Progress Report 2016 (2017), S 88
[5] M. Petriș et al., CBM Progress Report 2017 (2018)
[6] L. Radulescu et al., CBM Progress Report 2017 (2018)
[7] C. Simon et al., CBM Progress Report 2017 (2018)
[8] Ph. Weidenkaff, CBM Progress Report 2017 (2018)
[9] P. Lyu et al., CBM Progress Report 2017 (2018)
[10] D. Hu et al., CBM Progress Report 2017 (2018)
[11] I. Deppner and N. Herrmann, CBM Progress Report 2017 (2018)

Experiment beamline: none
Experiment collaboration: CBM
Experiment proposal: none
Accelerator infrastructure: SIS100
PSP codes: 1.1.1.5
Grants: BNBF 05P15VHFC1
Strategic university co-operation with: Heidelberg

The CBM FAIR Phase 0 project - eTOF at STAR

I. Deppner[1], N. Herrmann[1], the CBM-TOF collaboration

[1]University of Heidelberg

The FAIR Phase 0 program of TOF comprises among other tasks the installation, commissioning and operation of 36 eTOF-modules, using 108 CBM-TOF MRPC3a/b counters [1], during the beam energy scan campaign II (BESII) of the STAR experiment at BNL. The modules will be grouped in 12 sectors and will be attached on the east side pole tip of the magnet (conf. Fig 1). During the last year a substantial progress regarding this project was made.

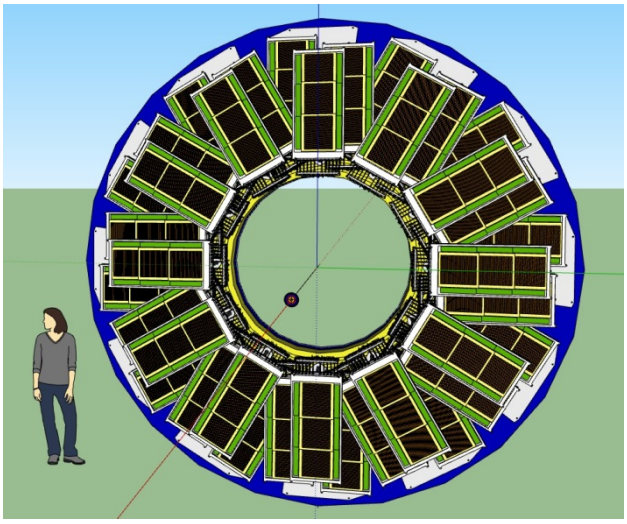

Figure 1: Conceptual design of the eTOF wall at STAR. The ”wheel” is composed of 36 module comprising 6912 readout channels.

The physical work of this project started with the installation of one module containing 2 MRPC3b counters at STAR in Jan. 2017 and operating it in the RUN17 (Mar. 17 - Jun. 17). The aim was to integrate our free streaming readout system in the trigger based readout system of STAR. It could be shown successfully that the first DAQ integration tests worked as expected (see last CBM Progress Report [2]). Currently software is developed in order to unpack the eTOF data and make them accessible to the STAR analysis framework. The test installation of the first module already delivered valuable information for a stable operation of our MRPC counters. After an accelerator intervention (un-planned beam loss event) one PADI FEE board stopped functioning pointing to the need for fast protection measures. After 2 month of operation both MRPC counters stopped working due to HV failure. This problem was analysed and cured by a modification in the design of the MRPC3b counter. These examples demonstrate the immense importance of the FAIR phase 0 programs in order to identify critical issues of the system under running conditions.

In the last year 3 modules for eTOF were produced. Two modules contain 3 MRPC3a counters each (with low resistive glass) manufactured at Nuctech in Beijing while 1 module is housing 3 MRPC3b counters build at USTC/Hefei. The module integration for the full wheel is carried out in Heidelberg. Figure 2 shows a photograph of the open module from the front side (left) and the back side (right). The 3 modules were shipped to BNL beginning of January 2018 and installed at the 6 o’clock position at the east pole tip (see Fig. 3). The readout system consists of the PADIX boards (inside the module box), a feed-through PCB, the TDC board with the GET4 V2.0 chip, a back-plane board distributing the power and the clock to the FEE cards, 5 AFCK boards sitting in a µTCA crate at 8 m distance from the modules and a FLIB board sitting in a rack mount PC located in the DAQ room about 50 m from the setup. The current connection between the back-plane board and the AFCK is copper cable (twisted pair) and will be re- placed with optical fiber after the RUN18. Then also the GBTx chip, sitting on the back-plane board, will be included in the readout chain. The connection between AFCK and FLIB is optical fiber.

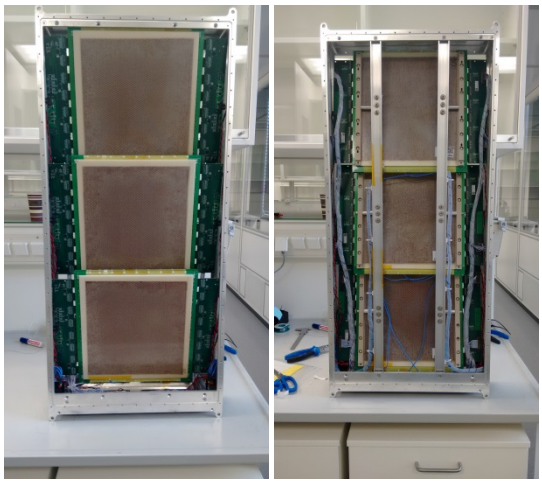

Figure 2: Open eTOF module - left: front side, right: back side.

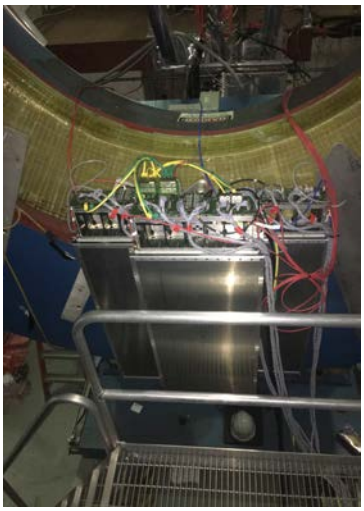

Figure 3: One sector mounted on the inner side of the pole tip.

In the meanwhile both institutes from China continued the mass production of the counters for the full eTOF wall (in total 150 counter). The production of the MRPC3a counters will be finished in March 2018 and 53 aut of 73 counters are shipped to Heidelberg. 25 of the MRPCa counters are devoted to the mCBM project. Figure 4 shows the production of MRPC3a counters in the clean room at Nuctech/Beijing. The clean room level is 100k. The production of the MRPC3b counter will be finished in July 2018. 5 counters are shipped to Heidelberg and integrated in the cosmic setup. The progress of the mass production as well as the QA procedure are summarized in [3, 4].

Figure 4: Mass production of MRPC3a counter in the clean room.

In order to coordinate and to discuss the progress as well as the open issues on the project two CBM-STAR meetings where organized during the last year. The first meeting took place at Darmstadt while the second meeting was carried out at Wuhan. Many fruitful discussion and solutions arises during these meetings. One example is the implementation of the eTOF geometry in the STAR simulation frame work (see Fig. 5).

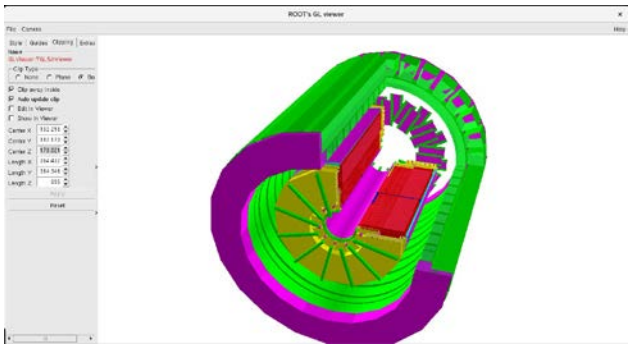

Figure 5: eTOF geometry included in the STAR simulation frame work.

The time line of the eTOF project is:
1) Jan 2018 - shipping and installation of one sector
2) Mar. - June 2018 - 2nd system integration test with one sector by participating in the Run18 beam time in STAR,
3) Mar. - Oct 2018 - Production and testing of 36 modules in Heidelberg
4) Sep 2018 - shipping of all 36 modules to BNL
5) Oct. - Feb. 2018 - Installation and commissioning of the eTOF syatem
6) 2019/2020 - Running in the BES II campaign
7) Summer 2021 - Decommissioning and shipping of all modules including infrastructure to FAIR

This report is also part of the CBM Progress Report 2017 (doi:10.15120/GSI-2018-00485)

References

[1] N. Herrmann et al. “CBM-TOF Technical Design Report”, http://repository.gsi.de/record/109024/files/, October 2014
[2] I. Deppner et al., TOF Summary, CBM Progress Report 2016 (2017)
[3] P. Lyu, CBM Progress Report 2017 (2018)
[4] D. Hu et al., CBM Progress Report 2017 (2018)

Experiment beamline: none
Experiment collaboration: CBM
Experiment proposal: none
Accelerator infrastructure: BNL-RHIC
PSP codes: 1.1.1.5
Grants: BNBF 05P15VHFC1
Strategic university co-operation with: Heidelberg

Development of muon detection system (MUCH) for the CBM experiment at FAIR

S. Chattopadhyay[1], A.K. Dubey[1], Z. Ahammed[1], J. Saini[1], P. Bhaduri[1], E. Nandy[1],V. Negi[1], M. Mandal[1],A. Kumar[1],C. Ghosh[1],S. Prasad[2], S. Biswas[2], S. Das[2], D. Emschermann[3], C. Schmidt[3], P. A. Loizeau[3], A. Senger[3],O. Singh[4], the CBM collaboration, and the FAIR@GSI division

[1]VECC, Kolkata, India; [2]Bose Institute, Kolkata, India; [3]GSI, Darmstadt, Germany,
[4]Aligarh Muslim University, Aligarh, India

The SIS-100 version of MUCH consists of five absorber segments with 4 detector stations sandwiched between them. While the first absorber is made of graphite, other absorbers are of iron. A gap of 10 cm houses the detector stations having 3 layers each consisting of varying number of chambers. The first and the second stations use GEM chambers to handle a hit rate of more than 400 KHz/cm^2. As the particle rate at the 3rd and 4th stations are considerably lower (maximum 5 KHz/cm^2 in Au+Au collisions at 10 AGeV), different technologies are being explored like high-rate RPC or straw tube chambers.

Two chambers fit to be placed in the 1st station are built at VECC-Kolkata and ready to be installed in the mini-CBM scheduled to take data in October 2018. The chambers (Fig. 1) use GEM foils from CERN custom-built for our configuration. Major features implemented in these chambers are (a) NS-2 technique for glue-less stretching (b) drift planes with opto-couplers connected to the HV line of each segment providing with a possibility of isolating the segment in case of any spark. This feature enables to use high-voltage segmentations using resistive chains thereby reducing the total cost of HV supply by a factor of 24 (the number of segments in each foil).

The readout planes of the chambers are having projective pads of varying sizes. Each pad covers 1 Degree in azimuth and equivalent radial distance. The chambers have been tested successfully with radioactive source (Fe-55, Sr-90) and ready to be installed in mini-CBM. A 1 cm thick Aluminium plate has been used to support the chamber and channels made inside the plate is being used for water-cooling. This setup has been tested to take data with Pb beam at SPS in November 2016.

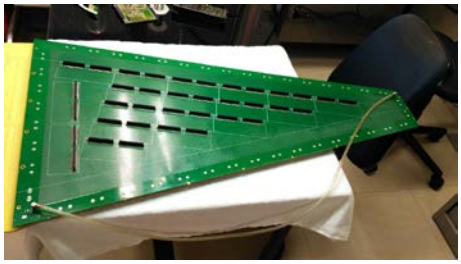

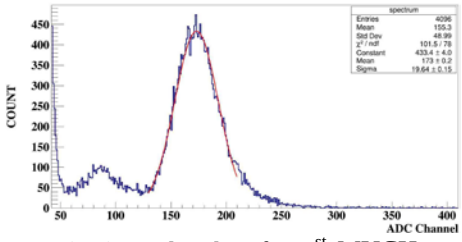

Fig.1 : (top) A chamber for 1st MUCH station (bottom) Fe-55 spectra

A low voltage distribution box (LVDB) has been developed to distribute LVs to the FEE boards. A FPGA-based system has been developed to control the operation of LVDB. A similar system has also been developed for the HV control. All components being used in the detector and supply systems have been tested with neutron and gamma sources to withstand a dose that is about a factor of two higher than estimated by FLUKA.

The MUCH system is being simulated using CBM-ROOT framework for measurement of LMVM and charmonia. The results obtained earlier have been found not to deteorirate using the most realistic geometry of the setup.

An ASIC called STS/MUCHXYTER have been developed for the MUCH readout and the version presently available has been connected to a GEM chamber for taking data with Sr-90 source. Even though the calibration is under progress, the readout shows clear source spot on the detector.

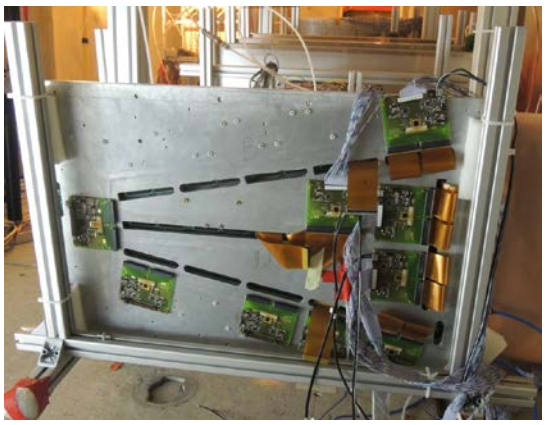

Fig.2: Al-plate for support and cooling of the GEM chambers. FEE boards are connected using small cables.

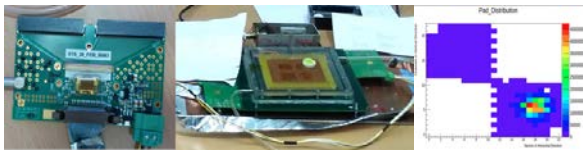

Fig.3: (left) STS-MUCHXYTER ASIC connected to a GEM chamber (right) beam spot seen online

A significant progress has been made on the mechanics of the MUCH system. Two major mechanical systems are absorbers and superframe to hold MUCH. Designs are in advanced stages and discussions are in progress with the prospective manufacturers.

One open area is to find a suitable technology for the 3rd and 4th stations of MUCH. Given the performance reported by ALICE muon chambers, two ALICE-muon RPCs have been tested with cosmics and with NINO and PADI electronics to provide >95% efficiency with cosmic muons. MUCH simulations using RPCs in the 3rd and 4th stations show good performance.

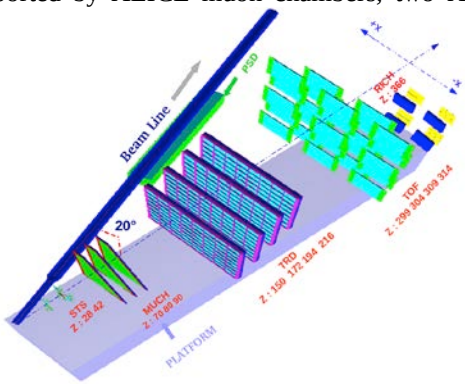

Fig. 4: 3 GEM chambers in miniCBM setup

Detailed setup has been developed to simulate the mini-iCBM setup including three GEM chambers. The digitization and formation of hits have been performed.

 DOI:10.15120/GR-2018-1

Preparation of a free-streaming DAQ system for mCBM@SIS18

D. Emschermann and C. Sturm for the CBM collaboration

The key objective of the Compressed Baryonic Matter experiment (CBM) at FAIR is to investigate the QCD phase diagram in the region of the highest net-baryon-densities by measuring nucleus-nucleus collisions. As a fixed-target experiment, CBM is consequently designed to cope with unprecedented collision rates up to 10 MHz which will allow studying extremely rare probes with high precision. To achieve the high rate capability, CBM will be equipped with fast and radiation hard detectors readout by a free-streaming data acquisition system transporting data with up to 1 TB/s to a large scale computer farm providing a first level event selection.

With mCBM@SIS18 we are presently constructing a CBM full-system test-setup at the GSI/FAIR host lab to study, commission and test the complex interplay of the different detector systems with the free-streaming data acquisition and the fast online event reconstruction and selection under realistic experiment conditions.

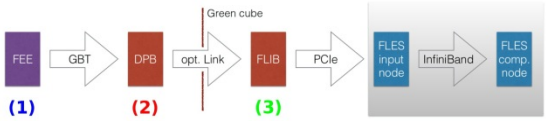

Figure 1: mCBM readout chain for the startup phase, based on DPB and FLIB. The mCBM subsystems are equipped with individual front-end electronics FEE (1). These front-ends are interfaced by the GBTx ASIC, which forwards the detector data via optical GBT link. All GBT links are received by the DBP layer located at 50 m distance in the DAQ container (2). The DPB is a FPGA based board which allows for subsystem specific pre-processing of the arriving data stream. A long optical link connects the DPB output to the FLIB board installed in the FLES input node in the Green IT Cube (3).

The detector stations will be equipped with final readout electronics containing ultra-fast and radiation-tolerant ASICs as front-end chips followed by CERN GBTx-based radiation-tolerant data aggregation units. Further down-stream, the data streams are handled by Data Processing Boards (DPB) containing powerful FPGAs and are forwarded via FLES Input Boards (FLIB), a PCIe based FPGA board, to a large-scale computer farm, the First-Level Event Selector (mFLES), which will perform on-line track and event reconstruction and selection, see Fig. 1.

The CBM detector front-ends are time-synchronized to the nanosecond level by the Timing and Fast Control (TFC) system. The detector front-end digitizes signals above threshold and assigns time stamps to hits. This data is then forwarded via an electrical connection to the GBTx readout board, where the electrical signals acquired through a large number of e-links are converted and merged into an optical GBT link operating at 4.48 Gbit/s. These GBT links are the detector interface to the Data AcQuisition (DAQ) chain.

On the road towards the full CBM DAQ system the mCBM DAQ system will be deployed in two phases. During phase I, the GBTx-based subsystems (mSTS, mMUCH, mTRD and mTOF) will be read out using already available readout chains based on existing prototype implementations of DPB and FLIB, see Fig. 1. As current prototype hardware, an AMC FMC Carrier Kintex (AFCK) board [1] is used for the DPB, a HiTech Global HTG-K700 PCIe board for the FLIB. Both boards are based on a Xilinx Kintex-7 FPGA. In phase II, DPB and FLIB will be replaced by a prototype of the Common Readout Interface (CRI) (see Fig. 2) in the FLES input stage, as it is foreseen for the CBM experiment. In addition, the mCBM subsystems (mRICH, mPSD) readout with FPGA TDCs chains will be added to the DAQ setup in 2019.

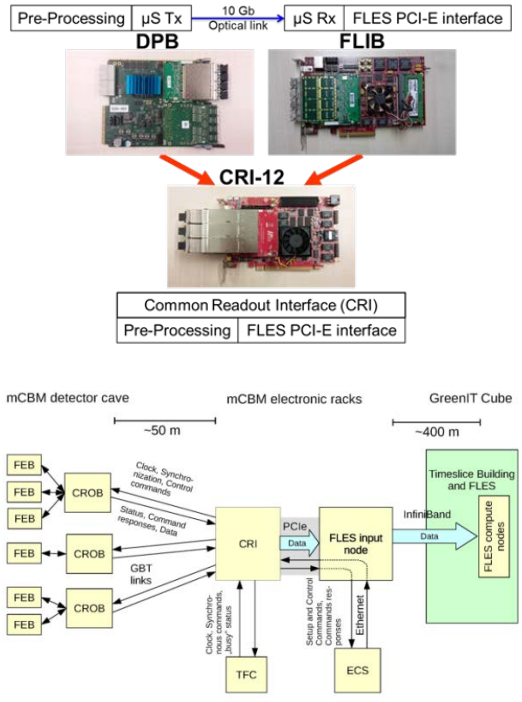

Figure 2: Upgrade of the mCBM DAQ in 2019, from two chained Kintex-7 devices to a single Ultrascale+ FPGA (top panel). This results to the final CBM DAQ scheme (bottom panel) [2].

References

[1] D. Hutter, J. de Cuveland, and V. Lindenstruth, Preparations for the mCBM FLES Setup, CBM Progress Report 2017, doi: 10.15120/GSI-2018-00485

[2] W.M. Zabołotny et al., Selection of hardware platform for CBM Common Readout Interface, Photonics Applications in Astronomy, Communications, Industry, and High Energy Physics Experiments 2017; 10445 (2017) 49, doi: 10.1117/12.2280938

Status of the CBM physics performance studies

I. Selyuzhenkov[1,2], I. Kres[3], C. Pauly[3], K.H. Kampert[3], M. Zyzak[1], I. Kisel[4], P. Kisel[1,5], I. Vassiliev[1], V. Klochkov[1,6], A. Senger[1], E. Bechtel[6], C. Blume[1,6], S. Glaessel[6], J. Book[6], H. Schuldes[6], M. Teklishyn[7], and H. Malygina[1] for the CBM collaboration

[1]GSI, Darmstadt, Germany; [2]MEPhI, Moscow, Russia; [3]Bergische Universität Wuppertal(BUW); [4]Frankfurt Institute for Advanced Studies(FIAS), Frankfurt, Germany; [5]JINR, Dubna, Russia; [6]Goethe-Universität Frankfurt, Frankfurt, Germany; [7]FAIR, Darmstadt, Germany

Introduction

The CBM experiment is designed to study the QCD phase diagram at high net-baryon densities and moderate temperatures with heavy-ion collisions at the high interaction rates. In this report we highlight the activities of the CBM Collaboration related to the physics performance studies.

π^0 reconstruction via double conversion

The produced heavy particles containing charm quarks, like J/ψ, and also rare vector mesons ω, ρ, φ can be detected via their leptonic decay ω/ρ/φ → e^+e^-. As leptons are insensitive to hadronic interaction with the dense medium, their leptonic decays offer a possibility to look into the early, dense phase of the fireball evolution. Due to their comparatively small production cross section, together with small branching ratio (BR) into e^+e^- a precise understanding of background is needed. A major source of background stems from decay of neutral pions into π^0 → γ+γ (BR 98.8%), aand π^0-Dalitz decays π^0 → e^++e^-+γ (BR 1.1%). Instead of measuring directly photons by using an electromagnetic calorimeter, the CBM-RICH detector is able to measure photons indirectly by detecting e^+e^--pairs stemming from conversion γ → e^+e^- in the target or in the material of the detectors. Two such reconstructed photons are then further combined to form a π^0.

The reconstruction efficiency for pions via double conversion is rather low (~ 10^{-4}), mainly due to the low conversion probability of the two photons. A precise acceptance and efficiency correction is required in order to quantitatively describe the π^0 background in dilepton studies. Two statistically independent Monte Carlo samples (each consists of 5 × 10^6 UrQMD events of central Au+Au collisions at 8 AGeV beam energy) are used to evaluate the analysis procedure. The first sample is used to derive a multi-dimensional (as a function of p_T and rapidity) acceptance and efficiency correction matrix. Using the fixed correction matrix, the data from the independent second sample (and also others in future) are analyzed. In Fig. 1 one can see the comparison between all generated (left panel) and reconstructed (middle panel) number of π^0 from the first simulated sample. The right plot shows their ratio, which determines the correction factors. These factors will be used for the realistic π^0 estimation from the second simulated sample. As can be seen from the different colors on the right plot of the Fig. 1, correction factors for different rapidity-p_T bins differ, therefore, the double conversion analysis has to be done for each rapidity-p_T bin separately, adding corresponding correction factors. Summing up all numbers of π^0 after the correction gives us the proper number of generated pions in the available acceptance.

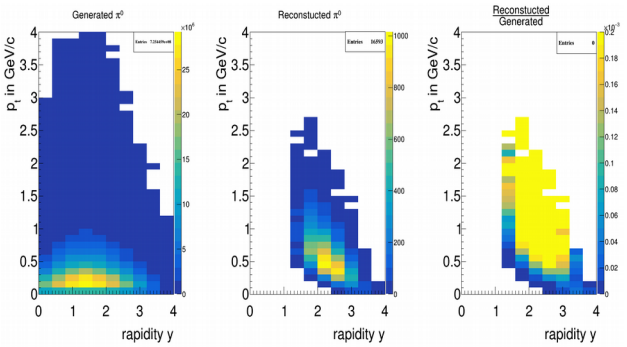

Figure 1: Phase-space coverage of all generated π^0 on the left plot, all reconstructed π^0 via conversion method on the middle plot, together with the their ratio on the right plot.

The corrected number of pions can be used for the temperature estimation of the emitting source. After summing up over rapidity to form 1-dimensional p_T distribution one can fit the resulting distribution and extract the corresponding temperature. In Fig. 2 one can see the comparison between reconstructed and generated p_T distributions together with the temperature fits.

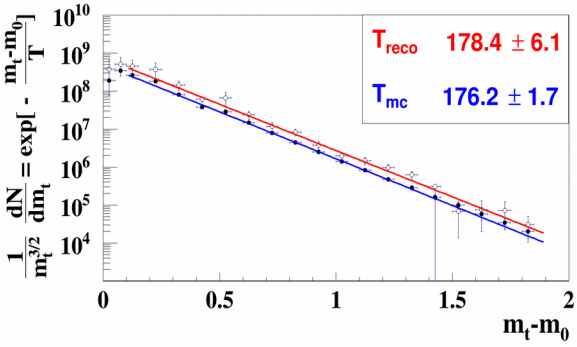

Figure 2: 1-dimensional p_T distributions of reconstructed π^0 after corrections (open circles) and simulated π^0.

Reconstruction of short-lived particles

The main goal of the short-lived particle analysis is to extract physics observables that characterize the system produced in a heavy-ion collision. One of such observables are particle yields as a function of momentum, rapidity, transverse mass, etc. In order to reconstruct short-lived particle spectra two methods were implemented in the KF Particle Finder package: side bands and background fit methods. The side bands method assumes that the back-

 DOI:10.15120/GR-2018-1

ground under the mass peak and around it has the same shape for all physics parameters. Under such assumption two kinds of spectra are collected for each parameter (p, rapidity, p_T, m_T) as well as two dimensional y-p_T and y-m_T spectra: signal+background within ±3σ of the peak and background in the region (3-6)σ around the peak. Then the background is normalized with respect to the integral of the background function in the region of ±3σ around the peak and subtracted from the signal+background spectra, that gives a reconstructed signal spectra.

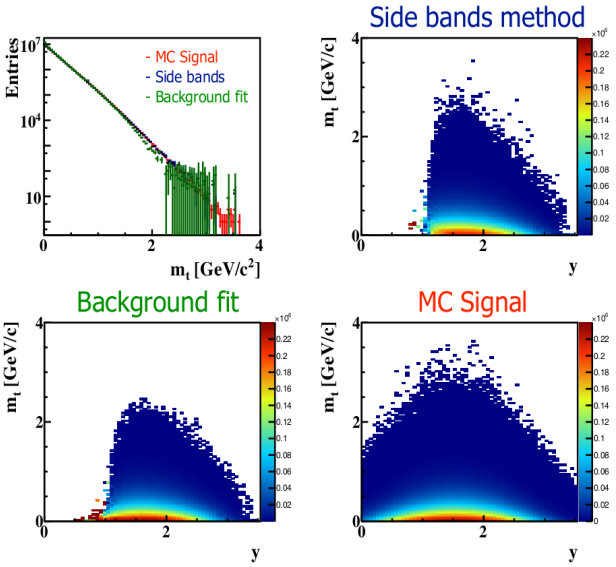

Figure 3: Efficiency corrected spectra of $K_s^0 \rightarrow \pi^+\pi^-$ decay as a function of m_t and y-m_t obtained by the side bands and background fit methods in comparison with the simulated Monte Carlo signal from 5M central Au+Au UrQMD collisions at 10 AGeV.

The second method which uses the background fit is implemented as follows: three dimensional histograms y-p_T -M and y-m_T-M are collected, where M is mass. Then the mass spectrum in each y-p_T or y-m_T bin is fitted with a signal+background function and the integral of the signal function provides the number of short-lived particles with given y and p_T or y and m_T respectively. The obtained number is filled to the corresponding bin of the signal spectra. Tools for collection of the efficiency plots were added to KF Particle Finder, that allow to reconstruct distributions of particles produced in the collision. Efficiency corrected m_T and y-m_T spectra obtained with both methods are shown in Fig. 3 for $K_s^0 \rightarrow \pi^+\pi^-$ decay in 5M central Au+Au UrQMD events at 10 AGeV. Reconstructed spectra are in a good agreement with each other and with the simulated Monte Carlo spectra.
The obtained m_T spectra can be further analyzed, for instance, in different rapidity bins, as it is shown in Fig. 4 - both reconstructed and simulated distributions are fitted with exponential functions, thus, providing the slope parameter. Under assumption, that produced particles are thermally distributed, the temperature can be extracted from the slope parameter.

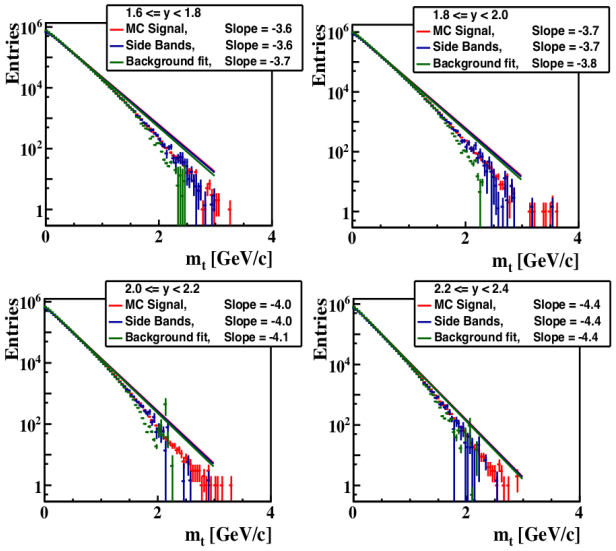

Figure 4: Reconstructed m_T signal in comparison to the simulated MC signal in different rapidity bins at an example of $K_s^0 \rightarrow \pi^+\pi^-$ obtained from 5M central Au+Au collisions.

Performance for directed flow measurement

The measurement of the anisotropic transverse flow is an important part of the CBM physics program. Due to the interaction among particles produced in a heavy-ion collision, the initial spatial asymmetry in the overlap region of the collision leads to the asymmetry in the direction of the particle's transverse momenta. This asymmetry can be measured via azimuthal distributions of produced particles with respect to the initial symmetry plane (reaction plane, RP) spanned by the impact parameter and the beam direction.
A sample of 5 million Au+Au collisions with beam momentum of 10 AGeV simulated with UrQMD event generator was used. Charge particles tracks were reconstructed using the Silicon Tracking System (STS) and Micro-Vertex Detector (MVD). The Projectile Spectator Detector (PSD) modules were grouped for analysis into three sets: central (PSD1), middle (PSD2) and outer (PSD3). Particle identification was done using Monte-Carlo information. Centrality determination was based on STS track multiplicity. The momentum asymmetry is quantified by constructing two-dimensional vectors q_n determined event-by-event from the STS tracks and calculated for three PSD module groups. Introducing a second harmonic vector helps to reduce non-flow correlations, such as contribution due to total momentum conservation. Imperfect acceptance and efficiency of the detector are biasing the azimuthal angle distribution of measured particles. A correction procedure for the q_n and Q vectors is implemented as a part of the QnCorrections framework.
Extracted values of the directed flow as a function of rapidity for negatively charged pions with reaction plane estimated from three different PSD subevents are shown in Fig. 5.

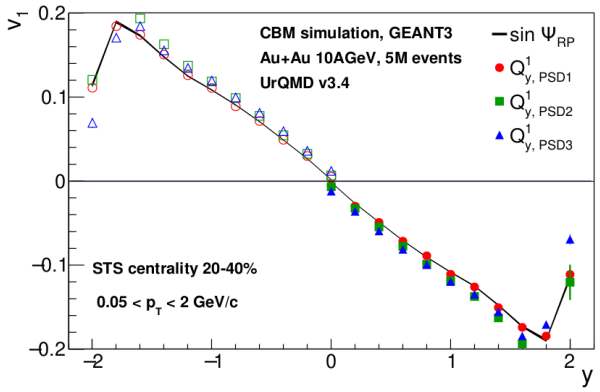

Figure 5: Directed flow of negatively charged pions for the 20-40% centrality class obtained using the y components of the PSD Q-vectors. Shaded area corresponds to v_1 calculated using MC-true reaction plane.

Di-muon measurement at low, intermediate and high invariant masses

The design of the CBM MUCH system consists of one absorber made of 60 cm carbon with additional Pb shielding around the beam pipe (5.7 degrees) and iron absorbers with thickness 20, 20, and 30 cm. Triplets of tracking detectors are mounted behind each absorber layer. Each tracking station behind the first and second absorber layer consists of 3 GEM detectors with high granularity in order to cope with the high particle density in these stations. The particle density behind the third and the fourth absorber is already significantly decreased, so that detectors with lower granularity could be used in order to reduce the number of channels.

The setup discussed above was optimized for measurements of the dimuon spectra in low invariant mass region. The Time-of-Flight (ToF) detector located 8 m downstream the target is used to suppress the background of protons and kaons. Figure 6 depicts the mass distributions for muons from ω (top) and for background (bottom) which are calculated using the time information. These simulations were performed for central Au+Au collisions at 8 AGeV generated with the UrQMD code assuming radial segmentation of 1 degree in stations 1 and 2, and 2 degrees in stations 3 and 4. The acceptance of the setup as a function of transverse momentum and rapidity is illustrated in the upper panel of Fig. 7.

An additional iron absorber of 1 m thickness behind the last detector station is required for measurements of the intermediate and high invariant mass regions. This study is devoted the investigation of the possibility to measure muon pairs over the full invariant mass spectrum. The simulations are based on the absorber system including the last absorber of 1 m thickness. In this case, the time measurements using the ToF detector are possible only for long tracks passing through all absorbers. Therefore, the soft muons are absorbed, and the acceptance of the reconstructed muons pairs will be shifted to forward rapidities (see central panel in Fig. 7). On the other hand, the signal-to-background ratio is very good, exceeding a value of 2 for omega mesons (see black histogram in Fig. 8). A possibility to shift the acceptance for dimuon signals back to midrapidity is to combine different types of tracks, for example long tracks with ToF information, and short tracks without ToF information. The acceptance for long-short and long-long combinations is shown in the lower panel of Fig. 7. The corresponding signal-to-background ratio is represented by the green histogram in Fig. 8.

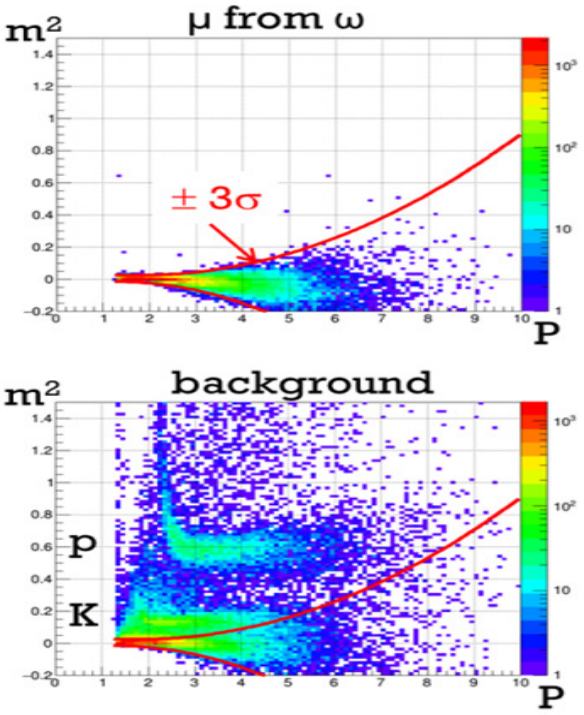

Figure 6: Mass squared versus momentum of muons distributions from omega meson decays (upper panel) and for protons, kaons and pions (lower panel) using ToF measurements. The red lines represent a 3 sigma selection of muon candidates by ToF.

In order to shift the acceptance further towards mid-rapidity, and simultaneously increase the signal-to-background ratio, one can consider an additional time-of-flight measurement in front of the last 1 m thick absorber. In this case, the contribution of short tracks to the background can be reduced, and all track combinations for muon pairs can be used: long-long, short-long, and short-short. Simulations have been performed with a ToF detector in station with a time resolution of 80, 200, 500 and 800 ps. Assuming a time resolution of 80 ps, the acceptance corresponds to the upper panel in Fig. 7, and the resulting signal-to-background ratio is represented by the red histogram in Fig. 8. For a much worse time resolution of 800 ps the signal-to-background ratio decreases by 35% only. When using only long-long and long-short track combinations together with the time measurement in station 4, the signal-to-background ratio improves further.

 DOI:10.15120/GR-2018-1

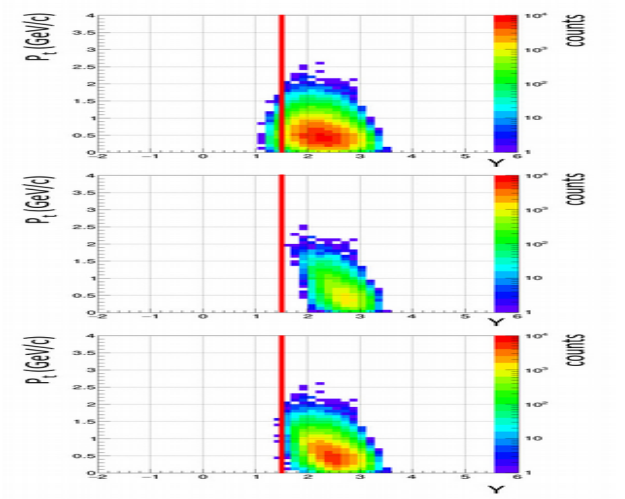

Figure 7: Acceptance for reconstructed muon pairs as a function of transverse momentum and rapidity. Upper panel: muon pairs from all muon track candidates. Middle panel: muon pairs from long tracks traversing 1 m iron absorber. Lower panel: muon pairs from short and long tracks. The red lines refer to mid-rapidity for 8 AGeV.

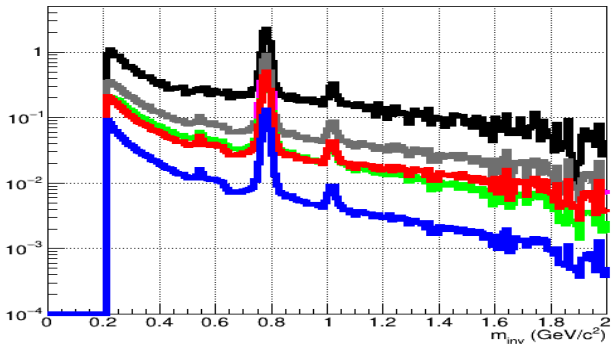

Figure 8: Signal-to-background ratio for muon pairs as a function of invariant mass for central Au+Au collisions at 8 AGeV. Black: muon pairs from long tracks with ToF information, Grey: muon pairs from long-long and long-short tracks, both with ToF information, Red: muon pairs from long-long, long-short, and short-short tracks, both with ToF information.

Dielectron measurements in Au+Au collisions

The measurement of dielectrons with sufficient signal-to-background ratio is essential for the CBM experiment. A good particle identification has to be provided in all momentum regions. For momenta below 6 GeV/c this can be done with the RICH detector. In the region of higher momenta the RICH loses its identification capabilities. The TRD can expand the particle identification and provide the necessary pion suppression to get access to the thermal radiation created in heavy-ion collisions.

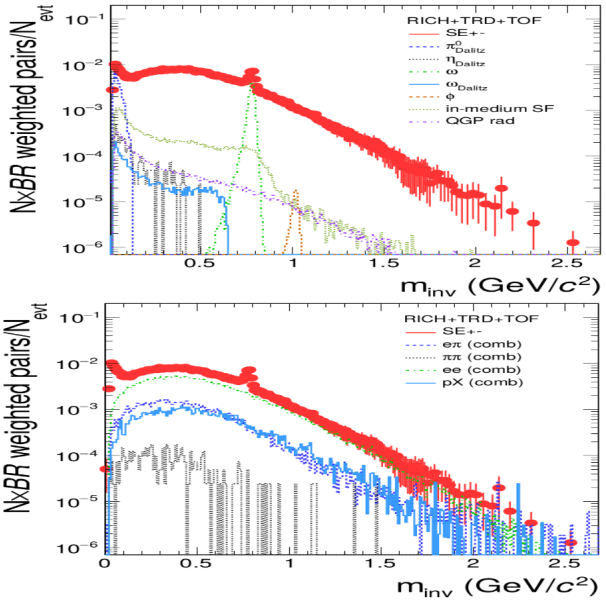

Figure 9: Invariant mass distribution for different unlike-sign pairs identified as electrons for central (10%) Au+Au collisions at 8 AGeV (red points), together with various signal channels (upper panel) and the combinatorial background contributions (lower panel). All contributions are weighted with their expected yield and branching ratio.

Figure 9 shows the invariant mass spectrum for different dielectron channels in the upper part. The simulation is done with 5 million Au+Au collisions at 8 AGeV beam energy for central (10%) events with the newest geometry of the TRD detector modules and four layers and a target thickness of 25 µm. A cocktail of low mass vector mesons (ρ, ω, ω dalitz and φ) as well as thermal radiation from the
hadronic and partonic medium is added via PLUTO generator. The electron identification for the RICH is done with the ANN output, tuned to a momentum independent efficiency of 90%, and for the TRD with the likelihood method tuned to 80% efficiency. The TOF identification uses β measurement to achieve an identification efficiency of ~ 90%. A p_T cut was used with a minimum of 0.2 GeV/c. The red points at the top panel of Fig. 9 show the total amount of reconstructed unlike-sign pairs which were identified as electrons. The signals of the in-medium and the QGP radiation are shown as violet and dark green dotted lines and can be accessed in the invariant mass range above 1 GeV/c^2 with a sufficient signal-to-background ratio. In the lower panel of Fig. 9 the corresponding background contributions are shown. The dotted green line presents the residual combinatorial dielectron pairs (e^+e^-) which are the most significant background contribution up to ~ 1.8 GeV/c^2. The other three lines consist of different hadronic combinations, which were misidentified as electrons but are strongly suppressed with respect to the e^+e^- component.

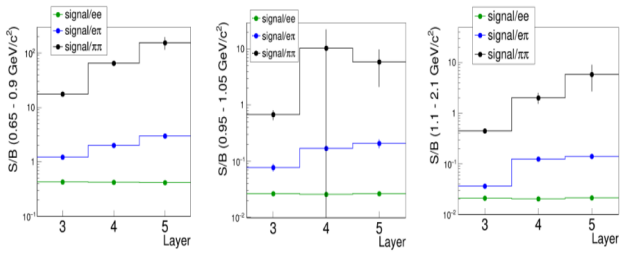

Figure 10: Total signal-to-background ratio in the range around the ω (0.65 − 0.9 GeV/c^2 - left), the φ (0.95 −1.05 GeV/c^2 - middle) and where the thermal radiation is expected to be dominant (1.1 − 2.1 GeV/c^2 - right).

To verify the best detector setup the simulation was also done for three and five TRD layers. Their performance can be quantified via the different signal-to-background ratios in the respective invariant mass regions as shown in Fig. 10. The four layer TRD setup shows a strong performance improvement in comparison to the three layer setup and provides sufficient identification for the requirements.

Hadron identification with the TRD

An important part of the CBM physics program is a high statistics measurement of double-Λ hypernuclei. Since up to now only very few double-Λ hypernuclei events have been identified, the measurement is considered to be a break-through in this field of physics. The Transition Radiation Detector (TRD) will significantly extend the number of hypernuclei states accessible within the program. For the identification of $^{6}_{\Lambda\Lambda}$He, which decays as $^{6}_{\Lambda\Lambda}$He → $^{5}_{\Lambda}$He+p+π and subsequently as $^{5}_{\Lambda}$He → ^{4}He+p+π , the separation of d and He is particularly important. The m/Z measurement of hadrons alone, as provided by the Time of Flight Detector (TOF), is not able to distinguish between the two different charge states. The TRD contributes to the separation of charged hadrons with a measurement of the specific energy loss. Fig. 11 shows how the identification of the light nuclei d and ^{4}He can be performed by combining TOF and TRD information.

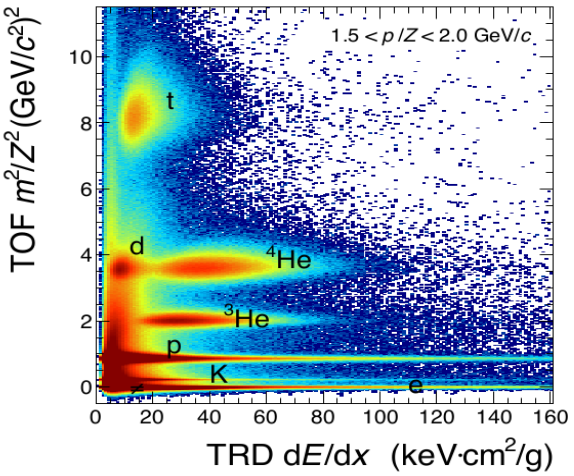

Figure 11: TOF versus TRD Mass squared distribution for 1.5 < *p/Z* < 2.0 GeV/c.

The distributions of the averaged energy loss signal *dE/dx* of d and ^{4}He, as reconstructed in the TRD for Au+Au collisions at 8 AGeV, are displayed in Fig. 12 for one momentum interval. A clear separation of d and ^{4}He is visible. The dE/dx distributions are fitted with a modified Gaussian, which includes the non-Gaussian tails of the distributions via the parameters α and β. Based on the corresponding energy loss resolution *σ(p/Z)/dE/dx(p/Z)*, the separation power can be determined for different particle species. The separation power for deuterons and ^{4}He for different detector geometries is shown in Fig. 13. A separation of d and ^{4}He on a level of σ ≥ 4 is achievable in the whole accessible momentum range with four TRD layers.

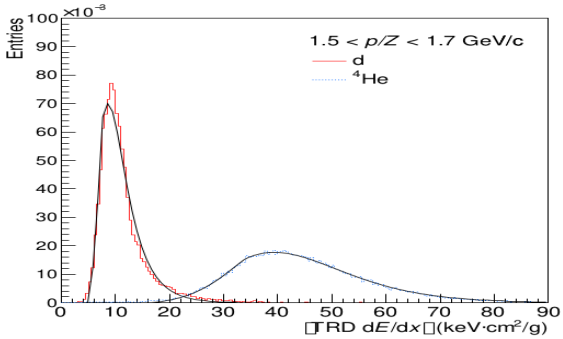

Figure 12: *dE/dx* distributions for d and ^{4}He, as reconstructed with the TRD, fitted with a modified Gaussian.

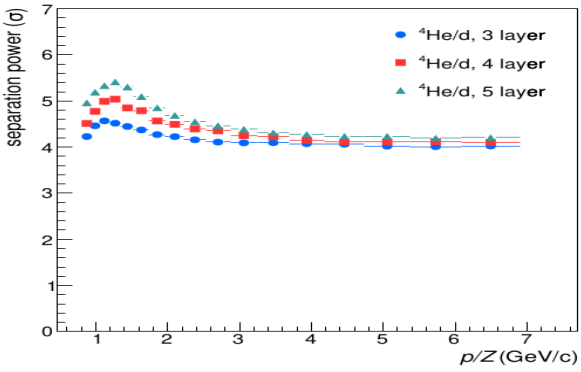

Figure 13: Separation power for d and ^{4}He as a function of momentum for setups with 3, 4 and 5 TRD layers.

Particle identification with the STS

Particle identification based on the energy loss in a thin absorber is a well-known technique in nuclear and particle physics. It can be naturally implemented in a tracking system by studying the energy loss Δ*E*/Δ*x* as function of the measured ratio of particle momentum and charge p/q. In the following we study the possibility of using the CBM-STS detector for particle identification in addition to the dedicated PID detectors (e.g., TOF). This way we expect to obtain a separation power for some particular cases such as low momentum particles not registered by the downstream detectors, decays inside the STS, and particles with the same m/Z ratio, e. g. ^{2}H and ^{4}He, which cannot be distinguished by means of a time-of-flight measurement alone. Since each track consists of several hits, each of which consists of two clusters, there are 2×N hits measurements of ΔE/Δx for a track. Each re-

 DOI:10.15120/GR-2018-1

constructed track has at least three hits in the STS. The chosen implementation for STS is based on the tracker geometry and readout electronics characteristics. The STS readout ASIC (STS-XYTER) has a dynamic range of 15 fC and a 5-bit flash ADC for each channel. These properties limit the implementation of the ΔE/Δx technique. If the charge in a given channel exceeds 15 fC (overflow), the energy loss measurement for the entire cluster (sum of all channels in the cluster) cannot be relied on.

For a proof of concept, we simulated 10^5 particles of various types (see Fig. 14) according to a thermal momentum distribution for Au+Au collisions at 10A GeV. A realistic detector response was involved in the simulation. An equivalent-noise charge of 1500e was used, which is 150−200% of the expected noise for a sensor connected to the readout electronics with a micro-cable; the threshold value was 3 × 1500 e = 4500e. Figure 1 shows that the energy loss measurement gives a reliable separation between single- and double-charged particles for the total momentum range, and separation between Hydrogen isotopes up to 2.5 GeV. The presence of clusters with overflow limits the application of the method in particular for heavy particles with low momentum. The efficiency is more than 99.99% for tritons and lighter particles, and 96.6% for the heaviest simulated particle ^{4}He (integrated over the whole momentum range). It is 100% for p > 2.5 GeV for all particles and drops for lower momenta.

The ΔE/Δx technique was tested on the example of ^{3}H reconstruction (see

Fig. 15). In this particular case it improves the signal-to-background ratio by a factor of 50 compared to using TOF alone for the identification of the decay products; the efficiency drops only by 0.3%. The method appears to be promising and shall be further developed for the implementation in the CBM software as one of the PID tools.

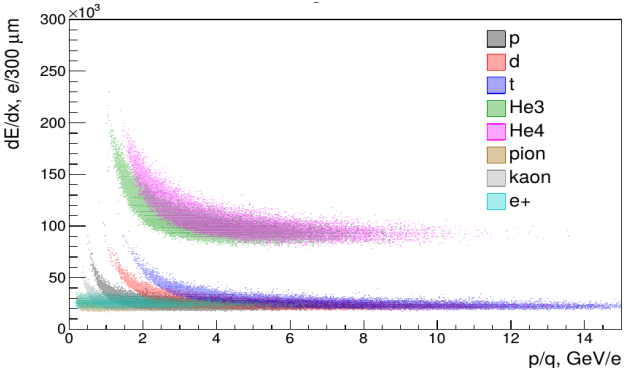

Figure 14: The reconstructed dE/dx normalized to the sensor thickness versus the reconstructed momentum-to-charge ratio from simulation of the CBM-STS.

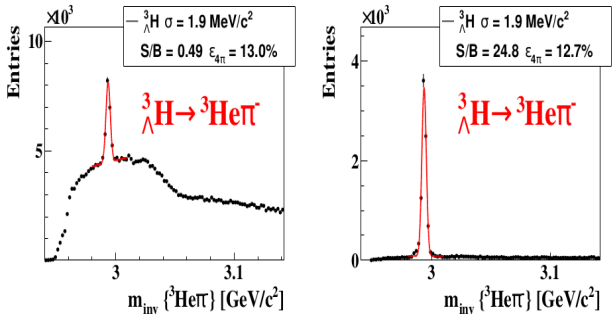

Figure 15: $^3_\Lambda$H reconstruction with TOF only (left) and with an additional PID from STS (right). 5×10^6 central Au+Au collisions at 10A GeV were simulated.

References

[1] [The CBM Collaboration], Chapter “Physics performance” in the CBM Progress Report 2017, DOI: 10.15120/GSI-2018-00485 (2018)

mCBM@SIS18 is on its way*

C. Sturm[1], D. Emschermann[1], J. de Cuveland[3], V. Friese[1], N. Herrmann[2], D. Hutter[3], P.-A. Loizeau[1], W. Niebur[1], A. Senger[1], F. Uhlig[1] , for the CBM collaboration

[1]GSI, Darmstadt, Germany; [2]Ruprecht-Karls-Universität Heidelberg, Germany, [3]Frankfurt Institute of Advanced Studies (FIAS), Frankfurt am Main, Germany.

The Compressed Baryonic Matter experiment (CBM) will explore the QCD phase diagram at the highest net-baryon densities by investigating nucleus-nucleus collisions in fixed-target mode at FAIR energies. The unique feature of CBM is its high-rate capability of up to 10^7 collisions per second, which will make it sensitive to extremely rare probes. In order to achieve these ambitious goals, CBM will employ fast and radiation-hard detectors as well as readout electronics. A novel, free-streaming data acquisition will be used, which aggregates the data sent by the self-triggered front-end electronics and pushes them to an online compute farm for data reconstruction and selection in real time.

By today, the design of the detector and electronics components for CBM is largely completed, and series production is going to start. The components were tested in the laboratory and in beam. Consequently, the next step is to test and optimize the operation of the full system of complex hard- and software components – from the detectors over the readout ASICs and the DAQ to on- and offline data processing and analysis – under realistic experiment conditions before the installation and commissioning of the full CBM detector setup. For this purpose we are presently installing a full-system test-setup for CBM at the GSI/FAIR host lab site under the name mCBM@SIS18 (”mini-CBM”, later shortened to mCBM). This test-setup will include detector modules from all CBM detector subsystems (MVD, STS, RICH, MUCH, TRD, TOF, ECAL and PSD see [1] - [6]) using prototypes or (pre-)series detector modules (mMVD, mSTS, mMUCH, mTRD, mTOF, mRICH, mECAL and mPSD).

Commissioning and running mCBM will complete our knowledge on proper functioning as well as on the performance of the CBM detector systems and their associated Front-End Electronics (FEE) before the final series production starts. The experiences gained during the complete mCBM campaign will significantly shorten the commissioning period for the full CBM experiment at SIS100.

Design of the test-setup

The mCBM test-setup will be positioned downstream a solid target under a polar angle of about 20° with respect to the primary beam, see Fig. 1 and 5. The present status of the mCBM engineering design is described in ref. [7]. mCBM does not comprise a magnetic field, and, therefore, will measure charged particles produced in nucleus-nucleus collisions traversing the detector stations following straight trajectories.

The tracking system comprises 2x STS (mSTS, see [8]), 3x MUCH (mMUCH) [9] and 4x TRD (mTRD) stations in total 9x tracking layers which provide redundant position information and allow to perform tracklet searches.

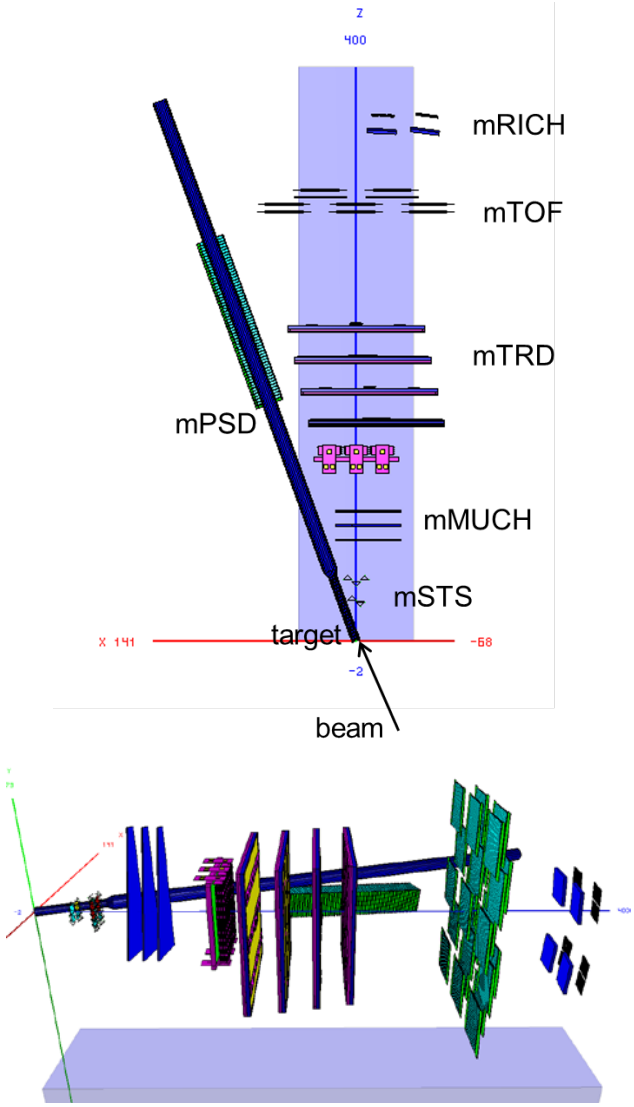

Figure 1: Top view (top panel) and side view (bottom panel) of the mCBM test setup (ROOT geometry) at the HTD cave. The detector stations are aligned at an emission angle of about θ_{lab}= 8° (beam pipe side, y = 0). Note, the GEM counters of the mMUCH subsystem are trapezoidal shaped (see lower panel), which is not visible in the top-view projection.

The setup will include a high-resolution time-of-flight system consisting of a fast and segmented diamond counter for time-zero (T_0) determination in front of the target as well as a TOF stop wall (mTOF) [10]. The mTOF detector modules are shown in Fig. 3 of [11]. An aerogel type RICH detector will be placed as the mRICH subsystem behind the mTOF detector and deliver a second measurement of the particle velocity in a selected ac-

 DOI:10.15120/GR-2018-1

ceptance window [12]. A small calorimeter (mECAL) will also be mounted behind the mTOF covering a reduced acceptance. Additionally, a PSD prototype-module (mPSD, see [13]) will be positioned directly under the beam pipe, 5° tilted relative to the beam axis while pointing to the target. In a later stage MVD stations (mMVD) will be added into the test-setup enabling a high-precision vertex reconstruction. However, the initial configuration of the mCBM test-setup is rather versatile and can be variably adapted according to the needs. Therefore, the detector stations are going to be mounted on sliders of a rail system on top of the mounting table.

The two mSTS stations and the 4^{th} layer of mTRD are centred in x and y. For tracks passing the active area of the mSTS, mMUCH, mTRD and mTOF subsystems the covered θ_{lab} range results to 8° – 32°. The overall acceptance is limited by the mSTS, which is located very close to the beam pipe [8] and cannot be moved further upstream.

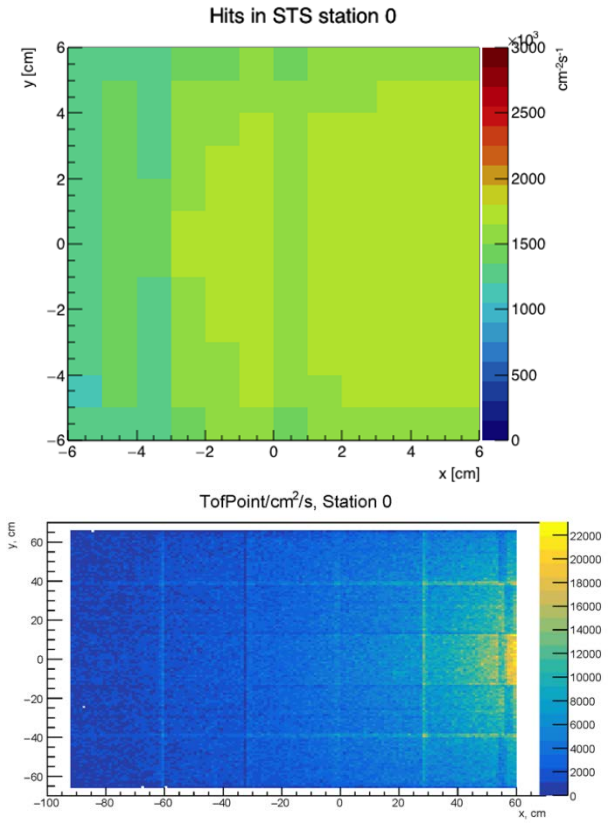

Figure 2: Hit rate within the first station of the mSTS (top panel) and of the mTOF (bottom panel). As input for the simulation, UrQMD events for minimum bias Au + Au col- lisions at 1.24 AGeV has been generated. δ-electrons have been taken into account.

Extensive Monte Carlo simulations have been performed to optimize the geometry of the setup. As input, events for minimum-bias Au+Au collisions at 1.24 AGeV have been generated with the UrQMD transport code. The complete mCBM geometry as shown in Fig. 1 has been implemented in CbmRoot and used for GEANT3 particle transport simulations taking δ-electrons into account. Within the mCBM acceptance an average charged-track-multiplicity yields to about 5 in minimum-bias and about 30 in central Au+Au collisions. In Fig. 2 hit rates normalized to 10^7 collisions per second (10^8 Au ions/s on a 10% interaction Au-target) are shown which have been obtained inside the first mSTS station (top panel) as well as in the mTOF stop wall (bottom panel). As shown, the hit rates result up to 1.8 MHz/cm^2 in the first mSTS station (mSTS0) and up to 22 kHz/cm^2 in the mTOF stop wall matching the design requirements of the CBM STS [1] as well as the CBM TOF [5] detector system. Here, δ-electrons enhance the hit rate within the first mSTS station by a factor of about 3.

The free-streaming DAQ system

The mCBM design focuses on the system performance aspect integrating existing (or currently under construction) prototype modules of all CBM detector subsystems into a common, high-performance free-streaming data acquisition (DAQ) system. The detector stations will be equipped with final readout electronics containing ultra-fast and radiation-tolerant ASICs as front-end chips followed by CERN GBTx-based radiation-tolerant data aggregation units. Further down-stream, the data streams are handled by Data Processing Boards (DPB) containing powerful FPGAs and are forwarded via FLES Input Boards (FLIB), a PCIe based FPGA board, to a large-scale computer farm, the First-Level Event Selector (mFLES, see [14]), which will perform on-line track and event reconstruction and selection, see Fig. 3.

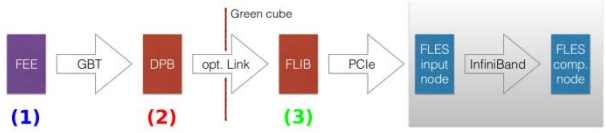

Figure 3: Envisaged mCBM readout chain for the startup phase, based on DPB and FLIB. The mCBM subsystems are equipped with individual front-end electronics FEE (1). These front-ends are interfaced by the GBTx ASIC, which forwards the detector data via optical GBT link. All GBT links are received by the DBP layer located at 50 m distance in the DAQ container (2). The DPB is a FPGA based board which allows for subsystem specific pre-processing of the arriving data stream. A long distance optical link connects the DPB output to the FLIB board installed in the FLES input node in the Green IT Cube (3).

The CBM detector front-ends are time-synchronized to the nanosecond level by the Timing and Fast Control (TFC) system. The detector front-end digitizes signals above threshold and assigns a time stamp to the hit. This data is then forwarded via an electrical connection to the GBTx readout board, where the electrical signals acquired through a large number of e-links are converted and merged into an optical GBT link operating at 4.48 Gbit/s. These GBT links are the detector interface to the Data AcQuisition (DAQ) chain.

On the road towards the full CBM DAQ system the mCBM DAQ system will be deployed in two phases. During phase I, the GBTx-based subsystems (mSTS, mMUCH, mTRD and mTOF) will be read out using already available readout chains based on existing prototype implementations of DPB and FLIB, see Fig. 3.

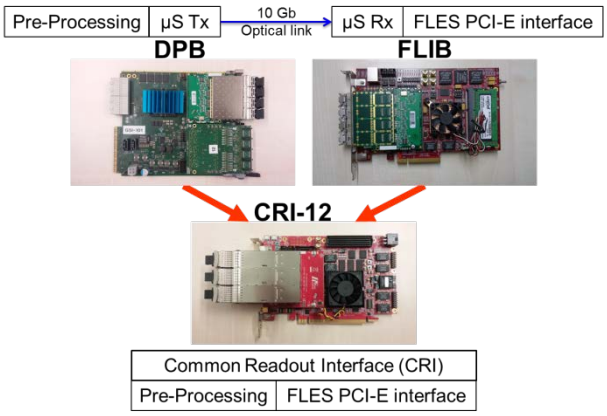

Figure 4: Upgrade of the mCBM DAQ in 2019.

As current prototype hardware, an AMC FMC Carrier Kintex (AFCK) board [15] is used for the DPB, a HiTech Global HTG-K700 PCIe board for the FLIB. Both boards are based on a Xilinx Kintex-7 FPGA. In phase II, DPB and FLIB will be replaced by a prototype of the Common Readout Interface (CRI) (see Fig. 4) in the FLES input stage, as it is foreseen for the CBM experiment. In addition, the mCBM subsystems (mRICH, mPSD) readout with FPGA TDCs chains will be added to the DAQ setup in 2019.

Reconstruction of the experimental area

The installation site for the mCBM test-setup is the detector test area named HTD in the GSI nomenclature (see Fig. 5) situated at the beam entrance of the experimental area cave-C (HTC) hosting the nuclear structure experiment R^3B. Although the space is very limited in the HTD area, the compact mCBM setup measuring a full length of about 4 m will fit into the HTD cave.

The arrangement of the HTD cave for the mCBM test-setup depends substantially on the incident angle of the beam as shown in Fig. 5. This also affects shielding measures which become necessary to make high-rate beam tests feasible up to CBM design collisions rates. Many iterations of radiation level simulations had been carried out using the FLUKA software package to fulfil the radiation safety requirements [16]. As one of the shielding measures, in particular to protect the R^3B experiment located in cave-C, a sandwich-like beam dump has been constructed consisting of 12x 12cm thick steel plates covered by 80 cm thick concrete blocks as visible in Fig. 6. A beam hole has been drilled up to the steel core (see Fig. 5) which will be blocked after irradiation.

Additional concrete blocks embedded into the chicane entrance have been placed directly in front of the R^3B target region (see Fig. 5 and 7). To block access into the HTD cave after high-rate beam-tests have taken place, a lockable entrance door is being installed. Up to four additional concrete layers with a thickness of 0.8 m each will be placed on top of the HTD cave ceiling.

As illustrated in Fig. 5, the incoming beam will be either transported to the R^3B experiment or deflected to the mCBM setup by a switching magnet (dipole magnet) mounted directly in front of cave-C carrying the name HTD MU1 in the GSI nomenclature. To date, beams had been deflected at an effective angle of 14.5° corresponding to an magnetic rigidity of Bρ = 10 Tm. Accordingly, the maximum kinetic energy for heavy projectiles like Au had been limited to 0.45 AGeV generating unrealistic conditions due to a large number of low-momentum fragments emitted during the collision. In order to exploit the full beam energy range of SIS18 we are going to exchange the vacuum chamber of the switching magnet by a spare chamber with vacuum outlets for 0° and 7.5°. With the given magnetic induction, beams will be bend on a radius of ρ = 11.25 m at top SIS18 energy which results to an effective deflection angle of 8.0°.

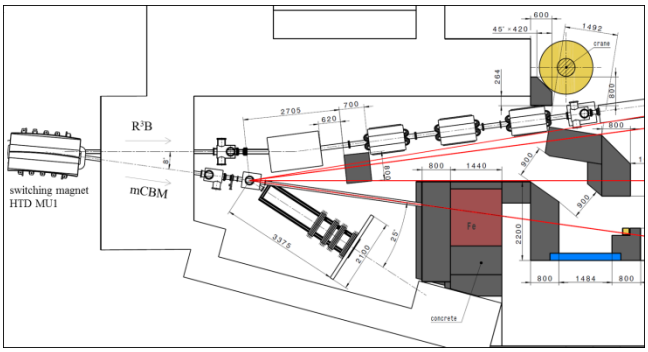

Figure 5: The modified mCBM cave (HTD) at the SIS18 facility of GSI/FAIR (as of August 31, 2017).

Figure 6: The Iron core of the beam dump is prepared for concrete pouring.

Figure 7: Chicane entrance to the mCBM cave (HTD).

 DOI:10.15120/GR-2018-1

Benchmarking the mCBM test-setup

To verify the performance of the CBM data taking concept the mCBM setup will be used to reconstruct physics observables that can be compared to published data. A feasibility study with the mCBM setup was performed using the Λ production probability in heavy-ion collisions as a benchmark observable. At SIS18 beam energies Λ baryons are produced close to or below the free NN production threshold. Thus their production probability is rather small posing a CBM-like challenge to the reconstruction and se- lection task.

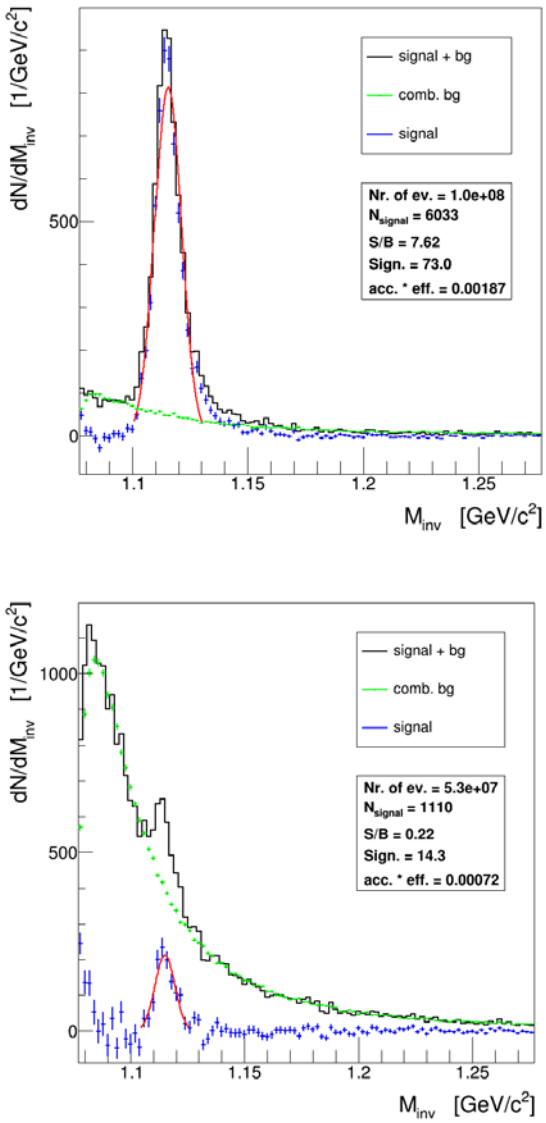

Figure 8: Λ-identification in minimum bias UrQMD events in Ni+Ni collisions at 1.93 AGeV (top) and in Au+Au at 1.24 AGeV (bottom). Invariant mass distributions are shown for (π-p) pair combinations (combinatorics) within events (black line, signal + bg), for pair combinations from mixed events (green symbols, comb. bg) and for the resulting distribution after subtraction (blue symbols, signal). Statistics information is obtained from a Gaussian fit to the subtracted distribution (red line).

Since mCBM does not include a magnetic field for momentum measurement, the reconstruction has to be done via time-of-flight (TOF) and track topology, assuming the pion and proton mass for (π-p) pair candidates. For simplicity, only STS and TOF hits are considered for the reconstruction algorithm. As geometry, the most recent mCBM setup has been used within the MC simulation as it is depicted in Fig. 1. Fig. 8 demonstrates that the limited information available is sufficient for Λ reconstruction. Improvements are certainly possible by tuning the selection cut values. As simulation input, 10^8 minimum bias events of the reactions Ni+Ni at an incident energy of 1.93 AGeV and $5.3 \cdot 10^7$ minimum bias events of Au+Au collisions at 1.24 AGeV have been generated with the UrQMD transport model [17]. The corresponding phase space coverage (efficiency in z-direction) for Ni+Ni collisions at 1.93 AGeV is shown in Fig. 9 demonstrating that the acceptance of mCBM is limited to a small angular range close to mid-rapidity.

For both benchmark collision systems published data from the FOPI collaboration are available in [18] as well as from the HADES collaboration in [19] that the mCBM results can be quantitatively compared to. It is worth noting that the technical goal and challenge is to reconstruct the invariant mass distributions shown in Fig. 8 within a time period of about 10 s data taking at SIS18, assuming 10^7 nucleus-nucleus collisions per second (10^8 ions per second bombarded on a 10 % interaction target).

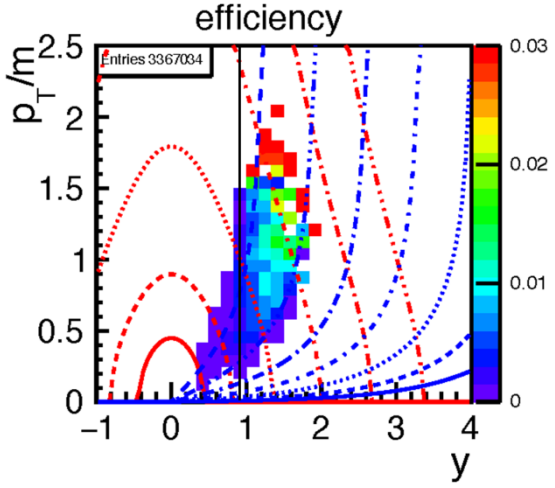

Figure 9: Efficiency of reconstructed Λ - baryons with mCBM produced in Ni+Ni collisions at 1.93 AGeV (input: events generated with UrQMD). Red and blue lines indicate constant laboratory momenta and laboratory polar angles, respectively. The black line marks mid-rapidity.

mCBM beamtime

Mid of 2017 a beamtime proposal had been submitted to the General Program Advisory Committee of GSI/FAIR (G-PAC) for the year 2018 (”development & commissioning”) with the focus on data transport, the data analysis as well as detector tests, and for the year 2019 (”approaching full performance”) implying the completion of subsystems, the high-rate data transport and data processing incl. online reconstruction. The applied beamtime has been fully granted by the G-PAC in September 2017.

All the background rejection strategies necessary to reconstruct rare probes with CBM at SIS100 can be prepared and exercised with mCBM. In addition, if the technical goals of mCBM are achieved, a measurement of the Λ production excitation function should become feasible. This was not yet measured in the SIS18 beam energy range thus offering a unique opportunity to contribute to world data, although the covered phase space is limited and therefore systematic errors become large when extrapolating to unmeasured regions.

The successful implementation and demonstration of the technical capabilities would also open the road to more relevant physics observables like the measurement of light hypernuclei. The beam time request for more physics oriented observables will be placed in the next beamtime period from 2020 – 2021, once the preliminary results are supporting the high expectations.

References

[1] J. Heuser, W. F.J. Müller, V. Pugatch, P. Senger, C.J. Schmidt, C. Sturm and U. Frankenfeld, Technical Design Report for the CBM Silicon Tracking System (STS),GSI-2013-05499, http://repository.gsi.de/record/54798

[2] S. Chattopadhyay, Y. P. Viyogi, P. Senger, W. F.J. Müller and C. J. Schmidt, Technical Design Report for the CBM: Muon Chambers (MuCh), GSI-2015-02580, https://repository.gsi.de/record/161297

[3] C. Höhne et al., Technical Design Report for the CBM Ring Imaging Cherenkov Detector (RICH), GSI-2014-00528, http://repository.gsi.de/record/65526

[4] C. Blume et al., Technical Design Report for the CBM Transition Radiation Detector (TRD), to be published

[5] N. Herrmann et al., Technical Design Report for the CBM Time-of-Flight System (TOF), GSI-2015-01999, https://repository.gsi.de/record/109024

[6] F. Guber and I. Selyuzhenkov, Technical Design Report for the CBM Projectile Spectator Detector (PSD), GSI-2015-02020 , https://repository.gsi.de/record/109059

[7] L. Radulescu, D. Emschermann, and A. Bercuci, CAD integration of the mCBM subsystems, CBM Progress Report 2017, 2018, DOI 10.15120/GSI-2018-00485

[8] O. Vasylyev et al., Progress with the integration of the mCBM Mini Silicon Tracking System, CBM Progress Report 2017, 2018, DOI 10.15120/GSI-2018-00485

[9] C. Ghosh et al., Development of a MUCH Cooling system for mCBM, CBM Progress Report 2017

[10] I. Deppner , N. Herrmann , and the CBM TOF working group, Time Of Flight Detector - Summary, CBM Progress Report 2017, 2018, DOI 10.15120/GSI-2018-00485

[11] The CBM eTOF working group, The TOF FAIR Phase 0 project - eTOF at STAR, CBM Progress Report 2017, 2018, DOI 10.15120/GSI-2018-00485

[12] G. Pitsch , S. Lebedev, and C. Höhne, Monte-Carlo Simulations of a mRICH detector with aerogel radiator in mCBM, CBM Progress Report 2017, 2018, DOI 10.15120/GSI-2018-00485

[13] F. Guber, mPSD at mCBM, CBM Progress Report 2017, 2018, DOI 10.15120/GSI-2018-00485

[14] D. Hutter , J. de Cuveland , and V. Lindenstruth, Preparations for the mCBM FLES Setup, CBM Progress Report 2017

[15] W.M. Zabołotny and G. Kasprowicz, "Data processing boards design for CBM experiment", Proc. SPIE 9290 (2014) 929023, doi:10.1117/12.2073377

[16] A. Senger et al. (CBM Collaboration), Concrete shielding and beam dump for mCBM, CBM Progress Report 2017, 2018, DOI 10.15120/GSI-2018-00485

[17] M. Bleicher et al., Relativistic Hadron-Hadron Collisions in the Ultra-Relativistic Quantum Molecular Dynamics Model, J. Phys. G: Nucl. Part. Phys. 25 (1999) 1859-1896

[18] M. Merschmeyer et al. (FOPI collaboration), K0 and Λ production in Ni+Ni collisions near threshold, Phys. Rev. C 76 (2007) 024906

[19] H. Schuldes et al. (HADES collaboration), Studying Strangeness Production with HADES, Web of Conferences 171, 01001 (2018), SQM2017

Experiment beamline: mCBM@SIS18
Experiment collaboration: CBM
Experiment proposal: S471
Accelerator infrastructure: SIS18 / HEST
PSP codes: 1.1.1
Grants:
GSI Helmholtzzentrum für Schwerionenforschung GmbH
Facility for Antiproton and Ion Research,
Helmholtz Gemeinschaft,
BMBF No. 05P12VHFC7, 05P2015, 05P15PXFCA, 05P15RGFCA, 05P12RGFCG, 05P15RFFC1, 05P12VTFCE, 05P15VHFC1, 05P15PMFC1, 05P16VTFC1, 05P16PMF1, 05P16PMFC1, 05P15ZAFC1,
HIC for FAIR Helmholtz International Center,
HGS-HIRe for FAIR,
Hessian Initiative for Excellence (LOEWE),
Cremlin - Connecting Russian and European Measures for Large-scale Reasearches Infrastructure,
European Union's Horizon 2020 research and innovation programme under grant agreement No.654166 and 654168, Helmholtz-YIG grant No.VH-NG-823,
Humboldt foundation, Germany
Strategic university co-operation with:
Darmstadt, Frankfurt-M, Gießen, Heidelberg

* This report is also part of the CBM Progress Report 2017, 2018, DOI 10.15120/GSI-2018-00485

D mesons Langevin propagation at SIS300-FAIR

G. Inghirami [1,2,3,4], H. Van Hees[1,2], S. Endres[1,2], J. Torres-Rincon[5] and M. Bleicher[1,2,3,4]

[1]FIAS, Frankfurt am Main, DE; [2]Goethe-Universität, Frankfurt am Main, DE; [3]GSI, Darmstadt, DE;
[4]J. von Neumann Institute for Computing, Jülich, DE; [5]Stony Brook University, Stony Brook, New York, USA

Heavy quarks represent an excellent tool to probe the properties of the medium which is supposed to form in relativistic heavy ion collisions, because they are produced in the very initial stages after the collision and their number is conserved until the hadrons they form decay by weak interaction, long time after the kinetic freezeout. Since their masses are considerably larger than the light quark masses, we can model their propagation into the medium by adopting a Langevin approach. In this work we perform the Langevin propagation of c and anti-c quarks in fixed target Au-Au collisions, with 25 AGeV beam energy, in the range of the future FAIR facility. In our simulations we neglect the back reaction of charm quarks and D mesons on the medium, allowing for the simultaneous propagation of many charm quarks at the same time, whose initial momentum distribution is computed by using Pythia 8.2. We compute the evolution of the background medium using both the UrQMD/hybrid [1] and the UrQMD/coarse graining [2] approaches, running simulations at fixed impact parameters b = 3 fm and b = 7 fm. We perform the hadronization by adopting an instantaneous coalescence model [3] in momentum space combined with Peterson fragmentation. We consider only the formation of D^+, D^0 mesons and their antiparticles. We take into account the effects of the finite baryon chemical potential on the values of the transport coefficients through a fugacity factor. The drag and diffusion coefficients in the partonic phase are computed within a resonance model [4], while the description of how the coefficients are derived in the case of D mesons can be found in ref. [5]. We study how variations in the centrality class and in the conditions for charm quark hadronization influence the elliptic flow and the nuclear modification factor of the final D and anti-D mesons.

We find that most of the final elliptic flow of D and anti-D mesons is built during the partonic phase, while the subsequent hadronic interactions seem to have a limited influence. Moreover, we find that the model of the dynamics of the medium and the hadronization procedure have a large impact on the magnitude and on the transverse momentum dependence of the elliptic flow and of the nuclear modification factor.

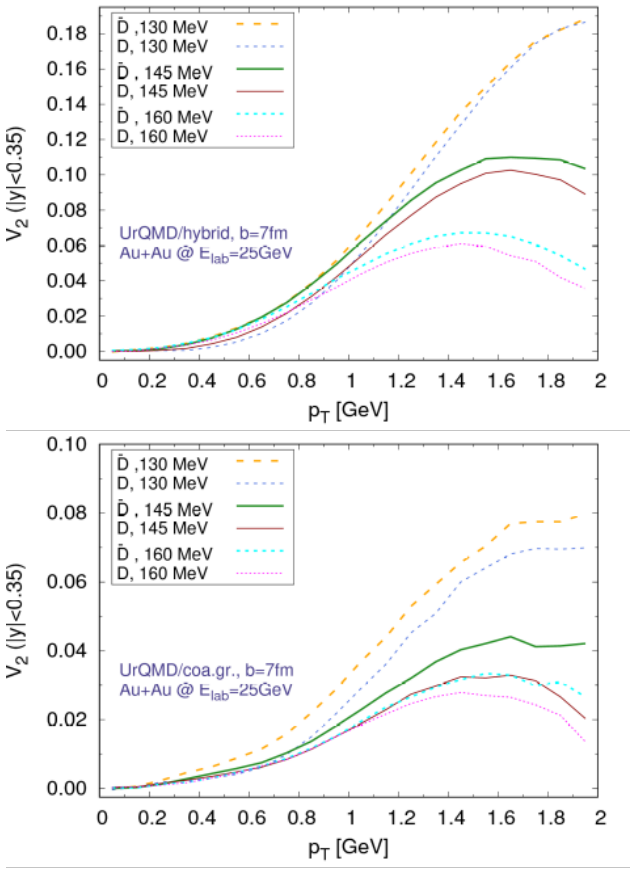

Figure 1: Elliptic flow of D and anti-D mesons (|y| < 0.35) within the UrQMD/hybrid (top) and UrQMD/coarse graining (bottom) approaches. Here we show the dependence on the hadronization temperature in Au+Au collisions at Elab = 25 AGeV at a fixed impact parameter b = 7 fm.

References

[1] H. Petersen, J. Steinheimer, G. Burau, M. Bleicher and H. Stöcker, Phys. Rev. C 78, 044901 (2008)

[2] S. Endres, H. van Hees, J. Weil and M. Bleicher, Phys. Rev. C 92, 014911 (2015)

[3] V. Greco, C. M. Ko and R. Rapp, Phys. Lett. B 595, 202 (2004)

[4] H. van Hees and R. Rapp, Phys. Rev. C 71, 034907 (2005)

[5] L. Tolos and J. M. Torres-Rincon Phys. Rev. D 88, 074019 (2013)

Grants: COST Action CA15213 (THOR)

Strategic university co-operation with: Frankfurt-M

CBM computing – progress, status and outlook

J. de Cuveland[1], V. Friese[2], P.-A. Loizeau[2], F. Uhlig[2], M. Zyzak[2]
for the CBM Computing Working Group

[1]FIAS, Frankfurt, Germany; [2]GSI, Darmstadt, Germany

The development of CBM software has, over the years, concentrated on simulation of nuclear collision events in the CBM detector setup, and reconstruction and analysis of the simulated data. The corresponding tools were widely used for studying the physics performance of the CBM detector.

With the advent of mCBM, which will start taking data in August 2018, new challenges appeared, which have to be met on a rather short timescale. mCBM will allow to test the entire data chain, from the front-end electronics through the DAQ chain to online and offline processing of experiment data on CPU. This will allow to scrutinise existing software concepts, but also enforces to accelerate the process of moving simulation and reconstruction from the event-by-event case to the handling of free-streaming data, corresponding to the real situation for CBM and mCBM. Moreover, issues not addressed so far, like the software needed to set-up, run and control the experiment, and, most of all, a framework concept of processing data in real-time, suddenly become very urgent.

To meet these challenges organisationally, the CBM software activities were structured and defined in a project-like manner, with the aim to distribute responsibilities, assess manpower, planning, timelines and milestones, and identify critical items and shortage of workforce. The following Computing Projects were defined (see Fig. 1):

- Experiment and Detector Control Systems (EDC): tools to configure and monitor detectors and DAQ
- Online Data Management (ODM): software to operate the online computing farm, receive data from the experiment, build time slices and deliver them to the compute nodes
- Data Processing Framework (DPF): the environment for data processing both online and offline
- Data Analysis Algorithms (ALG): algorithms for event reconstruction and common data analysis
- Simulation Software (SIM): enable detector simulation on the same level as real experiment raw data
- Offline Analysis Environment (OAE): develop strategies and tools for the offline analysis of large-scale data
- Software Development Infrastructure (INF): provide and maintain tools for collaborative software development and maintenance

The platform for coordination of and communication between the projects is the newly established Computing Board. In the following, we briefly report on the status and progress following the project structure.

Experiment and Detector Control system

The detector control was until now driven by beam-time activities and therefore mostly concerned systems with single detector type [1-3]. Following the establishment of the Computing Board, work is ongoing to define the tasks, interfaces and general specifications of the slow-control, detector-control and central experiment control systems. Prototypes of these systems will help for the operation of mCBM phase I and are necessary for efficient data taking with mCBM phase II.

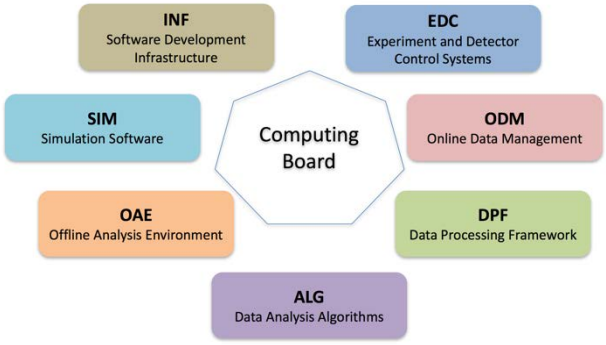

Figure 1: Computing project structure

Online Data Management

A demonstrator software that implements time slice building as well as the interfaces to detector links and online processing has been available for several years. This software, named *FlesNet* has already been used for online data taking in various CBM detector test setups and beam tests. It is still evolving, with recent work focusing on operational improvements for small and medium-sized setups. This includes the addition of a ZeroMQ-based transport complementing the existing RDMA-based transports [4].

With regard to the full SIS-100 setup, the scalability of the time slice building has been improved, including the demonstrator implementation of a new data-flow scheduler [5]. The work of the near future will cover additional features and tools that will also be beneficial to the upcoming operation of mCBM.

Data Processing Framework

The ROOT-based software framework employed by CBM for many years now allows to simulate, reconstruct and analyse physics events in an integrated environment. It, however, provides no inherent mechanism to parallelise the execution of tasks and thus make full use of the available computing architectures. This strongly limits its applicability for real-time data processing on the CBM compute nodes. First studies to introduce parallelism schemes into *CbmRoot* were undertaken [6, 7], but showed little performance gain owing to the structure of the reconstruction processing graph. In the future, the possibility to use the message-queue based *FairMQ* scheme, developed by the Scientific Computing group of GSI as extension to *FairRoot*, will be investigated.

 DOI:10.15120/GR-2018-1

Databases for various purposes (configuration, conditions, components) will be important ingredients to the framework. *FairDB* is currently used for managing the hardware component properties in several detector systems and may also be usable for other purposes [8].

Data Analysis Algorithms

The core reconstruction algorithm, the track finding in the STS, was already enabled to operate on free-streaming data. The event-building procedure from reconstructed STS tracks is also available and was tested with physics analysis [9]. The proper time-based input from cluster and hit finding, however, is currently only available for the STS and MUCH systems [7, 10]. Thus, current efforts are devoted to extend the existing time-based reconstruction to the downstream detectors (global tracking). Progress was made for tracking in the muon system [11, 16] and in the TRD [12]. In addition, the particle identification potential for light nuclei, relevant for the study of e.g., hyper-nuclei production, was investigated using the energy loss in the STS [13] and in the TRD [14]. Moreover, a first version of track finding in mCBM, which differs from the full CBM in the track model, was made available [15].

Development of the time-based procedure for reconstruction of global tracks is in progress. Two approaches are being considered at the moment: based on the *littrack* and the CA track finder algorithms. The *littrack* method is the current standard, and addition of the time measurement to the reconstruction scheme is a straightforward solution. However, it is based on the track following algorithm using STS tracks as seeds, which makes it complicated to be applied for the detector alignment task. In its turn, the CA track finder in STS is already fully adapted for time-based reconstruction and expansion of the method to the downstream detectors is currently being implemented [16]. The task of the time-based global track finder requires realistic description of the time response of cluster and hit finding algorithms, which will be addressed in the nearest future. Based on this realistic input, the existing solutions for global tracking will be compared w.r.t. performance in order to arrive at an optimal solution.

Simulation Software

The two major ingredients for simulations are the description of the detector geometry and a model for the detailed detector response (digitizer). The detector geometries for CBM were consolidated; by now, all detector systems deliver the geometry in the ROOT *TGeoManager* format as agreed on for standalone visualisation and management through a database (see [17-19]). Geometry descriptions for all detector system participating in mCBM are also available. In order to manage the increasing number of geometry versions for the detector system for different contexts / setups and provide them in a controlled and user-friendly way, the development of a Geometry Database was continued; a prototype is now available for testing [20].

Time-based version of all digitizers were provided (see [18, 21]), which is of particular importance for the modelling of the actual data stream from both mCBM and CBM. Together with a (simplified) software representation of the time-slice building, the simulation output is now logically equivalent to the raw data expected from the data acquisition. It is, however yet on the *digi* (ROOT) level and does not include all details of the time slice building (e.g., micro-slice sub-structure). Similarly, not all relevant features (e.g., data loss due to pile-up from different events) are yet included in all digitizers; this will be the task for the immediate future.

The next issues to be addressed by simulation software are thus: the proper treatment of inter-event pile-up in the digitizers, the inclusion of not event-correlated background sources into the simulations (see [22, 23]) and the description of the data stream in the actual raw data format.

Offline Analysis Environment

Considerations to organise the offline analysis of the huge amount of data CBM will archive when starting operations in 2024 have not started yet in earnest. A strategy will be developed in close cooperation with the other FAIR experiments, in particular with PANDA as the other data-intensive experiment, and with FAIR/GSI-IT. First steps to develop a common FAIR computing model, of which the CBM computing model will be one part, will be taken in 2018, with the aim to arrive at a Technical Design Report in 2020.

Software Development Infrastructure

The basic tools to enable an effective and collaborative software development are in place and operational since several years.

- Software distribution: *CbmRoot*, comprising simulation, reconstruction and analysis software, is distributed through a *subversion* repository hosted on a GSI server. Several packages (*KFParticle*, *KFParticleFinder*, *FlesNet*), are hosted separately on *git* servers and are integrated into *CbmRoot* in the build process. The movement of the entire CBM software to a *git* repository is one of the tasks for the next future.
- Build system: We use *CMake* to build *CbmRoot*, which takes also care of the integration of external packages. Shell scripts for the installation of external packages and of *FairRoot* are provided. The installation is supported on all Linux flavours as well as for OS X.
- Documentation: By convention, documentation is provided in-code in *Doxygen* format. The documentation is generated nightly on a GSI server, which provides a browser-based output [24]. Additional requirements on documentation are to be defined by the Computing Projects.
- Software integrity management: the possibility to perform regular tests (nightly or on commit) is provided through a *CDash* system. Tests are to be defined by the Computing Projects. The test results are furnished on a web server [25].
- Project management and communication: The collaborative platform for software development in

CBM is a *Redmine* instance [26]. It integrates a browser front-end to the repository, systems for issues, news, forum and Wiki, and project planning facilities. The *Redmine* system is also used for some hardware projects.

The development tools and the deployment of servers are subject to constant maintenance and further development following the needs of the Computing Projects.

This report is also part of the CBM Progress Report 2017 (doi:10.15120/GSI-2018-00485).

References

[1] P. Klaus et al., *The Detector Control System for the MVD prototype PRESTO*, CBM-PR2017*, p. 12

[2] J. Bendarouach and C. Höhne, *Design of a control and monitoring system for the mirror alignment of the CBM RICH detector*, CBM-PR2017, p. 59

[3] V. Negi, J. Saini and S. Chattopadhyay, *Design and development of error resilient control system of Low Voltage Distribution Board for CBM-MUCH detector*, CBM-PR2017, p. 79

[4] J. de Cuveland et al., *A FLESnet transport using ZeroMQ*, CBM-PR2017, p. 129

[5] F. Salem et al., *Data-flow scheduling for a scalable FLESnet*, CBM-PR2017, p. 130

[6] M. Prokudin, *Parallelization of CbmRoot at task level*, CBM-PR2017, p. 132

[7] V. Singhal et al., *Parallelization of cluster and hit finding for the CBM-MUCH*, CBM-PR2017, p. 144

[8] D. Bertini and E. Lavrik, *Progress with FairDB development*, CBM-PR2017, p. 133

[9] V. Akishina et al., *Reconstruction of time-slices in CBM at high interaction rates*, CBM-PR 2017, p. 145

[10] V. Friese, *Time-based cluster finding in the CBM-STS detector*, CBM-PR2017, p. 143

[11] A. Zinchenko and V. Ladygin, *Application of the vector finding-based track reconstruction method for the CBM muon setup*, CBM-PR2017, p. 146

[12] O. Derenoskaya, T. Ablyazimov and V. Ivanov, *Towards $J/\psi \to e^+e^-$ triggering with the CBM-TRD*, CBM-PR2017, p. 148

[13] H. Malygina et al., *Investigation into the particle identification potential of the CBM-STS*, CBM-PR2017, p. 160

[14] S. Gläßel et al., *Hadron identification via energy loss measurements with the TRD*, CBM-PR2017, p. 156

[15] T. Ablyazimov, V. Friese and V. Ivanov, *Using the binned tracker in mCBM*, CBM-PR2017, p. 189

[16] V. Akishina, I. Kisel and M. Zyzak, *Kalman Filter track fit for the CBM STS and MUCH detector systems*, CBM-PR2017, p. 147

[17] P. Klaus et al., *Update on the CBM MVD geometry*, CBM-PR2017, p. 135

[18] L. Lebedev, E. Ovcharenko and C. Höhne, *RICH software status*, CBM-PR2017, p. 138

[19] O. Singh et al., *Description of the CBM-MUCH geometry in ROOT format*, CBM-PR2017, p. 140

[20] E. Akishina et al., *Geometry database for the CBM experiment*, CBM-PR2017, p. 142

[21] A. Bercuci et al., *Time-based CbmRoot simulations of the Bucharest TRD prototype for mCBM*, CBM-PR2017, p. 186

[22] V. Friese, *Implementation of electronic noise in the simulation of the CBM-STS*, CBM-PR2017, p. 137

[23] A. Senger, *Time-based track reconstruction in STS with δ-electrons*, CBM-PR2017, p. 136

[24] http://cbmroot.gsi.de/cbm-doc/daily/html/index.html

[25] https://cdash.gsi.de/index.php?project=CbmRoot

[26] https://redmine.cbm.gsi.de/projects/cbmroot

.

* I. Selyuzhenkov and A. Toia (eds.), CBM Progress Report 2017, Darmstadt 2018, ISBN 978-3-9815227-5-4, doi:10.15120/GSI-2018-00485

HADES activities and status 2017

The HADES collaboration

GSI Helmholtzzentrum für Schwerionenforschung

Introduction

The main goal of the HADES experiment is to explore the microscopic structure of dense baryonic matter. HADES experiments performed in the last years in nucleus-nucleus and proton-nucleus reactions have shown the important role played by the propagation of far off-shell ρ mesons due to their coupling to baryonic resonances in hadronic matter, visible as an excess radiation of the e^+e^- production above conventional sources for invariant masses below the vector meson poles. To provide a reference to these medium effects and to study the electromagnetic structure of the baryonic resonances an important programme has been developed by the HADES collaboration to investigated elementary reactions like pp, quasi-free ′n′p and recently πp.

Studying reactions with proton and pion beams on proton (liquid H_2 or polyethylene) targets is indeed an important element of the HADES program. Besides measurements of production cross sections, which provide an essential reference for heavy-ion collisions, also the elementary reaction mechanisms are studied. In particular, the role of baryonic resonances is investigated in both strangeness and dielectron production.

Recent physics results

Results from 2012 Au+Au run

The time-of-flight (TOF) resolution of HADES has been improved by using additional information in the calibration procedure and by assessing the quality of the TOF detector and its readiness for the upcoming experimental runs at SIS18 (see contribution of G. Kornakov).

We have also improved our analysis techniques of weakly decaying hadrons, like neutral kaons and hyperons, by applying machine learning techniques to the recognition of the decay topologies. To train such algorithms high statistics signal and background samples are needed. In our analysis the signal sample is obtained from a simulation, while the background sample is generated by combining tracks from different real events. Figure 1 shows a comparison between the resulting invariant-mass spectra when either using the hard topology cuts from [1] or when using a trained neural network. It is evident that the neural network based approach provides a gain of up to 200% in the yield of reconstructed Λ hyperons, when optimized for significance of the signal.

In addition, we have started to refine the analysis of protons and light nuclei, with a specific emphasis on the amount of thermalization of the created system and the nucleon coalescence parameter.

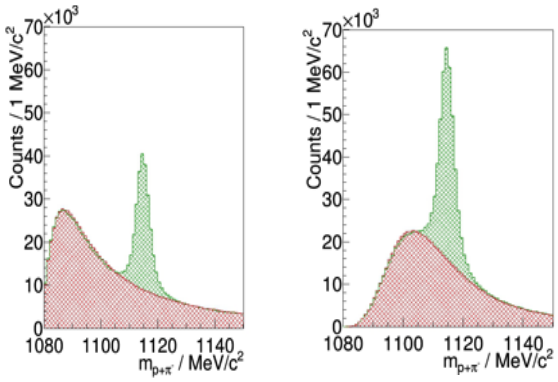

Figure 1: Reconstructed Λ mass spectrum in Au+Au collisions obtained with hard cuts [1] (left) and using a neural network (right). The signal is shown in green and the uncorrelated background in red.

Because of their self-analysing nature, weak decays can be used to measure the average spin orientation of the mother particle and interpret this as a signal of a possible global spin polarization. We have analyzed a significant Λ sample and extracted the centrality dependence of the polarisation parameter (see report of F. Kornas).

We have furthermore made a step forward towards understanding the transverse momentum spectra of charged pions in terms of their production from the thermalized system (see report of M. Gumberidze).

The studies on directed (v_1) and elliptic (v_2) flow of identified particles have been further extended. In addition to the multi-differential analysis for protons and pions (see 2016 GSI reports by B. Kardan and M. Gumberidze), now also the v_1 and v_2 of deuterons and tritons have been investigated as a function of transverse momentum and rapidity. After normalizing p_t and v_2 with the mass number A, the elliptic flow of p, d and t exhibits a clear scaling at mid-rapdity, as expected within a simple nucleon coalescence picture. Furthermore, higher moments of proton flow, v_3 and v_4, with respect to the first order reaction plane have been investigated.

First results on two-pion HBT correlations have been obtained as well. A special algorithm for the reduction of the effect of close track pairs had to be implemented for this analysis. The study was performed for negatively charged pions and allowed to extract the radius parameters R_{long}, R_{out}, and R_{side} as a function of pair momentum k_t and collision centrality. A significant k_t-dependence of the radius parameters is observed, in line with the expectation for a radially expanding source as it is also visible in the mass dependence of the p_t-spectra of identified single particles.

We have finally performed a comprehensive dilepton analysis for the Au+Au data and were able to extract significant medium modifications of hadron properties,

based on an established NN reference spectrum [2,3]. The excess yield has been quantitatively understood as thermal radiation emitted from the hot and dense fireball. Above an invariant mass of 0.4 GeV/c, the observed spectral shape of the excess radiation for the 40% most central collisions, corrected for the acceptance of the spectrometer, exhibits an almost exponential shape, consistent with an average temperature of the transient fireball of around 72 MeV. The absence of a bump in the vector meson pole mass region indicates a "melting" of the ρ meson in the medium.

We have extracted the multi-differential pattern of dilepton emission, including transverse mass, rapidity, helicity and azimuthal anisotropy distributions, for several centrality bins (see report of S. Harabasz).

Results from 2014 pion beam run

In 2014 a pioneering campaign investigating pion-nucleus collisions (π + C, W) at an incident momentum of 1.7 GeV/c was carried out with HADES at the GSI pion beam facility. This allowed to investigate in-medium effects on the strange mesons K^-, K^+, and ϕ in cold nuclear matter.

Previous studies indicated a moderately repulsive KN potential for kaons (K^+, K^0), while the antikaons (K^-) are expected to propagate in an attractive potential with a considerable imaginary part. Antikaon absorption processes in nuclear matter mediated by strangeness exchange reactions on one (KN $\rightarrow$ πY) or more nucleons (KNN $\rightarrow$ YN) contribute sizeably. A similar study pf the phi meson is also of considerable interest. And this concerns not only the significant feed-down into the K^- as observed in sub-threshold Au+Au collisions and elementary p+p reactions close to the ϕ production threshold. Of even more importance is the ϕ absorption in cold nuclear matter, resulting in a widening of the ϕ natural width.

Yet another interesting topic that can be addressed with pion-nucleus reactions is the study of hyperon propagation within nuclear matter. In the discussion of the equation of state of neutron stars the properties of the Λ are of considerable interest as its interacton with one or several nucleons enters various theoretical models. Since pion-induced reactions happen mostly on the nuclear surface, the lambda is also produces there and subsequently traverses the nucleous where it can rescatter on a nucleon. A measurement of the exclusive channel π^-+p $\rightarrow$ K + Λ with an additional recoil proton offers the opportunity to study the ΛN interaction in nuclear matter through a comparison of the data with transport models. A preliminary analysis of the HADES data shows that this process can indeed be isolated experimentally.

Production of e+e- pairs was measured in another run using the GSI pion beam at a lower momentum of 0.685 GeV/c impinging on polyethylene (PE) and carbon targets.

To allow for a more direct study of the baryonic contributions to the pair spectrum, we performed an exclusive analysis by applying invariant-mass and missing-mass cuts.

We have selected 1500 events corresponding to the free or quasi-free pi-p $\rightarrow$ ne^+e^- reaction. The comparison to model predictions is on-going. Using the Partial Wave Analysis (PWA) of the two-pion production measured in an energy scan in the same experiment, this excess can be interpreted as an off-shell contribution, consistent with the Vector Meson Dominance model (see report of F. Scozzi).

A parametrization of the angular distributions using the spin density formalism was also performed, allowing for the first time to get important information on the helicity structure of baryon electromagnetic transitions in the time like region.

The neutral pion and eta contributions were reconstructed in pi-PE reactions at 0.685 GeV/c using the photon conversion method. The preliminary extracted cross sections fit well to the world data (see repport of J.-H. Otto).

Status of the upgrade projects

With the start of FAIR Phase-0, most of the HADES detector systems will have reached an age of over 15 years. In order to keep the detector operational, an upgrade program has been started: For reasons of better photon detection efficiency, (1) the UV detector of the RICH has been replaced by MAPMTs, and (2) the Pre-Shower detector (polar angle coverage from 18 to 45 degree) has been replaced by a full-fledged electromagnetic calorimeter (ECAL). Moreover, the success of the experimental program addressing elementary reactions motivated the instrumentation of the acceptance region between polar angles of 0.5 to 6.5 degree with a straw-tube tracker. Most of these upgrade projects profit by close synergies with instrumentation projects of other FAIR collaborations (PANDA and CBM).

Electromagnetic Calorimeter

The addition of an electromagnetic calorimeter (ECAL) to HADES will moreover allow to study by photon measurements new reaction channels involving e.g. the production of neutral mesons, as well as neutral Λ(1405) or Σ(1385) resonances in elementary and heavy-ion reactions. Another advantage is the resulting improvement of the electron-to-pion separation at large momenta. ECAL is based on 978 lead glass modules recycled from the OPAL experiment. It is divided into 6 sectors, and it covers forward angles of $16^\circ < \theta < 45^\circ$ and almost the full azimuthal angle. The Technical Design Report had already been approved in 2014 by the FAIR ECE. The project is carried out by groups from Rez, Krakow, Moscow, Bratislava, Frankfurt, Darmstadt, Munich and GSI.

The readout of the detector is based on PaDiWa AMPS boards [4] (charge-to-width measurement) developed especially for the calorimeter and connected to a TRB3 [5] setup. The second generation of the 8-channel PaDiWa-AMPS front-end boards was assembled at GSI EE, tested in the laboratory and meanwhile the four completed sectors of the ECAL have been equipped (see report of A. Rost). A dedicated optical monitoring system has been de-

 DOI:10.15120/GR-2018-1

veloped for the ECAL. It is based on a laser LED and a microlens array with optical fibers which allows to send light pulsed of defined intensity into each single ECAL module for calibration purposes.

In the current funding concept, photomultipliers of two different types are installed. The limited budget forces the HADES collaboration, other than recommended by the ECE, to partly reuse 1.5" EMI 9903KB photomultipliers recovered from the MIRAC (WA98) detector; for the rest, new 3" Hamamatsu R6091 photomultipliers have been purchased.

RICH Photon Detector

The MWPC based gaseous RICH VUV photon detector with its CsI photon converter is currently being replaced by an arrangement of multi-anode photo multiplier tubes (MAPMTs, Hamamatsu H12700C) with blue-enhanced high quantum efficiency photo cathodes. The detector modules composed of 6 MAPMTs and integrated together with all required readout electronics on a backplane are developed together with CBM and will also be used as UV photon detectors in the CBM RICH. The pixel size (5.8×5.8 mm^2) of these devices perfectly matches the pad geometry of the old MWPC detector and guarantees reasonable position resolution of single photon hits and efficient ring image recognition on the 0.92 m^2 sensitive area. The MAPMTs are arranged on two aluminum carrier frames such as to fit as close as possible to the focal surface of the RICH mirror. Altogether 428 MAPMTs (27392 readout channels in total) arranged on 74 super-modules with 3×2 individual MAPMTs each will be mounted inside the existing gas tight detector chamber and flushed with nitrogen. A schematic view of the new RICH configuration and the design of the new photon detector device is depicted in Fig. 2.

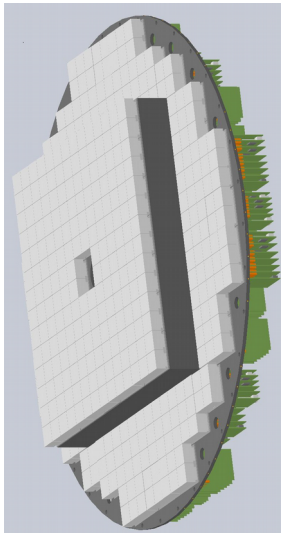

Figure 2: Schematic view of the redesigned HADES RICH photon detector and read-out configuration.

The newly developed readout front-end (DiRich) comprises pulse amplification, discrimination, time-to-digital conversion and time-over-threshold measurement for single photon signals from each individual MAPMT pixel. Twelve densely packed DiRich cards serve six MAPMTs and are arranged on a super-module backplane together with a power- and combiner card providing connection to the TRBnet of the HADES data acquisition system. Laser measurements with MAPMTs and final DiRICH prototypes show the expected performance with respect to single photo electron detection efficiency and rate capability.

The high quantum and single photo electron detection efficiency, low cross talk probability, and a new versatile ring finder algorithm lead to an expected superb single e^+/e^- identification efficiency across the whole detector area, in spite of the very short radiator length at small polar angles. In particular, the ring finder allows to efficiently discriminate overlapping rings even for very close e^+e^- pairs with opening angles down to $\delta\Omega \simeq 3^\circ$. Simulations done with conservative detector parameters promise a significant reduction of the misidentified combinatorial e^+e^- pair background also in heavy-ion reactions.

The new RICH photon detector will be ready for the 2018 beam times.

New Forward Detector System

To extend the acceptance of the HADES Spectrometer towards lower polar angles, 0.5° – 6.5°, a dedicated Forward Detector is being constructed. This detection system consists of two tracking stations placed 3.1 and 4.6 m downstream of the target and is based on straw tubes. It is followed by a high precision time-of-flight wall based on RPC technology and a high granularity scintillator based hodoscope. As this detector will operate in a field-free region the particle identification has to be performed based on dE/dx and time-of-flight measurements. Additionally, the straw tube tracking stations will be used for reconstruction of off-vertex decays.

The two stations of the Forward Tracking Detector are each composed of 8 layers of self-supporting straw tubes with 10 mm diameter. The layers are built from vertical straws rotated by 0, 90, 0, 90 and 0, 90, −45, 45 degree around the beam axis. The position resolution of the detector amounts to around 150µm which, for the given detector geometry, provides track reconstruction with angular resolution of $\sigma_\theta = 0.5$ mrad for 2 GeV protons. The Straw Trackers are currently assembled by the Krakow and FZ Juelich teams, based on developments for the PANDA Forward Tracker. LIP Coimbra is producing the Forward RPC.

The increase of acceptance will play a significant role in studies of N (π) + N and p + A reactions where this detector is essential for exclusive channel reconstruction and PWA analyses of hyperon production and for studies of decays like $\Lambda \rightarrow p\pi^-$, Λ^* (Σ^*) $\rightarrow \Lambda e^+ e^-$ (hyperon transition form-factors) and $\Xi^- \rightarrow \Lambda\pi^-$. For heavy-ion reactions the Forward Detector will consist only of an highly granular plastic scintillator (the other two components will be removed). The detector will then focus on reaction plane reconstruction and precise centrality measurements.

Start Detector Upgrade

For experiments with HADES, a radiation hard and fast beam detector is required. The detector is placed directly in the beam either close in front of the target (START) and in some configurations also at the exit of the RICH detector (VETO). To properly handle the rates the detector has to be segmented and radiation hard. The time resolution of the START should be so good (time-zero measurement with $\sigma_{t0} < 50$ ps) that the time-of-flight measurement is not deteriorated by it. While this is mandatory for proton- and pion-beam induced reactions, in case of heavy-ion collisions, the time-zero determination is further improved by taking the average of a properly corrected stop measurements of all charged particles in the acceptance. These requirements can in general be fulfilled by utilizing single-crystal Chemical Vapor Deposition (scCVD) diamond based detectors. High counting rate capability of the diamond detector (up to 107 ions/s/mm^2) has been shown in the Au+Au run. The measured radiation damage to the diamond material by Au ions has been quantified and it has been shown that while the energy resolution of a degraded detector is reduced significantly, its timing properties are, however, worsened only slightly. A similar concept for T0 measurement will be used during the 2018 Ag+Ag run.

The detection of minimum-ionizing particles remains challenging since one has to deal with very small amounts of induced charge carriers while the expected high rates require special emphasis on the read-out electronics. A read-out concept for diamond detectors for minimum ionising particles will be based on the already well established TRB3 (Trigger and readout board - version 3) platform developed at GSI. The board provides 260 high precision (RMS < 12 ps) multi-hit FPGA-TDC channels and serves as a flexible data acquisition system (DAQ). The available comprehensive software package allows on-line monitoring capabilities including basic analysis. A large variety of front-end electronics is available in order to extend its functionality.

MDC FEE Upgrade

The about 27.000 sense wires of the HADES drift chambers are currently read out by means of dedicated front-end electronics mounted on the frames of the detectors. The analog section is based on the ASD-8 ASIC featuring amplification, shaping and discrimination with a common threshold per 8 channels and a typical integration time of 7 – 8 ns. A semi-customized ASIC for time digitization provides both, drift time and valuable time-over-threshold information. Built nearly 20 years ago, the system suffers from an increasing number of dead channels and the data transfer bandwidth turned meanwhile out to be a limiting factor of the DAQ. Moreover, in high-rate applications it is recommended to employ multi-hit capability of the read-out to avoid efficiency losses due to occupied channels fired by random coincidences (notably δ electrons). Also, a higher detection sensitivity is desirable to increase the stability of the detector under high load by lowering the gas gain. Besides that, the HADES tracking algorithms would accept slightly worse spatial resolution while profiting from an improved noise immunity.

Pursued by groups from Frankfurt and GSI, state-of-the-art solutions based on available ASICs (the ASD-8 is no longer on the market) and time digitization realized in FPGAs are being studied in order to replace the old FEE in the near future. A promising replacement candidate is the PASTTREC ASIC, developed at the Jagiellonian University, Krakow, for reading out straw tubes of the PANDA experiment and future forward tracking in HADES. This chip is currently at the focus of our investigations. It is supplemented by a high precision FPGA-based TDC, implemented on a TRB3 board. In parallel, a cost-efficient and lightweight, but coarsely binned (500 ps) FPGA-based prototype TDC was successfully tested and is now foreseen to replace the currently used dedicated TDC ASICs. To arrive at conclusive performance results, the tests are being conducted under realistic conditions in direct comparison to the present ASIC. To do so, a spare drift chamber is employed and both signal-to-noise and dE/dx, as well as time resolution are systematically characterized with radioactive sources and cosmic rays. Furthermore, a test beam time took place at the Jülich Cooler Synchroton COSY in October 2017.

One key issue is the compatibility of the present flex-based signal routing and the PASTTREC ASIC mounted on a customized board, which significantly affects the noise immunity together with determining the optimum parameter settings of the PASTTREC chip. Due to the arrangement of two stereo angle layers, it is possible to assess the drift time (and spatial) resolution by correlating adjacent drift cells. This study, together with beam tests, will help to answer the other key question on the possibility of assigning an ASIC optimized for straw tube signals – which deliver more charge (operation at 2 bar and longer track path in a straw tube cell) – to read out the mini (cell) drift chambers of HADES. The final decision on the replacement of the existing electronics is foreseen to take place in the first half of 2018. A new MDC read-out is then scheduled to be available for the year 2020.

 DOI:10.15120/GR-2018-1

References

[1] T. Scheib, "*Λ and K^0 Production in Au+Au collisions at 1.23A GeV"*, Ph. D. thesis, U. Frankfurt (2017).
[2] P. Sellheim, "*Reconstruction of the low-mass dielectron signal in 1.23A GeV Au+Au collisions"*, Ph. D. thesis, U. Frankfurt (2017).
[3] S. Harabasz, "*Reconstruction of virtual photons from Au+Au collisions at 1.23 GeV/u*", Ph. D. thesis, TU Darmstadt and Jagellonian U. Krakow (2017).
[4] A. Rost et al., "A flexible FPGA-based QDC and TDC for the HADES and the CBM calorimeters", Jinst 12, C02047 (2017).
[5] C. Ugur et al., "*264 Channel TDC Platform applying 65 channel high precision FPGA-based TDCs*", in IEEE Nordic Mediterranean Workshop on Time-to-Digital Converters, IEEE NoMe TDC 1 (2013).

Experiment beamline: HADES
Experiment collaboration: HADES
Experiment proposals: S333, S407, S447
Accelerator infrastructure: SIS18
PSP codes: 1.1.2
Grants: BMBF 05P12CRGHE HZDR Dresden; BMBF 05P12RGGHM, U. Gießen; BMBF 05P15PXFCA, U. Wuppertal; BMBF 05P15WOFCA, TU München; Helmholtz Alliance HA216/EMMI; HIC for FAIR (LOEWE).
Strategic university co-operations with: Darmstadt, Dresden, Frankfurt am Main, Giessen, TUM, Wuppertal

Performance of the plastic scintillator Time-of-Flight Wall of HADES during the Au+Au run

G. Kornakov[1] for the HADES Collaboration

[1] TU Darmstadt, Germany.

The performance of the HADES TOF plastic scintillator wall [1] has been studied in great detail. This study had a twofold purpose: The first one was an attempt to improve the time-of-flight resolution by including additional information in the calibration procedure. The second one was to assess the quality of the detector and its readiness for the upcoming experiments.

The adoption of a TRB [2] based data acquisition scheme required new front-end electronics. The new boards based on the NINO chip [3] encode into the leading edge and width of a digital pulse the arrival time and (integral) charge of the signal read out on both sides of the scintillator coupled to Photo-Multipliers (PMTs). A consequence of these changes is a position dependent relation between the arrival time and the width of the TRB signal. Therefore, the goal of the new calibration strategy was to incorporate to the sequence of procedures the local dependence between the measured charge and time, the so-called "walk correction". For such a purpose the time-charge relation was studied in 20 equally long sections (bins) along the scintillator rods. Figure 1 shows such a correlation for a single bin of one rod. The reference time was calculated using the measured momentum and flight distance of particles identified in the tracking detector using the specific energy loss. With this, the dependence can be modelled by a linear combination of exponential and power-law functions, which are used during the calibration procedure to remove the walk effect from the data.

The measured time-of-flight and position along the rod can be reconstructed using the half-sum and half-difference of both times multiplied by the light group-velocity in the scintillator. Following previous works, the timing could be improved if instead of the half-sum a weighted average is used [4].

The result of these procedures is shown for minimum ionizing particles in Figure 2. Timing precisions of the order of 130 ps where achieved for the shortest rods of 1475 mm, degrading slightly to 160 ps due to signal attenuation in the longest rods of 2365 mm.

This result confirms the excellent time capabilities of the TOF Wall and its readiness for the upcoming experiments with both heavy and light beams.

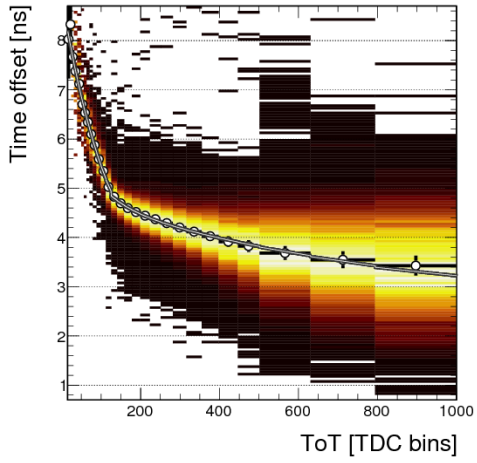

Figure 1: Example of a time-charge dependence measured in one longitudinal bin of a scintillator rod. The white circles correspond to the median of the distribution and the line is a fit consisting of a linear combination of exponential and power-law functions.

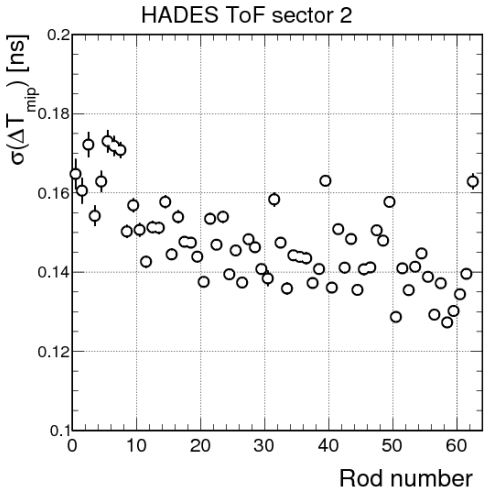

Figure 2: Timing performance for minimum ionizing particles of one of the sectors of the scintillator wall.

References

[1] C. Agodi et al., Nucl. Instrum. Meth. A 492 (2002) 14.
[2] I. Fröhlich et al., IEEE Trans. Nucl. Sci. 55 59. (2008)
[3] F. Anghinolfi et al., Nucl. Instrum. Meth. A 533 (2004) 183-187.
[4] M. Kurata et al., Nucl. Instrum. Meth. A 349 (1994)

Experiment beamline: HADES
Experiment collaboration: HADES
Experiment proposal: S407
Accelerator infrastructure: SIS18
PSP codes: none
Grants: VH-NG-823, Helmholtz Alliance HA216/EMMI
Strategic university co-operation with: Darmstadt

 DOI:10.15120/GR-2018-1

Benchmarking new front-end electronics for the HADES drift chambers

M. Wiebusch[1], C. Wendisch[2], J. Pietraszko[2], C. Müntz[1], J. Stroth[1,2] for the HADES Collaboration

[1] Goethe Universität, Frankfurt, Germany, [2] GSI, Darmstadt

Upgrading the digital part of the HADES MDC read-out system in preparation for SIS-100 requests a re-design of the analog part as well. Instead of re-using the ASD8 ASICS we want to benchmark a modern amplifier-shaper-discriminator chip, the PASTTREC ASIC [1], developed by JU Krakow, w.r.t. to precision in time and energy loss measurement.

Figure 1:

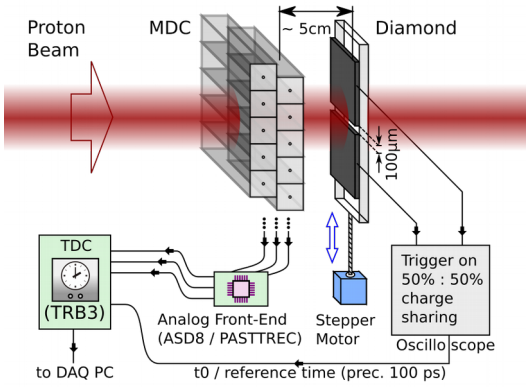

Sketch of the COSY beam test set-up to assess timing precision of the joint system comprising a drift chamber and different read-out electronics.

The timing precision, being the most crucial performance parameter of the joint system of detector and read-out electronics, was assessed during a beam test at the COSY accelerator in Juelich using a proton beam with a momentum of 2.7 GeV/c. As shown in figure 1, a diamond detector [2] served to provide trigger, reference time and position of protons in a narrow slice (<100 µm) of the beam, parallel to the sensing wire, and thus allows to select perpendicular tracks at any position within a drift cell.

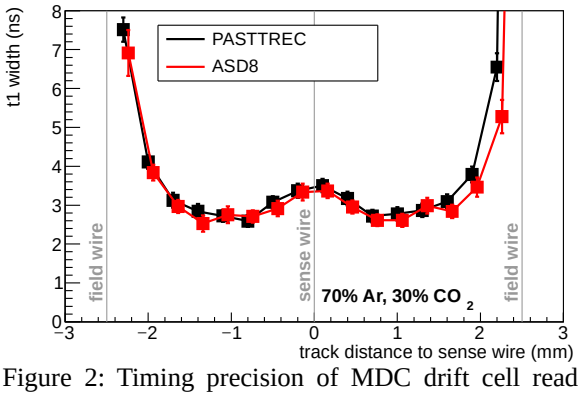

Figure 2: Timing precision of MDC drift cell read out with ASD8 and PASTTREC ASIC as a function of track position within the cell. Shown is the sigma of a gaussian fit of the coincidence time spectrum.

The resulting time precision is illustrated in figure 2. Within the error bars, PASTTREC (when walk correction is applied to the data) can achieve a similar, though slightly worse, timing precision as ASD8, i.e. ~3 ns in the inner regions of the cell. These results improve upon earlier measurements at the GSI Detector Lab via tracking of cosmic muons, because access to higher statistics allowed for finding better ASIC settings.

Concerning energy loss measurement precision, both ASICs were tested with a ^{55}Fe X-ray source irradiating a drift chamber operated at various high voltages. The pulse charge spectrum (figure 3) was derived from the recorded time-over-threshold spectrum by applying a calibration function which was recorded by means of a programmable pulse generator. In contrast to ASD8, PASTTREC was able to separate the main X-ray peak from the argon escape peak at and even below the HV working point.

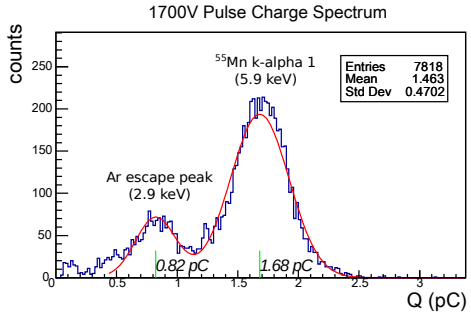

Figure 3: Calibrated charge spectrum (derived from TOT distribution) of MDC irradiated with a ^{55}Fe X-ray source and recorded with PASTTREC.

References

[1] G. Korcyl et al., "Readout electronics and data acquisition for gaseous tracking detectors," in IEEE Transactions on Nuclear Science, vol. PP, no. 99, pp. 1-1. doi: 10.1109/TNS.2017.2786464

[2] J. Pietraszko et al., doi:10.15120/GR-2015-1-MU-NQM-HADES-28

Experiment beamline: HADES
Experiment collaboration: HADES
Experiment proposal: S477
Accelerator infrastructure: SIS18
PSP codes: 1.1.2
Grants: GSI strategic partnerships (FuE), HIC for FAIR, BMBF(05P15RFFCA)
Strategic university co-operation with: Frankfurt-M

The PaDiWa-AMPS2 TDC and QDC front-end electronics for the HADES Electromagnetic Calorimeter

A. Rost[1], I. Fröhlich[2], T. Galatyuk[1,3], H. Kayan[3], J. Michel[2], A. Prozorov[4], M. Traxler[3] for the HADES collaboration

[1]TU Darmstadt, Darmstadt, Germany; [2]Goethe Universität, Frankfurt am Main, Germany; [3]GSI, Darmstadt, Germany; [4]Nuclear Physics Institute of ASCR, Rez, Czech Republic

The second generation of the 8 channel PaDiWa-AMPS front-end board was assembled at GSI department for Experiment Electronics (GSI EE). The board implements precise TDC and QDC measurements optimized to read out the 978 PMTs of the HADES-electromagnetic calorimeter (ECAL) [1]. The measurement principle [2] is to integrate the signals and to encode the results in the width of the digital output pulses. High precision is achieved by implementing a modified Wilkinson-ADC method, so actively discharging the integrated signal results in a fast crossing of the threshold. The lengths of the digital pulses are measured by the well-established TRB3 (General Purpose Trigger and Readout Board - version 3) platform [3].

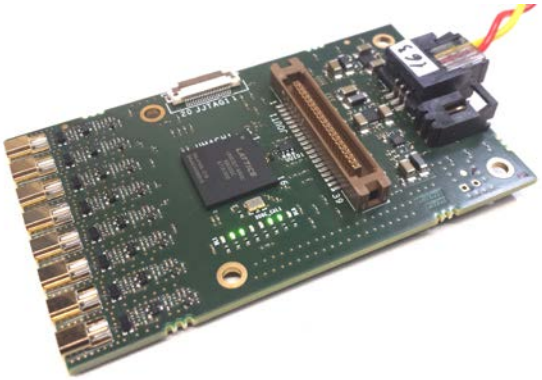

Figure 1: Photography of the PaDiWa-AMPS2 front-end board.

The circuitry of the front-end board is based on the Come&Kiss1 principle, where analogue electronics is used only for the amplification stage and integration, while other tasks, e.g. discrimination, threshold settings, delay generation for discharging and the LVDS drivers are implemented in a field-programmable gate array (FPGA). The second version of the PaDiWa-AMPS2 front-end board is shown in Fig. 1.

Because of the new layout in combination with a smaller package size, the routing of the signal lines have been optimized for better timing precision and reduced crosstalk. The concept of using a transformer in the input stage in order to galvanically isolate the ground was carefully tested. In laboratory measurements it has been shown that the transformer improved the signal to noise ratio. The charge measurement precision (resolution of the system defined as sigma/mean of the charge distribution) as a function of the measured charge has been determined with a pulse-generator. The results are shown in Fig. 2. A time precision of 20 ps and a relative charge precision below 0.5% (for ECAL PMT pulses >1 V) was reached.

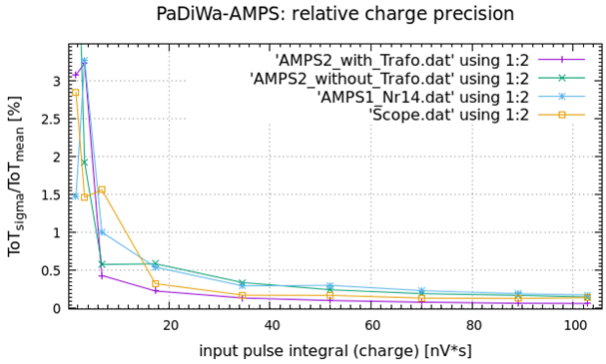

Figure 2: Relative charge precision of the PaDiWa-AMPS2 board compared to PadiWa-AMPS1 and a Oscilloscope reference measurement.

The HADES ECAL detector is currently under construction. The mass production of 150 PaDiWa-AMPS2 front-end boards was done by the GSI EE. The read-out electronics will be installed by end of spring 2018 and fully commissioned with cosmic muons and LED signals. A production beam time with the HADES spectrometer is planned in August 2018. Four sectors of the ECAL will be in place for the 2018 beam time to enable the photon measurement.

References

[1] W. Czyzycki et al., Electromagnetic Calorimeter for HADES, [1109.5550]

[2] A. Rost et al., 2017, “A flexible FPGA based QDC and TDC for the HADES and the CBM calorimeters”, JINST 12 C02047

[3] M. Traxler et al., “A Precise Multi-Channel QDC FEE utilizing FPGAs as Discriminators and Delay Elements Based on the TRB3 as TDC and Readout Platform”, GSI Scientific Report 2013

Experiment beamline: HADES
Experiment collaboration: HADES
Experiment proposal: none
Accelerator infrastructure: SIS18
PSP codes: none
Grants: Work supported by the DFG through GRK 2128 and VH-NG-823.
Strategic university co-operation with: Darmstadt

1 use commercial elements & keep it small and simple

 DOI:10.15120/GR-2018-1

Application of micron-size plasma for investigations of HADES Mini Drift Chamber (MDC) cells with an unique laser driven test facility

X. Fan[1], L. Naumann[1], M. Siebold[1], D. Stach[1], C. Wendisch[2], M. Wiebusch[3]

[1] HZDR, Dresden, [2] GSI, Darmstadt, [3] Goethe Universität, Frankfurt, Germany

To investigate the electron drift and amplification in gaseous detectors a high precision laser driven detector test facility has been developed at the Helmholtz-Zentrum Dresden-Rossendorf, using a pulsed UV laser beam with 257 nm wavelength, 10^{-2} to 10^{5} Hz frequency and 10^{11} to 10^{13} W/cm^2 energy density [1]. A multi-photon ionization process generates electrons and ions in micron-size beam envelope within radii of $r_{x,y} = 10$ µm and Debye length $l_z = \pm 100$ µm. An adaptable drift chamber detector (s. fig.1) has been designed to create the real electric field topology of each of all six different Mini Drift Detector cells of the MDC II plane of the HADES spectrometer [2]. Due to the anode wire alignment of ±40°, ±20° and ±0° (with respect to the cathode wires in adjacent wire layer), in each different drift cell type a different anomalous radial electrical field distribution is formed. With an increased precision in knowledge of the local field topology, we assume to increase the track reconstruction quality of the HADES spectrometer, and for the future, improve in optimizing cell geometries. The laser beam is focused into the detector with a well-defined 3D position, start time and number of primary electrons.

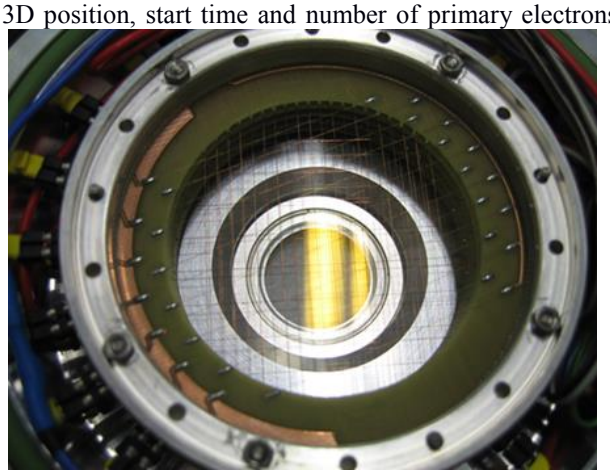

Figure 1: Drift chamber inside the opened gas tight box.

The start time signal, taken from the laser pulse has a resolution of 2 ps (FWHM). This signal triggers the data acquisition (DAQ) of five readout channels, on which read-out electronics with ASD-8 and PASTTREC [3] ASICs have been tested. 2D and 3D drift velocity distributions have been measured for different counting gas mixtures of Ar/CO_2. Figure 2 shows the nearly perfect radial symmetry in the +0° cell with exception of the four corners, which are defined by the shortest distance between field wires and cathode layers. Electrons generated in the corners were delayed there due to the gas properties and low electrical field strength. The Electron drift-velocity is constant over a wide range of more than 70% of the drift cell (see fit in fig.3) and amounts to (62±0.3) µm/ns.

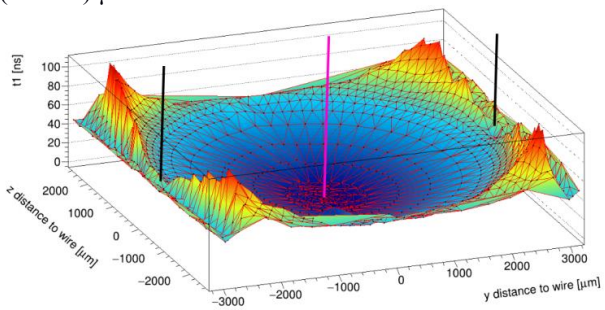

Figure 2: Mean drift time (t1) as function of the laser ionization point inside a drift cell, (1290 data points, each contains 8000 events) measured on an area orthogonal to the (+0°) anode wire (pink), between two field wires (black) and two cathode layers at z = ±2500 µm.

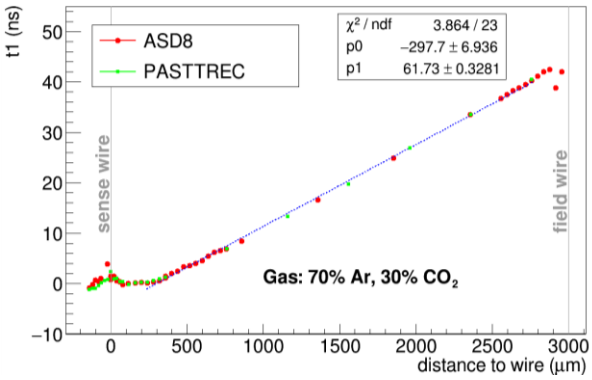

Figure 3: Measured mean drift time (t1) as a function of the distance perpendicular to sense wire, obtained for both amplifier ASICs at z=0, $U_{field} = U_{cathode} = -1.7$ kV.

Close to the anode wire the Debye length of the plasma disturbs the measurement. The drift time distribution has a standard deviation of 0.5 to 1.0 ns, this allows in case of a laser induced point source to deduce the spatial resolution of 30 to 60 µm for the HADES-MDC II with the used ASICs.

References

[1] L. Naumann et al., JINST 9 (2014) C10009
[2] G. Agakishiev et al.,Eur.Phys.J. A 41(2009) 243
[3] G. Korcyl et al., IEEE TNS, V. PP,N. 99 (2017)

Experiment beamline: HADES
Experiment collaboration: HADES
Experiment proposal: S477
PSP codes: 1.1.2.
Grants: HGS-HIRe**,** GSI strategic partnerships (FuE), HIC for FAIR, BMBF(05P15RFFCA)
Strategic university co-operation with: Frankfurt-M

Machine learning for weak decay recognition in heavy-ion collisions

S. Spies[1] and M. Lorenz[1] for the HADES collaboration

[1]Goethe-University, Frankfurt

The production of quark flavor is one of the most important observables in heavy-ion collisions. At SIS 18 energies this corresponds mainly to the production of strangeness. In contrast to hadron production in elementary N+N collisions, in heavy-ion reactions additional multi-step processes do occur and the production of e.g. strange hadrons below their free N+N threshold is possible by accumulation of energy. Therefore, the investigation of sub-threshold strangeness production is one of the most promising probes, as it contains newly produced quarks, it is sensitive to the amount of energy provided from the created system [1].

The recent experimental observations challenge the understanding of sub-threshold strangeness production: The first simultaneous measurement of K^- and Φ mesons in central heavy-ion collisions below a kinetic beam energy of 10A GeV by HADES revealed that the Φ/ K^- multiplicity ratio is found to be surprisingly high with a value of 0.52±0.16. Consequently, the different slopes of the K^+ and K^- transverse-mass spectra can be explained solely by feed-down, which substantially softens the spectra of K^- mesons. Hence, the different slopes do not imply diverging freeze-out temperatures of these two mesons caused by unequal coupling to baryons, as suggested commonly [2].

Yet, any detailed understanding of strangeness production and propagation in heavy-ion reactions requires information on all production channels of all particles with open or hidden strangeness. Therefore, the analysis is extended to further particles carrying strangeness such as K^0 mesons and Λ hyperons. They decay via the weak interaction and can be reconstructed through their decay products. Data on these hadrons in central Au+Au collisions at kinetic beam energies below 2A GeV have never been published before. Due to their decay via the weak interaction, these particles have a characteristic decay topology, which can be used to suppress combinatorial background. As most of the particles produced in heavy-ion collisions result from strong processes and are hence emitted from the interaction point of the two colliding ions, the latter one can be reconstructed from the intersection point of all reconstructed charged particle trajectories in the detector. Due to the weak decay, a fraction of e.g. Λ hyperons decay a few centimeter away from their creation point (cτ=7.89 cm). Hence, one can search for trajectories which meet in space (secondary vertex) separated by a given distance from the reaction vertex. Applying such selection criteria the combinatorial background of random pion proton combinations is more strongly suppressed than the signal of truly correlated pion-proton pairs. The drawback of this method is the low efficiency, usually of a few per mill.

Machine learning methods e.g. based on artificial neural networks are a very promising tool to overcome this shortcoming. Such algorithms can be trained to recognize specific correlations, resulting in higher reconstruction efficiencies compared to a series of hard cuts. We applied the methodology of machine learning for the recognition of weak decay topologies for the first time for heavy-ion collision data within HADES. For the training of such algorithms high statistic signal and background samples are needed. For the signal sample, we use a simulation, while the background sample is generated by combining tracks from different events, which are by definition uncorrelated.

Analysis results

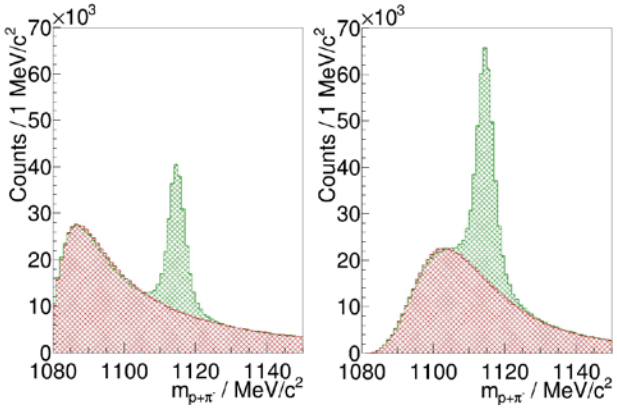

Figure 1: Λ mass spectrum from data with hard cuts from [3] (left) and using a neural network (right), signal is shown green and combinatorial background red.

Figure 1 shows a comparison between the resulting invariant mass spectra using only the hard topology cuts from [3] and with the use of a neural network. The analysis based on the neural network provides a gain of about 200% in the amount of reconstructed Λ hyperons, when optimized for significance of the signal.

References

[1] S. Weissenborn, D. Chatterjee and J. Schaffner-Bielich, Nucl. Phys. A 881 (2012) 62.

[2] J. Adamczewski-Musch et al. [HADES Collaboration], Physics Letters B 778 (2018) 403-407.

[3] T. Scheib, Λ and K^0_s Production in Au+Au Collisions at 1.23A GeV, Ph.D. thesis U. Frankfurt, 2017

Experiment beamline: HADES
Experiment collaboration: HADES
Experiment proposal: none
Accelerator infrastructure: UNILAC / SIS18
Grants:
Strategic university co-operation with: Frankfurt-M

 DOI:10.15120/GR-2018-1

Strange meson production in pion-nucleus collisions at 1.7 GeV/c

J. Wirth[1,2], L. Fabbietti[1,2], A. Scordo[3] and the HADES collaboration

[1]Excellence Cluster Universe, Technische Universität München, Garching, Germany; [2]Physik Department, Technische Universität München, Garching, Germany; [3]INFN Laboratori Nazionali di Frascati, Frascati, Italy

The production of strange mesons in pion-nucleus reactions allows for a quantitative study of in-medium effects such as re-scattering and absorption processes at a well-defined density (ρ_0). In 2014 the versatile HADES setup at the GSI pion beam facility [1] provided a worldwide unique opportunity to study open and hidden strange mesons (K^+, K^- and ϕ) in cold nuclear matter generated in pion-nucleus reactions ($\pi^- + A,\ A = C,\ W$) at an incident pion beam momentum of 1.7 GeV/c.

In the case of the kaons (K^+, K^0) several hints for the existence of a moderately repulsive KN potential for the kaons (K^+, K^0) exist [2]. On the contrary, the antikaons (K^-) are expected to propagate in an attractive potential with a considerable imaginary part. Antikaons can be absorbed in nuclear matter via strangeness exchange processes on one ($K^-N \rightarrow Y\pi$) or more nucleons ($K^-NN \rightarrow YN$). Furthermore, the study of the ϕ meson production and absorption ($\phi \rightarrow K^+K^-, BR = 48.9 \pm 0.5\%$ [3]) of light (C) and heavy (W) nuclei is essential. Since, the absorption of the ϕ meson in cold nuclear matter has been interpreted as a proof of the widening of the ϕ natural width [4]. Besides, ϕ decays may substantially affect the observed K^- abundance. In subthreshold 1.23 AGeV $Au + Au$ collisions a surprisingly high ϕ/K^- ratio with a value of 0.52 ± 0.16 was obtained [5]. Also in elementary $p + p$ close to threshold the ϕ meson is a sizeable source for the K^- production [6].

Both charged kaons are identified by means of the time-of-flight (Target T0 Detector/RPC/TOF) and momentum measurements with the drift chambers (MDCs) combined with the toroidal magnet field. To enhance the signal to background ratio, both kaons are pre-selected by their specific energy loss in the MDCs.

Figure 1 shows the mass distribution of the K^- in the polar angle and momentum interval of $15.0 \leq \theta[°] < 27.5$ and $430 \leq p\ [MeV/c] < 500$ in the RPC detector. The neutral ϕ meson is reconstructed in terms of the invariant mass of K^+K^- pairs as shown in Fig. 2 in the polar angle and momentum interval of $15.0 \leq \theta[°] < 27.5$ and $500 \leq p\ [MeV/c] < 1250$.

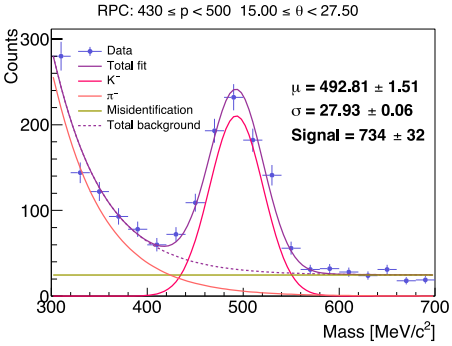

Figure 1: Reconstructed K^- mass spectrum in a specific $p - \theta$ region (see legend) for the RPC in $\pi^- + C$ collsions. The K^- signal is represented by a Gaussian (magenta line). The background is composed of an exponential function for the pions (pink line) and a polynomial (green line).

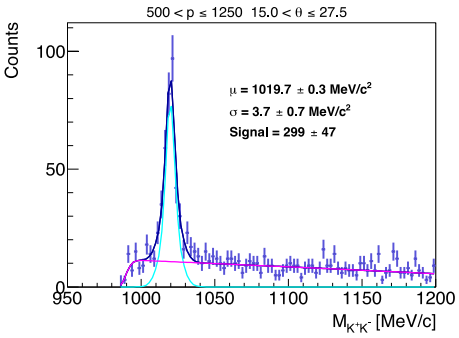

Figure 2: Invariant mass distribution of K^+K^- pairs in a specific $p - \theta$ region (see legend) in $\pi^- + C$ collsions.

References

[1] J. Adamczewski-Musch et al. [HADES Collaboration], Eur. Phys. J. A 53 (2017) 188
[2] G. Agakishiev et al. [HADES Collaboration], Phys. Rev. C 90 (2014) 054906
[3] C. Patrignani et al. [Particle Data Group Collaboration], Chin. Phys. C 40 (2016) 100001
[4] D. Cabrera et al., Nucl. Phys. A 733 (2004) 130
[5] J. Adamczewski-Musch et al. [HADES Collaboration], Phys. Lett. B 778 (2018) 403
[6] Q. J. Ye et al. [ANKE Collaboration], Phys. Rev. C 85 (2012) 035211

Experiment beamline: HADES@SIS18
Experiment collaboration: HADES
Experiment proposal: S333
Grants: SFB Sonderforschungsbereich 1258 “Neutrinos und Dunkle Materie in der Astro- und Teilchenphysik (NDM)“, GSI F&E TMLFRG1316 CBM-RICH
Strategic university co-operation with: none

A non-binomial model for efficiency corrections to particle number cumulants

R. Holzmann[1], and the HADES collaboration

[1]GSI, Darmstadt, Germany

Fluctuations of conserved quantities (e.g. baryon number, strangeness, charge) are considered among the most promising probes of the QCD phase diagram [1]. Fluctuations are usually quantified in terms of the cumulants of the observed particle distributions and detector efficiency corrections are applied in order to obtain the true cumulants. This is generally done [2] assuming the efficiency to be of binomial type, i.e. assuming that the detection processes of multiple particles in any given event are independent.

In the binomial model, the probability of detecting p out of M emitted particles in an event can be written:

$$P_p^M = C_M^p \epsilon^p (1-\epsilon)^{M-p} . \quad (1)$$

By expanding the $(1-\epsilon)^{M-p}$ term in Eq. (1) and averaging P_p^M over all events one finds a relationship between the average probability to observe p particles and the so-called factorial moments $\langle F_n \rangle$ of the true particle distribution:

$$P_p = \sum_{m=p}^{\infty} (-1)^{m-p} \frac{\langle F_m \rangle}{m!} C_m^p \epsilon^m . \quad (2)$$

Using Eq. (2) one retrieves the well-known relation between measured and true factorial moments [3]:

$$\langle f_n \rangle = \epsilon^n \langle F_n \rangle . \quad (3)$$

Real-life detectors are commonly designed with a finite occupancy: they can register only a limited number of particles per given event and consequently their detection efficiency decreases with increasing particle number. This effect can be studied in simulations and for HADES the efficiency drop was found to be of order 10% - 15%.

We therefore propose a new, fully analytical, non-binomial model which naturally incorporates efficiency losses resulting from an increasing particle number. Our model strictly applies to detectors segmented into a finite number N of modules of given solid angle Ω such that the total solid angle covered (or total efficiency) is $\varepsilon = N\Omega$. Any given module can fire when hit by a particle, but only once, i.e. multiple hits of a module are not distinguishable from single hits. Following [3, 4], the detection probability in Eq. (1) transforms into:

$$P_{Np}^M = C_N^p \sum_{l=0}^{p} (-1)^{p-l} C_p^l \left[1 - \frac{(N-l)}{N}\epsilon\right]^M , \quad (4)$$

and the factorial moments relation of Eq. (3) into:

$$\langle f_n \rangle = \sum_{m=n}^{N} \langle F_m \rangle \frac{(-1)^m}{m!} \frac{\epsilon^m}{N^m} \sum_{k=n}^{m} C_N^k k(k-1)\cdots \cdots (k-n+1) \sum_{l=0}^{k} (-1)^k C_k^l (N-l)^m . \quad (5)$$

Figure 1 below illustrates the influence of the detector segmentation on the drop of efficiency with multiplicity.

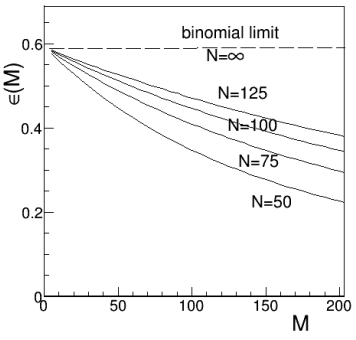

Figure 1: Non-binomial efficiencies as function of the particle multiplicity M for ε = 0.59 and N = 50 – 125.

For a "continuous" detector like HADES a strict hardware segmentation into N distinct modules is not realized, but an effective segmentation $\tilde{N}$ can still be introduced, with $\tilde{N}$ and ε adjusted to describe the observed (or simulated) efficiency behavior $\epsilon = \epsilon(M)$.

References

[1] M. Asakawa and M. Kitazawa, Prog. Part. Nucl. Phys. 90 (2016) 299.
[2] A. Bzdak and V. Koch, Phys. Rev. C 91, (2015) 027901.
[3] S.Y. Van der Werf, Nucl. Inst. Meth. 153 (1978) 221.
[4] G. Bellia et al., Nucl. Inst. Meth. 226 (1984) 424.

Experiment beamline: HADES
Experiment collaboration: HADES
Experiment proposals: S407, S447
Accelerator infrastructure: SIS18
PSP codes: 1.1.2
Grants: none
Strategic university co-operation with: none

 DOI:10.15120/GR-2018-1

π^0 and η production in π^-+PE collisions at 690 MeV/c beam momentum

J. Otto[1] for the HADES collaboration

[1]Justus-Liebig Universität, Gießen, Germany

In this work we present the analysis of neutral mesons (π^0 and η) in π^- + *polyethylene (PE, [-CH_2-CH_2-]$_n$)* data at a beam momentum of *p = 690 MeV/c* taken by HADES in summer 2014. As HADES does not employ an electromagnetic calorimeter, detection is performed via conversion of decay photons *(π^0 / η → γγ / γγ*→ $e^+e^+e^-e^-$).*

First, lepton identification is performed with rather soft cuts on the particle sample: To do so we require the momentum to be smaller than *1 GeV/c*, an energy loss in the MDCs of less than *12 MeV*, a reconstructed mass *m < 100 MeV/c^2* and *0.8 < β < 1.2*. Since di-leptons originating from conversion are characterized by small opening angles, we allow for hit sharing in the inner MDCs. Accordingly we cut on opening angles smaller than 10° when reconstructing unlike-sign lepton-pairs to reduce combinatorial background. Simulation shows that π^0 (η) mesons produced at our energies mainly decay into 2γ with opening angles *15° < θ_{lab} < 45°* (*115° < θ_{lab} < 145)*. After the formation of lepton-quadruplets from our pair sample we cut on the specified ranges of opening angles between two photon candidates. Clear signals of π^0 and η production with background contribution at the percent level are observed. Figure 1 shows the reconstructed invariant mass spectrum after all cuts. 632 entries in the π^0 mass range and 93 entries in the η mass range are counted.

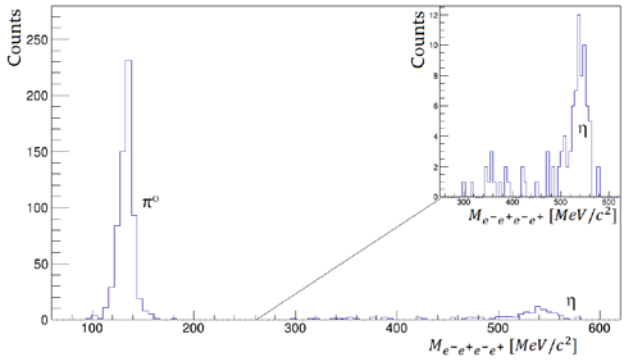

Figure 1: Reconstructed invariant mass spectrum of two detected di-lepton pairs after cuts.

In order to extract π^0 and η cross sections, raw data have to be corrected for detector inefficiency, geometrical acceptance and be properly normalized. We performed an efficiency correction in p_t-y bins based on PLUTO simulations of the $\pi^-p \rightarrow \pi^0/\eta + n$ reactions and subsequent decay as $\pi^0/\eta \rightarrow \gamma\gamma/\gamma\gamma^*$.

We derived integrated efficiencies of

$$\epsilon_{\pi^0} = (4.80 \pm 0.22) \cdot 10^{-6}$$

$$\epsilon_{\eta} = (2.60 \pm 0.05) \cdot 10^{-5}$$

These values include the conversion probability in the target region of HADES, geometrical acceptance and reconstruction efficiency with all cuts applied. Errors shown are statistical only.

Normalizing on elastic scattering [1,2] we can derive cross sections for π^0 and η production in π^- + *PE*

$$\sigma_{\pi^0} = \frac{\sigma_{el}}{N_{ev}^{el}} \cdot \frac{N_{\pi^0}}{\epsilon_{\pi^0} \cdot N_{ev}^{\pi^0}} = (12.68 \pm 1.08)\, mb$$

$$\sigma_{\eta} = \frac{\sigma_{el}}{N_{ev}^{el}} \cdot \frac{N_{\eta}}{\epsilon_{\eta} \cdot N_{ev}^{\eta}} = (0.836 \pm 0.105)\, mb$$

using $\frac{\sigma_{el}}{N_{ev}^{el}} = 0.88 \cdot 10^{-7} mb$ [1,2]

HADES has also measured the reaction π^- + *C*. Analysing this data accordingly we are able to subtract the carbon fraction in our data and derive a cross section for π^0 production in π^- +*p* (for the η, statistics is too small):

$$\sigma_{\pi^0}^{\pi^-+p} = \frac{\sigma_{el}}{N_{ev}^{el}} \cdot < \pi^0 >_p = (14.39 \pm 2.73)\, mb$$

with $< \pi^0 > = \frac{N_{\pi^0}}{\epsilon_{\pi^0} \cdot N_{ev}^{\pi^0}}$

and $< \pi^0 >_{PE} = < \pi^0 >_p + \frac{2}{3} < \pi^0 >_C$ [1,2]

In literature we find values for the π^0 and η production in π^- +*p* collisions at *690 MeV/c* beam momentum listed as:

$$\sigma_{\pi^0}^{\pi^-+p} = 16.5\, mb \text{ [3]}$$

$$\sigma_{\eta}^{\pi^-+p} = 0.5\, mb \text{ [4]}$$

Our result for the π^0 cross section in π^- +*p* is in agreement with literature. For the η we can not compare directly as our cross section is related to π^- +*PE*. Besides the statistical errors shown, our analysis has systematic errors which are being estimated. Those mainly originate from missing production processes in our simulation with three particles in the final state leading to significant differences in the momentum distribution in experiment and simulation, and therefore influence our efficiency.

References

[1] F. Scozzi [HADES collab.], EPJ Web Conf. 137 (2017) 05023

[2] W. Przygoda [HADES collab.], EPJ Web Conf. 130 (2016) 01021

[3] Landolt-Börnstein Database, values received from P. Salabura.

[4] D. Rönchen et al., Coupled-channel dynamics in the reactions πN → πN, ηN, KΛ, KΣ, EPJA49(2013)44.

Experiment beamline: HADES
Experiment collaboration: HADES
Accelerator infrastructure: SIS18
Grants: GSI strategic partnership
Strategic university co-operation with: Gießen

Exclusive Λ analysis to study hyperon scattering in medium

S. Maurus[1], L. Fabbietti[1], for the HADES collaboration

[1]Excellence Cluster Universe, Technische Universität München, Boltzmannstr. 2, D-85748, Garching, Germany

Since several years the study of the Λ, the lightest hyperon, is of special interest in several topics, like the equation of state. In vacuum, the elastic interaction between the proton and the Λ-p already has been measured in scattering experiments, constraining theoretical models. [1].

Still, the in-medium properties of the Λ-p system lacks any data point from the experimental side.

In July 2014 a dedicated secondary pion beam campaign was performed with the HADES detector setup impinging on a tungsten (W) and carbon (C) target with an incident beam-momentum of 1.7 GeV/c. As pion reactions are happening close to the surface [2], also the lambdas are created here, traversing the whole nucleus and therefore they form an ideal system to study the lambda in-medium properties.

Our approach is to use the exclusive channel $\pi^- + p \rightarrow K^0 + \Lambda$ where the Λ eventually can interact elastically with its surrounding ($\Lambda + \mathrm{p} \rightarrow \Lambda + \mathrm{p}$). This may provide information on lambda proton scattering and shed light on the in medium properties of the lightest hyperon.

This channel is isolated by searching for a matching charge pattern ($K^0 \rightarrow \pi^+ + \pi^-, \Lambda \rightarrow \mathrm{p} + \pi^-, p$) with 3 positive and 2 negative charged particle candidates.

Further, the particle identification of these particle candidates is based on their characteristic energyloss in the MDCs and their velocity β, measured in the time of flight sub-detector system in combination with the momentum.

In addition, a mass cut further reduces the chance of a wrong identification of these candidates, reducing the background.

Caused by the multiple appearance of particles (p, π^-) in the final state, an event hypothesis is necessary, to assign these particles to their correct mother (K^0, Λ). The best combination is found when both invariant masses (p, π^-) and (π^+, π^-) are best matching to their nominal value (Λ, K^0). The invariant mass of (π^+, π^-) vs. (p, π^-) for the best combination is illustrated in Fig. 1, subtracted by their PDG mass.

To be sensitive to the in-medium behaviour of the Λ an angle difference is extracted, which is constructed as follows:

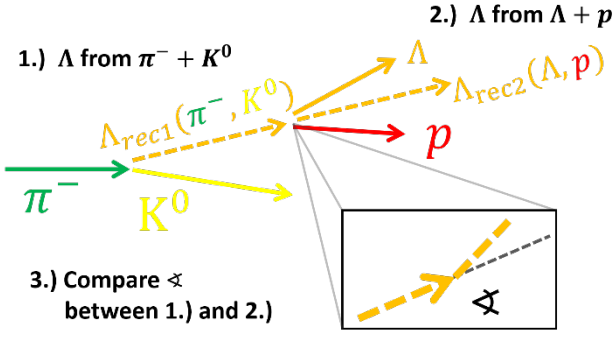

Fig.2 Construction of the observable.

Based on the incident π^- beam in combination with the measured K^0, the Λ momentum can be inferred (Λ_{rec1}) right after its creation. Now this Λ is reconstructed from the measured Λ in the detector in combination with the measured proton. If we assume a single reaction, the sum of the measured Λ and p gives us the Λ before the reaction (Λ_{rec2}). Now the angle between (Λ_{rec1}) (Λ_{rec2}) is evaluated, as sketched in Fig. 2. In theory they should be perfectly aligned. As both protons have an unknown start momentum, arising from the fermi-momentum and we are facing limited resolution, this distribution will be shifted and smeared. Nevertheless, these effects are included in the simulation framework.

The next step in this analysis will include the creation of templates for all different production channels and scenarios which can happen inside the nucleus.

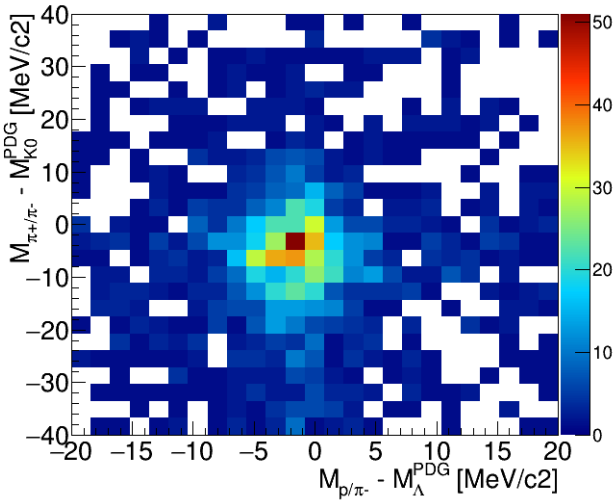

Fig.1 Invariant mass of (π^+, π^-) vs inv. mass of (p, π^-), subtracted by the nominal mass of K^0 and Λ, respectivley. Only the best combination is shown. Details see text.

References

[1] J. Haidenbauer et al., Nucl. Phys. A 915 (2013)24
[2] Benabderrahmane et al. Phys. Rev. Lett. 102, 182501 (2009)

Experiment beamline: HADES
Experiment collaboration: HADES
Experiment proposal: S333
Grants: BMBF HADES: "Verbundprojekt 05P2015", GSI F&E TMLFRG1316 CBM-RICH

 DOI:10.15120/GR-2018-1

Fit to transverse momentum spectra of dileptons measured by HADES

S. Harabasz[1] for the HADES collaboration

[1]Technische Universität Darmstadt, Germany

Virtual photons are penetrating probes emitted throughout the whole evolution of the fireball formed in collisions of heavy ions and therefore they are well suited for studying the properties of strongly interacting matter at extreme conditions.

The analysis of Au+Au collisions at $\sqrt{s_{\mathrm{NN}}} = 2.42$ GeV measured by HADES showed [1] that the invariant mass distribution of dileptons has a Boltzmann shape, which leads to the conjecture, that the temperature of the emitting source, at least the one averaged over the evolution of the system, can be read out from the inverse slope of the mass spectrum.

To do this in a proper way, it is essential to understand which probability density function of invariant mass corresponds to a thermal phase-space distribution. The derivation quoted e.g. in [2] shows that the correct parametrization is

$$\frac{\mathrm{d}N}{\mathrm{d}M} \propto V\tau \frac{\mathrm{Im}\Pi_{\mathrm{em}}(M;T)}{M^2} 4\pi M^2 T\, K_1\left(\frac{M}{T}\right),$$

where V, τ and T are the volume, lifetime and temperature of the fireball, respectively, $\mathrm{Im}\Pi_{\mathrm{em}}$ is the vector meson spectral function, and K_1 is a modified Bessel function of the second kind. This form is obtained after integrating out rapidity. Moreover, the fit has to be made in the range of invariant masses high enough such that the shape of the spectrum is governed by the Boltzmann distribution (Bessel function) and not by the spectral function, so that the latter one can be treated as approximately proportional to M^2. Therefore, the fraction in the above formula is a constant. While at SPS and RHIC energies the temperature can be extracted from the spectra above 1.2 GeV/c^2, at SIS18, where the expected temperature is about four times lower, the fit starting at 0.3 GeV/c^2 would yield a slope parameter that could be compared on the same footing [3]. In addition, in this mass range the argument of the Bessel function can be treated as large enough to justify its known approximation by $K_1(x) \underset{x\to\infty}{\longrightarrow} \sqrt{\pi/2x}\exp(-x)$, which leads to:

$$\frac{\mathrm{d}N}{\mathrm{d}M} \propto V\tau(2\pi MT)^{3/2}\exp\left(-\frac{M}{T}\right)$$

and one gets the well-known representation (cf. [4]):

$$\frac{\mathrm{d}N}{\mathrm{d}M} \propto M^{3/2}\exp\left(-\frac{M}{T}\right)$$

On the other hand, starting from a Boltzmann distribution, and assuming that the spectral function varies little with transverse momentum, one can arrive, by nearly identical mathematical reasoning, to the parametrization:

$$\frac{1}{p_t}\frac{dN}{dp_t} \propto m_t K_1\left(\frac{m_t}{T}\right) \qquad (1)$$

which is exact and does not require any approximation, especially that $m_t \gg T$ is certainly not fulfilled in the low part of the transverse momentum spectra for low invariant masses.

These arguments can be tested with HADES data. The transverse momentum distributions, together with fits of Eq. (1) are shown in Fig. 1. The rather good description of the spectra is visible, which confirms the assumption of the thermal radiation. Particularly, the approximate exponential fit would not reproduce properly the convexity of the spectra. The slope parameters from the fit are shown as well.

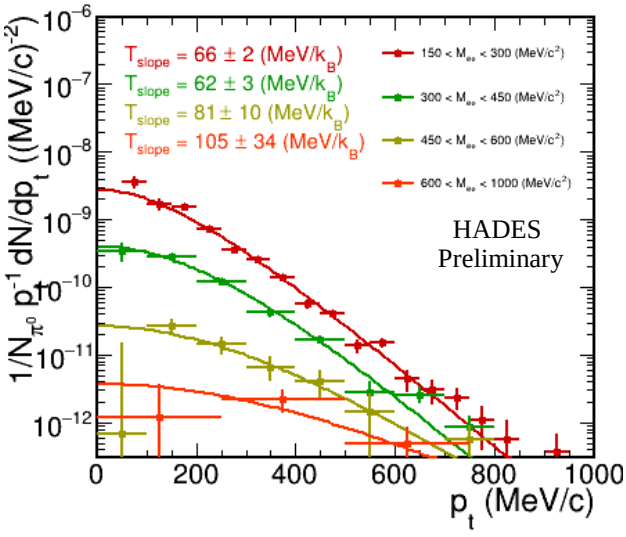

Figure 1. Transverse momentum distributions of dileptons measured by HADES in different invariant mass bins together with fits of Eq. (1).

Another necessary condition is the consistency between the slope parameter extracted from the fit to the invariant mass and the one from the transverse momentum fits, extrapolated to mass zero. This will be tested and discussed in a future publication.

References

[1] P. Sellheim, PhD thesis, Goethe-Universität Frankfurt am Main, 2017, S. Harabasz, PhD thesis, Technische Universität Darmstadt and Jagiellonian University in Cracow, 2017

[2] F. Seck, Master's thesis, Technische Universität Darmstadt, 2015

[3] T. Galatyuk et al., Eur.Phys.J. A52 (2016) 131

[4] H.R. Schmidt and J. Schukraft, J.Phys. G19 (1993) 1705

Experiment beamline: HADES
Experiment collaboration: HADES
Experiment proposal: S407
Accelerator infrastructure: SIS18
PSP codes: none
Grants: VH-NG-823, Helmholtz Alliance HA216/EMMI
Strategic university co-operation with: Darmstadt

Understanding the transverse mass spectra of charged pions measured in Au+Au at 1.23 AGeV collisions with HADES

M. Gumberidze[1] for the HADES collaboration

[1]Technische Universität, Darmstadt, Germany

It is well established that hadron abundances in ultra-relativistic heavy-ion collision can be described with a statistical partition function with fitted temperature T and baryon chemical potential μB. It is interesting to validate if also the spectra of particles at low energies are consistent with thermal production at chemical freeze-out. For such a study Therminator [1] has been used as Monte Carlo event generator. Therminator was previously designed for studying particle production in relativistic heavy-ion collisions performed at different experimental facilities, e.g. SPS, RHIC and LHC.

Therminator assumes that the fireball freezes out at a predefined hypersurface in space-time at given temperature- and bayro-chemical potential. While the program accepts any boost-invariant flow profile, two common flow profiles, the Blast Wave and the Cracow model are already implemented. At this single freeze-out particles abundances are determined by the temperature and baryon chemical potential via the Cooper-Frye formalism.

The parameters used for the Blast Wave model calculations T = 53 MeV, μB = 803 MeV were taken from [2]. This assumes that the collision system investigated by HADES freezes out along the “universal freeze-out line”. This curve can be parameterized by <E>/<N> approximately equal to 1 GeV. A collective expansion velocity (β) on the order of 0.36 has been extracted from the same HADES data sample [3] using blast-wave parameterization.

In Fig. 1 mid-rapidity transverse mass spectra of negative and positive pions for the 5% most central collisions are shown in comparison to a cocktail of various sources of pion production obtained from Therminator. Since Therminator simulates also the decays of resonances, the final spectra contain primordial and secondary contributions (the primordial particles are emitted directly from the fireball, while the secondary particles come from resonance decays). Simulated spectra have been scaled up by a factor of 0.7 and 0.5 for negative and positive pions respectively in order to compare slope of the spectra.
We observe good agreement between the data and the model results for low transverse mass region (mT < 400 MeV/c2). On the other hand, the model results underpredict the data for higher transverse masses. This can be interpreted as contribution from decays of higher lying resonances produced in hot/dense matter [4]. This conjecture is presently being checked with transport models.

References

[1] A.Kisiel, T.Taluc, W.Broniowski and W. Florkowski, Comput. Phys. Commun., 174: 669-687 (2006).
[2] J.Cleymans et.al., Phys. Rev. C73 (2006) 034905
[3] H.Schuldes (HADES Coll.) ”Studying Stramgeness Production with HADES” proceedings SQM2017
[4]. C. Muentz et. al. Z. Phys. A 357(1997) 399

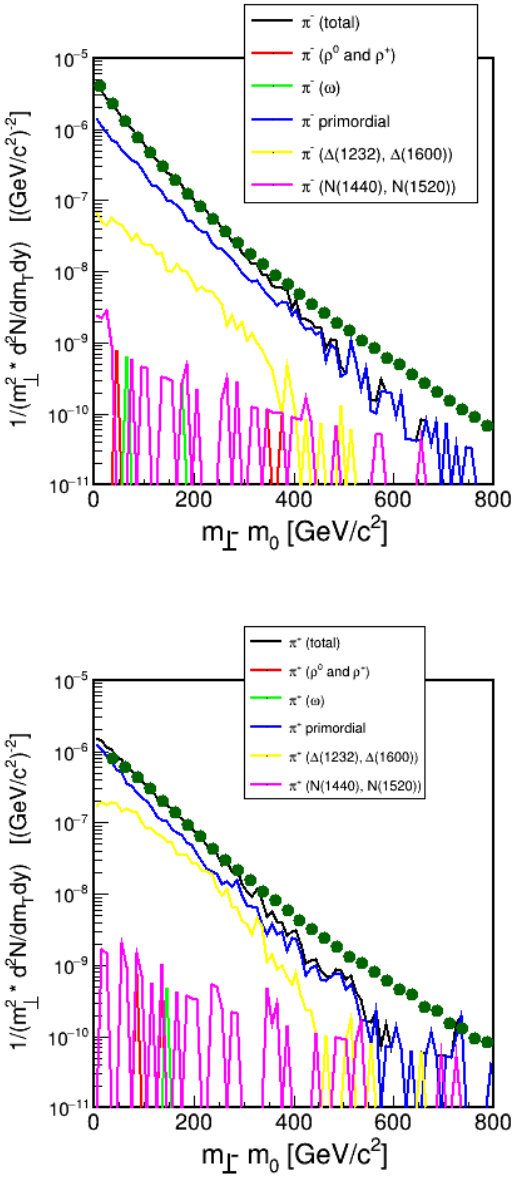

Figure 1. Transverse mass spectrum for negative (upper) and positive pions (lower) compared to the model.

Experiment beamline: HADES
Experiment collaboration: HADES
Experiment proposal: S407
Accelerator infrastructure: UNILAC / SIS18
Grants: VH-NG-823, Helzholtz Alliance HA216/EMMI
Strategic university co-operation with: TU Darmstadt

 DOI:10.15120/GR-2018-1

Protons and light nuclei in Au+Au collisions at 1.23A GeV measured with HADES

M. Szala[1] for the HADES collaboration

[1]Goethe-Universität Frankfurt, Germany

By varying the collision system and the beam energy of heavy ion collisions one can access broad areas of the phase diagram of strongly interacting matter.
We have carried out a detailed moment analysis of proton multiplicity distributions of Au+Au collisions with 1.23A GeV [1]. As the fully conserved quantity investigated here is the baryon number, further investigations will focus on including protons bound in the light nuclei formed in Au+Au collisions to the analysis.
A first estimate of the produced nuclei can be made using the β versus momentum correlation, which is used for particle identification (see Fig. 1). It turns out that the created system is a baryonic dominated system and the ratio between proton and deuteron multiplicity is approximately 0.3. Hence, indeed a significant contribution of protons is indeed bound in deuterons and light nuclei.

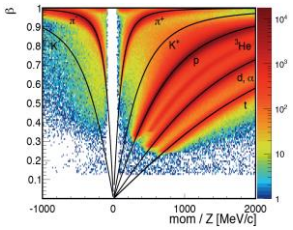

Figure 1: Correlation between measured time-of-flight β and particle momentum. Black lines correspond to the expected values of the different particles.

Furthermore by studying the light nuclei, one can also estimate the degree of thermalization of the system by comparing e.g. transverse rapidity distributions to longitudinal rapidity distributions. Also the mechanism for the production of the nuclei can be examined in detail and confronted with phenomenological models, e.g. formation of coalescence versus thermal production.
In order to calculate the count rate of protons, in this analysis the phase space is divided into cells along the rapidity and transverse mass axis. These cells were chosen to cover an interval of 0.09 < y < 1.59 in 0.1 steps for rapidity and 0-1000 MeV/c^2 in 25 MeV/c^2 steps along m_t-m_0. For every reduced transverse mass bin the mass spectra is plotted and the proton countrate is extracted using a multi-gaussian fit.
The resulting transverse mass spectra extracted for various rapidities are subsequently corrected for detector acceptance and efficiency. The resulting corrected number of counts is divided by m_t^2 in order to easily compare to a thermal distribution and a blast wave.
From these spectra, information about the freeze-out in form of the kinetic freeze-out temperature T_{kin} and characteristics of the radial flow in form of the radial expansion velocity β_r can be derived.

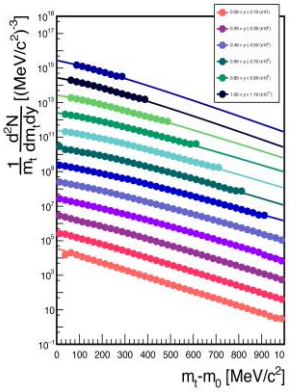

Figure 2: Corrected transverse mass spectra of protons for the 0-40% most central events, scaled by 1/m_t. Each spectrum is multiplied by a power of 10 and fitted using a blast wave function.
To estimate the multiplicities, the spectra have to be extrapolated to full phase space. One approach for extrapolation is by using blast wave functions fitted to the data:

$$\frac{1}{m_t}\frac{d^2N}{dm_t dy} = \int_0^R A m_t K_1\left(\frac{m_t \cosh(\rho)}{T_{kin}}\right) I_0\left(\frac{p_t \sinh(\rho)}{T_{kin}}\right) r dr$$

with A being a constant, $\rho(r) = tanh^{-1}(\beta_r(r))$, K_1 and I_0 are two modified Bessel functions ans the transverse geometric radius of the source is denoted by R.
The transverse velocity field $\beta_r(r))$ can be derived as

$$\beta_r(r) = \beta_s \left[\frac{r}{R}\right]^n \text{, with n = 1.}$$

According to formula a blast wave was fitted to the data (shown in Fig. 2). For this β and T are extracted in a global χ^2 scan over all data points.
Further steps in the analysis will be the centrality dependend analysis and the extension to the analysis of light nuclei in order to reconstruct the complete kinematics of participating baryons.

References

[1] GSI Scientific Report 2016, [10.15120/GR-2017-1] (p. 108)
[2] H. Schuldes, PhD thesis, Frankfurt (2016)

Experiment beamline: HADES
Experiment collaboration: HADES
Experiment proposal: S407
Accelerator infrastructure: SIS18
PSP codes: 1.1.2.
Grants: GSI strategic partnerships (FuE), HIC for FAIR, BMBF(05P15RFFCA)
Strategic university co-operation with: Frankfurt-M

Λ polarization in Au+Au collisions at $\sqrt{s_{NN}} = 2.42$GeV investigated with HADES

F. Kornas[1] for the HADES collaboration

[1]TU Darmstadt, Darmstadt, Germany

Λ hyperons can be used as a probe for possible vortical effects in the early stages of heavy-ion collisions since their weak decays preserve information about their polarization due to parity violation [1,2].

A good candidate to search for such an effect is the Λ hyperon with its decay channel $\Lambda \to p + \pi^-$. The polarization can be described by proton azimuthal angle in the Λ frame ϕ_p^* with respect to the total orbital angular momentum L [3]. Since L is always perpendicular to the reaction plane Ψ_{RP}, the reconstructed event plane Ψ_{EP} can be used as a measure for L, taking into account its resolution R_{EP}:

$$P_\Lambda = \frac{8}{\pi \alpha_\Lambda} \frac{\langle \sin(\Psi_{EP} - \phi_p^*) \rangle}{R_{EP}} \qquad (1)$$

Here $\alpha_\Lambda = 0.642 \pm 0.013$ [4] is the corresponding decay parameter and the brackets denote the average over all Λs and events.

Previous measurements by the STAR collaboration indicate an enhancement of the Λ and $\bar{\Lambda}$ polarization in Au+Au collisions towards lowest collision energy, $\sqrt{s_{NN}} = 7.7$ GeV [5] while there is no polarization found at the highest collision energy, $\sqrt{s_{NN}} = 200$ GeV [3].

At a center-of-mass energy of $\sqrt{s_{NN}} = 2.42$ GeV, seven billion events of Au+Au collisions were recorded with HADES in april 2012. After event selection and track reconstruction, the decay daughters of Λ candiates were selected first using a cut on their mass times charge of $0.3\ GeV/c^2 < m \cdot q/e < 1.3\ GeV/c^2$ for the proton and $-0.3\ GeV/c^2 < m \cdot q/e < 0\ GeV/c^2$ for the pions. All identified protons and pions in one event are combined to Λ candidates. Possible Λ candidates are selected by the parameters of the decay topology: the offset of both daughter tracks to the event vertex, the closest distance of these tracks as a possible decay vertex, the distance of the Λ track to the event vertex and the flight distance of the Λ with a lifetime of $c\tau \sim 8\ cm$. The distributions of these variables from simulated thermal Λs embedded into UrQMD [6] are handed to the TMVA to train a neural network to distinguish between signal and background. The mixed-event method is used to generate the background. This results in one cut parameter, the discriminant which is a weighted sum of all the input parameters. In the current analysis, various cuts are applied to the Λ candidates in order to guarantee a high purity sample after the TMVA is performed.

The discriminant is optimised on the significance which results in $\sim 3 \cdot 10^5 \Lambda$s remaining for $0 - 40\%$ centrality which is enough statistics to perform this analysis. The results of this sample of Λs for 10% centrality classes is shown in Figure 1 for three different mass bins. For the sidebands the $2 - 4\sigma$ range around the fitted Λ peak is taken, while for the Λs the 2σ region around the mean value is used as an input. The signal-to-background ratio in this region is 3.7 for the most peripheral bin and drops down to 1.3 in the most central case. The significance is in the range of $sig \sim 200$.

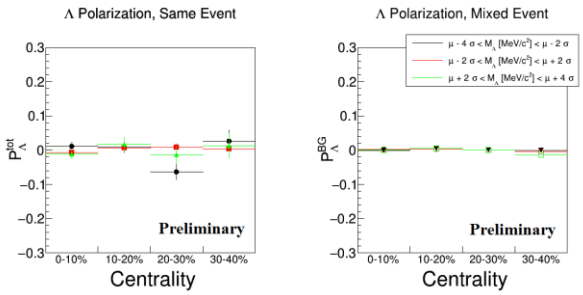

Figure 1: Λ Polarization in Au+Au collisions at $\sqrt{s_{NN}} = 2.42$ GeV in comparison to the sideband of the mass spectrum as a function of the centrality of the collision. In the left panel, the results are shown for the same event while in the right panel the results from the mixed-event are shown.

As a proof of principle the Λs from the mixed-event are not polarized. Yet for the same-event analysis the measured polarization is comparable to zero. For sure, one has to be aware of the effects of a limited detector acceptance. The results shown here are integrated values over rapidity and transverse momentum. The p_t and rapidity dependent analysis will be performed in the near future. Nevertheless, one has to correct for the finite geometrical coverage of the detector. The effects of the limited detector acceptance are discussed in [7] and will be investigated for the case of HADES.

References

[1] Z.-T. Liang and X.-N. Wang, Phys. Rev. Lett. 94, 102301 (2005).
[2] Z.-T. Liang and X.-N. Wang, Phys. Lett B 629, 20 (2005).
[3] B. I. Abelev et. al. (STAR Collaboration), Phys. Rev. C 77, 061902(R) (2008).
[4] Review of Particle Physics, Chin. Phys. C 38, 090001 (2014).
[5] L. Adamczyk et. al. (STAR Collaboration), Nature 548, 62 (2017).
[6] S. A. Bass et. al., Prog. Part. Nucl. Phys. 41 (1998) 255-369.
[7] S. Lan et. al., arXiv:1710.03895 (2017).

Experiment beamline: HADES
Experiment collaboration: HADES
Experiment proposal: S407
Accelerator infrastructure: UNILAC/SIS 18
PSP codes: none
Grants: VH-NG-823, Helmholtz Alliance HA216/EMMI
Strategic university co-operation with: Darmstadt

 DOI:10.15120/GR-2018-1

Dilepton production in pion induced reactions with HADES

F. Scozzi[1,2] for the HADES collaboration

[1]TU Darmstadt, Germany; [2]Institut de Physique Nucleaire Orsay, CNRS-IN2P3, Univ. Paris-Sud, Paris

The HADES experimental program on pion-beam induced reactions was recently started at GSI [1,2]. The π-nucleon reaction is an ideal probe to study baryon resonances. In particular, the dilepton (e^+e^-) production is used to investigate baryon resonance Dalitz decays ($R \to Ne^+e^-$), which provides access to the time-like electromagnetic structure of baryon transitions.

The e^+e^- production was measured in a test experiment using the GSI pion beam at a momentum of 0.685 GeV/c impinging on polyethylene and carbon targets [3]. The standard algorithm to identify leptons (**ring finder**) is based on finding ring patterns induced by the Cherenkov photons in the RICH detector. In addition, a matching between the reconstructed ring centre and a lepton track candidate is required. In case of small number of reconstructed photons per ring the efficiency of the lepton reconstruction can be improved using another method, the so-called **backtracking**. Here, one starts from lepton candidate tracks extrapolated to the RICH and searches for corresponding hits with looser constraints than in the ring finder method. After a careful tuning of the simulated RICH response, a realistic description of the RICH observables and of the efficiencies of the reconstruction algorithms in the simulation could be achieved. This is demonstrated in Fig.1, where the dilepton invariant mass spectra obtained for each algorithm after efficiency corrections are compared. The backtracking algorithm reaches an efficiency about factor 3 three higher, which is important, in particular when considering the low e^+e^- yield in the invariant mass region above π^0.

To allow for a more direct study of the baryonic contributions, events from the π^0 and η Dalitz decays present in the inclusive spectra can be efficiently rejected by applying conditions on invariant mass ($M_{ee} > 140\ MeV/c^2$and missing mass ($M_{miss} > 1040\ MeV/c^2$). In this way, about 1500 events corresponding to free or quasi-free $\pi^- p \to ne^+e^-$ reaction were selected, with a contribution of about 66% of pion carbon events. The comparison to model predictions is on-going, but it is already clear that a significant excess above expected contributions assuming point-like baryon Dalitz decays is present in the dilepton invariant mass distribution. Based on a Partial Wave Analysis (PWA) of the two-pion production measured in an energy scan in the same experiment, this excess can be interpreted as an off-shell ρ contribution, consistent with the Vector Dominance Model (VDM). These studies have a direct impact on the modelling of the emissivity of strongly interacting matter, which is based on VDM [4].

A parametrization of the angular distributions using the spin density formalism was also performed. It allows for the first time to extract important information on the helicity structure of baryon electromagnetic transitions in the time like region [5].

In future, we propose to extend these measurements to the third resonance region ($\sqrt{s} \sim 1.7\ GeV$), with higher statistics, taking advantage of the foreseen improvement of the beam intensity and of the upgraded HADES detector, including in particular the new Electro Magnetic Calorimeter and a new Forward Detector.

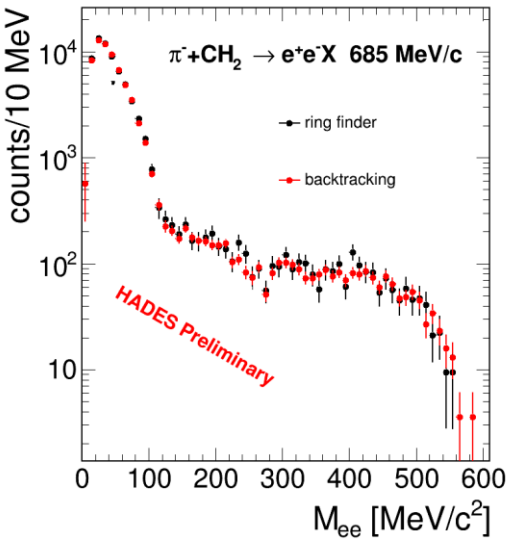

Figure 1: Efficiency corrected yield e^+e^- pairs reconstructed using the ring finder (black dots) and the backtracking algorithm (red dots). The data was taken for a pion beam at a central momentum of 0.685 GeV/c impinging on a polyethylene target.

References

[1] J. Adamczewski-Musch *et al.*, (HADES collaboration) Eur. Phys. J. A53 (2017) 188
[2] J. Diaz *et al.*, Nucl.Instrum.Meth. A478 (2002)
[3] F. Scozzi *et al.*, (HADES collaboration) EPJ Web Conf. 137 (2017) 05023
[4] R. Rapp and J. Wambach, Adv.Nucl.Phys. 25 (2000)
[5] E. Speranza *et al.*, Phys.Lett. B764 (2017)

Experiment beamline: HADES
Experiment collaboration: HADES
Experiment proposal: S333
Accelerator infrastructure: SIS18
PSP codes: 1.1.2
Grants: VH-NG-823 TU Darmstadt and CNRS/IN2P3 IPN Orsay
Strategic university co-operation with: Darmstadt

 DOI:10.15120/GR-2018-1

Characterisation of a cascaded power supply for use with multi-GEM stacks

P. Gasik[1,2], L. Fabbietti[1,2] and the ALICE Collaboration

[1]Physik Department E62, TU München, 85748 Garching, Germany;
[2]Excellence Cluster 'Origin and Structure of the Universe', 85748 Garching, Germany

The ALICE Collaboration will undertake a major upgrade of the detector apparatus in view of the LHC Runs 3 and 4 (2021 to 2029). In particular, new readout chambers will be installed in the TPC, replacing currently used Multi Wire Proportional Chambers with Gas-Electron-Multiplier-(GEM)-based detectors. New chambers employ stacks of four GEM foils, which require a High-Voltage system with eight HV power channels. This can be realised by employing a passive voltage divider (resistor chain), eight independent HV channels (each referring its potential to ground) or a novel system of eight "cascaded" HV channels that sit on top of each other (each referring its potential to the channel below) generating a cascade of high voltages.

In the first scenario, all fields and GEM voltages are defined by the resistor values and cannot be changed easily during the detector operation. Independent HV channels give full flexibility in choosing GEM voltages, however, the potential differences between subsequent channels may increase substantially in case of a spark discharge event or emergency shutdown of all channels caused by a power supply trip. Measurements performed at the Technical University of Munich have shown that the time difference between switching subsequent HV channels off may reach several hundreds of milliseconds. This can easily result in large potential differences across GEMs causing their irreversible damage.

The cascaded PS system was characterised in terms of its reaction on a discharge event and different tripping modes. Measurements were performed with a prototype delivered by ISEG GmbH. All tests were done using a GEM-PCB Simulator [1], an equivalent of a ~0.17 m^2 large quadruple GEM stack of an ALICE Inner Readout Chamber. Measurements included realistic cable lengths and protection resistor values. Differential voltages on the HV channels were monitored with 1:10 and 1:100 scope test probes via decoupling capacitors. Self-made 1:1000 probes were used to monitor absolute voltages on a long-timescale.

A discharge event is induced using a Gas Discharge Tube connected across a capacitor representing a single GEM segment (~5 nF). We do not measure any significant over-voltages across GEM foils and GEM segments other than the sparking one. Small voltage variations observed in the subsequent GEMs are due to the capacitive coupling of the foils and may cause increase of the potential difference across a GEM at a single-volts level.

The time-characteristics of the cascaded power supply is measured for different tripping modes after detection of an overcurrent:

- turn channel off with ramp,
- turn channel off without ramp,
- turn all channels off without ramp.

A relay is used to create a short across a single GEM segment and trigger a trip.

In case of the single-channel reaction, we do not observe any significant voltage increase across non-tripping GEMs. Occasional few-volts increase due to the capacitive coupling of the subsequent foils does not pose a threat to the GEMs. It is worth to mention that in case no software delay is specified between an overcurrent detection and turning the HV channel off, the intrinsic system delay varies between 10 and 20 ms. This means that the voltage across GEM may be reduced immediately after spark detection, before the nominal potential difference is reached (the typical re-charging time of a 100 cm^2 segment, powered via 10 MΩ protection resistor, is ~200 ms).

The most crucial issue is a measurement of the last tripping mode, when all channels are switched off without ramp (emergency shutdown of the PS). By construction, no overvoltage is expected across any of GEMs, as the HV channels of the cascaded PS are stacked in a row as in case of the passive voltage divider. The latter is confirmed in our tests where we measure time delays between switching off subsequent channels. In a series of measurements where the emergency shut down is triggered in different HV channels, we observe that all channels are switched off at the same moment (see Fig. 1) and no overvoltage is created across any of the GEMs in the stack.

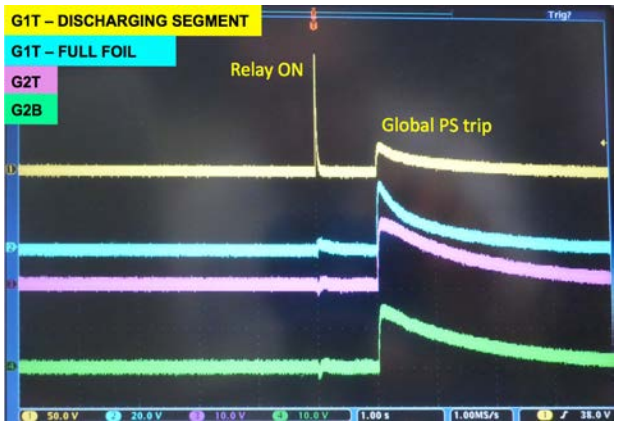

Figure 1: Reaction of the cascaded PS to an overcurrent detected in one of the channels (Relay ON). All channels are switched off at the same moment (within <1 ms). A one-second reaction-delay was set in the PS software.

In summary, the measurements presented in this report assure safe operation of GEM-stacks with the cascaded power supplies that are considered as a baseline PS system for the ALICE TPC upgrade.

References

[1] P. Gasik, "Quadruple GEM-PCB Simulator", GSI Scientific Report 2016, doi:10.15120/GR-2017-1.

Experiment beamline: none
Experiment collaboration: CERN-ALICE
Experiment proposal: none
Accelerator infrastructure: CERN-LHC
PSP codes: none
Grants: Excellenzcluster Universe 'Origin and Structure of the Universe' DFG EClust 153, BMBF ALICE 'Verbundprojekt 05P2015'
Strategic university co-operation with: none

 DOI:10.15120/GR-2018-1

Measurement of J/ψ production as a function of event multiplicity in pp collisions at √s = 13 TeV with ALICE*

S. Weber[1,2], for the ALICE collaboration

[1]GSI, Darmstadt, Germany; [2]TU Darmstadt, Germany

The event multiplicity dependent production of charmonium gives insight into QCD processes and particularly the interplay between the hard and soft mechanisms in particle production. ALICE has performed multiplicity dependent measurements of inclusive J/ψ production at mid and forward rapidity in pp collisions at √s = 7 TeV [1], reaching multiplicities of about 4 times the mean value. The results are consistent with a stronger than linear increase with multiplicity, similar to results for open-charm hadrons and J/ψ originating from beauty-hadron decays ("non-prompt" J/ψ) [2].

A new measurement of J/ψ production as a function of event multiplicity was performed with the ALICE detector [3] in pp collisions at √s = 13 TeV. Using a trigger on high event multiplicities, based on a large deposited charge in the ALICE V0 scintillator arrays at forward and backward rapidity, mid-rapidity multiplicities of about 7 times the mean value in minimum bias collisions were reached. High p_T J/ψ (p_T > 8 GeV/c) were obtained from data triggered by the EMCAL electromagnetic calorimeter. The signal was extracted from the dielectron decay channel in the ALICE central barrel. Particle identification was performed with the TPC detector, for high p_T ,together with the EMCAL PID information.

Figure 1 shows the self-normalized J/ψ yield as a function of charged-particle multiplicity in four p_T bins. A stronger increase for higher p_T is observed, in qualitative agreement with predictions from the PYTHIA8 model [4]. Within this model, the increase of J/ψ production can be understood from production in multi-parton interactions (MPI).

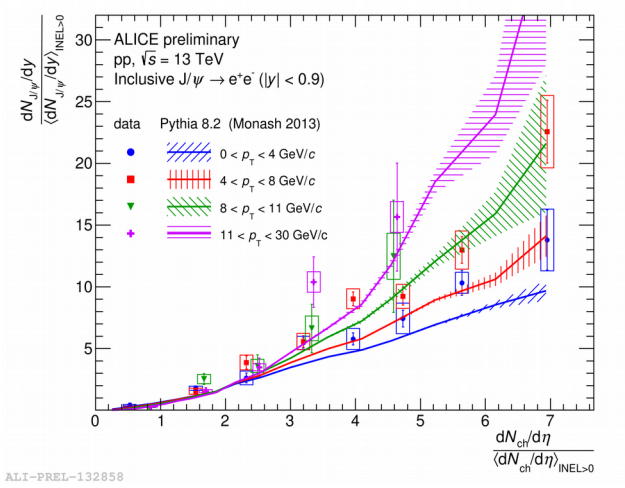

Figure 1: Multiplicity dependence of inclusive J/ψ production at mid-rapidity at √s = 13 TeV in four transverse momentum bins, comparison to PYTHIA8.

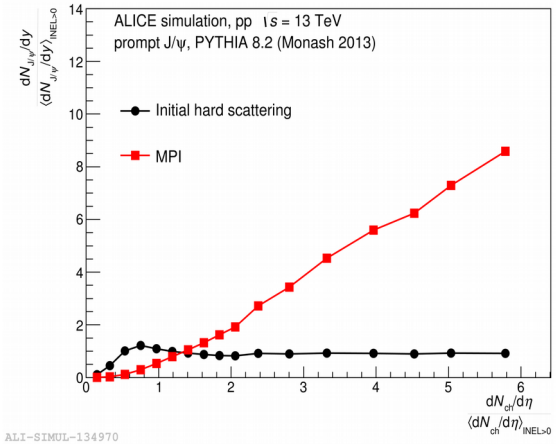

Figure 2: PYTHIA8 prediction for multiplicity dependence of prompt J/ψ production from initial hard scatterings and from MPI in pp collisions at √s = 13 TeV.

Figure 2 shows the PYTHIA8 prediction for the self-normalized yield of prompt J/ψ (excluding beauty-hadron decays) as a function of charged-particle multiplicity for J/ψ produced in the initial hard scattering of the event, and for J/ψ produced in subsequent ones from the MPI framework. It can be seen that initially produced J/ψ are independent of the charged-particle multiplicity, so the contribution of J/ψ from MPI is vital for the understanding of the data.

References

[1] B. Abelev, et al., Phys. Lett. B712 (2012) 165–175.
[2] J. Adam, et al., JHEP 09 (2015) 148.
[3] K. Aamodt, et al., JINST 3 (2008) S08002.
[4] T. Sjostrand, S. Mrenna, P. Z. Skands, Comput. Phys. Commun. 178 (2008) 852–867.

*Work supported by BMBF, GSI, HGS-HIRe, HIC4-FAIR, H-QM, TU Darmstadt

Σ^0 baryon production in pp collisions at $\sqrt{s}$ = 13 TeV measured with the ALICE experiment*

A. Mathis[1,2] and L. Fabbietti[1,2], for the ALICE collaboration

[1]Technische Universität München, Physik Department E62, Garching, Germany
[2]Excellence Cluster 'Origin and Structure of the Universe', Garching, Germany

To present day, only very little is known about the interaction between Σ baryons and nucleons (Σ-N). This is due to the fact that up to now, Σ hypernuclei have not been observed yet and moreover, scattering data for Σ hyperon beams are scarce. Hence, the Σ-N interaction remains to be probed. For other hyperons, the situation is somewhat better, in particular for the case of the Λ. Recently, much progress has been made for the case of the Λ-N interaction by employing femtoscopy as a complementary method compared to scattering data. In the context of femtoscopic measurements, it is also interesting to quantify the feed-down from the Σ^0 which decays almost exclusively into a Λ baryon and a photon [1] to the final state of interest containing a Λ. At low collision energies close to the NN threshold, the production cross-sections $\sigma_\Lambda/\sigma_\Sigma \approx 10$ [2] suggest a feed-down of ~ 10%. For larger energies, however, according to isospin considerations, the ratio is expected to approach 1/3 [3] as the Λ is represented in an isospin singlet state while the Σ^0 belongs to an isospin triplet representation. Hence, if sufficient energy is available in the reaction, three different Σ states can be excited but only one Λ state.

A study of the Σ-N, and the hyperon-nucleon interaction in general is also of interest in the context of the study of the content of neutron stars. Even though, as recently demonstrated, gravitational wave observations of binary neutron star mergers are a powerful tool to determine the neutron star equation of state (EOS), the latter still remains a puzzle. In particular, for the description of such a system in the presence of hyperons a thorough understanding of the hyperon-nucleon interaction is mandatory.

As a first step, we measure the production of the Σ^0 baryon at an unprecedented high energy of $\sqrt{s}$ = 13 TeV in pp collisions with the ALICE detector. For the analysis, all available data are employed, which account to about 1×10^9 events collected with a minimum-bias trigger. For the reconstruction of the Σ^0 the dominant decay channel $\Sigma^0 \rightarrow \Lambda\ \gamma$ is exploited. The Λ is then subsequently identified via its decay into a charged pion and a proton (BR ~ 63.9 % [1]) employing the dE/dx information provided by the ALICE Time Projection Chamber. The energy of the photon is typically too low to allow for the employment of ALICE's electromagnetic calorimeter. Instead, the photon conversion method is used which relies on the identification of the dielectron pair produced in the conversion of a photon in the detector material, $\gamma \rightarrow e^+e^-$. For the case of ALICE, the corresponding probability is about 8 %. The four-momentum vector of the Λ is then combined with a dielectron pair and the resulting invariant mass is depicted in Fig. 1. The background is described by a forth-order polynomial (dotted line) and the signal is parametrized by a single Gaussian.

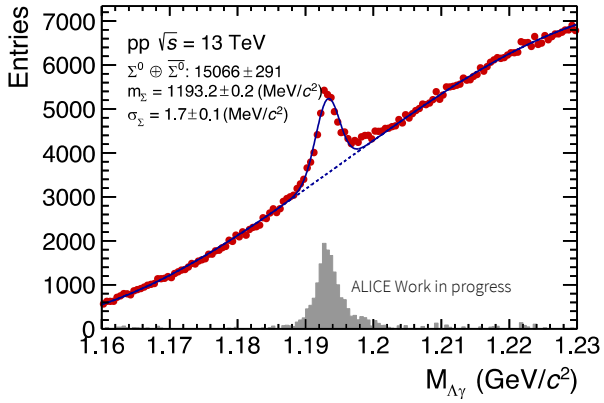

Figure 1: Invariant mass of the Λ and a dielectron pair. The dotted line depicts the combinatorial background and the signal is parametrized by a Gaussian. The grey histogram displays the signal after subtraction of the background.

A global fit of the spectrum yields in total about 15,000 Σ^0 baryons candidates at a signal-to-noise ratio of about 0.2. After correcting the spectra for acceptance and efficiency, this analysis will yield the Σ^0 production cross-section and the Σ^0/Λ ratio at an unprecedented high energy of $\sqrt{s}$ = 13 TeV together with a comparison to event generators such as PYTHIA [4]. Moreover, with more data being reconstructed, the feasibility of p-Σ^0 femtoscopy will be checked, possibly allowing to constrain the Σ-N interaction for the first time. Additionally, with the available statistics, a study of all relevant decay channels ($\Sigma^0 \rightarrow \Lambda\ \gamma$, $\Sigma^0 \rightarrow \Lambda\ \gamma\ \gamma$ and $\Sigma^0 \rightarrow \Lambda\ e^+e^-$ [1]) may be at hand and the feasibility will be explored, which for the first time would allow for a relative measurement of the corresponding branching ratios.

References

[1] K.A. Olive *et al.*, Chin. Phys. C, 38, 0900001 (2014).
[2] P.Kowina *et al.*, Eur. Phys. J. A 22, 293-299 (2004).
[3] H.Landolt, R.Börnstein, Landolt-B.12, (1988).
[4] T. Sjöstrand, S. Mrenna, and P. Skands, Journal of High Energy Physics 2006 no. 05, (2006) 026.

*) Work supported by the DFG Excellenzcluster Universe, "Origin and Structure of the Universe" (DFG EClust 153), BMBF ALICE „Verbundprojekt 05P2015" and the Collaborative Research Center "Neutrinos und Dunkle Materie in der Astro- und Teilchenphysik (NDM)" (SFB 1258).

 DOI:10.15120/GR-2018-1

Baryon Femtoscopy in p–Pb Collisions at 5.02 TeV

B. Hohlweger[1,2] and L. Fabbietti[1,2], for the ALICE collaboration

[1]Technische Universität München, Physik Department E62, Garching Germany,[2]Excellence Cluster `Origin and Structure of the Universe`, Garching, Germany

Understanding the interaction of hyperons at finite densities is fundamental in order to understand the role of strange degrees of freedom in the Equation of State (EoS) of neutron stars. Scattering data for hyperons does not allow to discriminate between models of baryon-hyperon interaction. Therefore, femtoscopy has been proposed to study the interaction of these pairs. The observable in femtoscopic analysis is the two-particle correlation function, defined as

$$C(\boldsymbol{p}_1,\boldsymbol{p}_2) = \frac{P(\boldsymbol{p}_1,\boldsymbol{p}_2)}{P(\boldsymbol{p}_1)P(\boldsymbol{p}_2)} = C(k) = \int S(\boldsymbol{r},k)|\psi(\boldsymbol{r},k)|^2 d\boldsymbol{r}, \quad (1)$$

where $P(\boldsymbol{p}_1,\boldsymbol{p}_2)$ is the conditional probability of finding a particle pair with a momentum $\boldsymbol{p}_1$and $\boldsymbol{p}_2$ in the same event, while $P(\boldsymbol{p}_i)$ is the single particle probability of independently finding the particles with momentum $\boldsymbol{p}_i$. This quantity can also be viewed as a function of the relative momentum k in the pair center of mass frame and is related to the product of source function $S(\boldsymbol{r},k)$ and wave function $\psi(\boldsymbol{r},k)$ [2]. The sensitivity to the interaction arises from the wave function, which is obtained by solving the Schrödinger equation incorporating the interaction potential of a given pair. The source is typically described by a Gaussian distribution and is assumed to be the same for all baryon pairs.

In a recent study in p–Nb collisions at √s = 3.5 GeV [1] and in pp collisions at √s = 7 TeV it has been shown that the correlation function for p-Λ pairs develops a sensitivity to different scattering parameters. It was however apparent that more statistics would allow for stronger constraints on different models and for this purpose, the analysis was extended to data from p–Pb collisions at $\sqrt{s_{NN}}$ =5.02 TeV. After applying event selection criteria, around 600 million events are available to analyse pairs of p-Λ and p-Ξ. The Λ hyperon is identified via its decay into a charged pion and proton (BR ~63.9%), which subsequently are identified by the dE/dx measurement in the Time Projection Chamber (TPC). The resulting sample has a purity of around 96%. The Ξ hyperon is identified via its decay into a Λ and a pion (BR ~99.9%). A first signal of Ξ's in the invariant mass distribution is depicted in Fig. 1, where a purity of around 87% is reached. The experimental correlation function for p-p, p-Λ and p-Ξ pairs is then obtained by constructing the relative momentum distribution from pairs in the same event $N_{SE}(k)$ and of uncorrelated pairs $N_{ME}(k)$ where each particle is from a different event. The correlation function is obtained by dividing the $N_{SE}(k)$ by $N_{ME}(k)$.

The Correlation Analysis Tool using the Schrödinger Equation (CATS) [3] framework has been employed in the calculation of the proton-hyperon interaction. For p-Λ pairs the interaction has been described by χ_{EFT} potentials at LO and NLO. In the case of p-Ξ pairs a preliminary local potential from the HAL Lattice QCD collaboration [4] has been adopted. The correlation function, as shown in Eq. (1), depends both on the source size and the undergoing potential. Studying the source with p-p pairs, where the interaction potential is well known, allows to reduce the uncertainty arising from the size of the emitting source and permits to set tighter constraints on the strong potential of more exotic pairs as baryon-hyperon or hyperon-hyperon. In the p–Pb system the size of the source depends on the impact parameter and its variations are expected to be larger than in the elementary collisions. The geometry of the emitting source can be studied by using the p-p correlation function binned in several multiplicity classes. The results of this study will provide the necessary input to perform a final combined fit of baryon-baryon pairs in the p–Pb collision system and to ultimately constrain the interaction potentials for baryon-hyperon pairs.

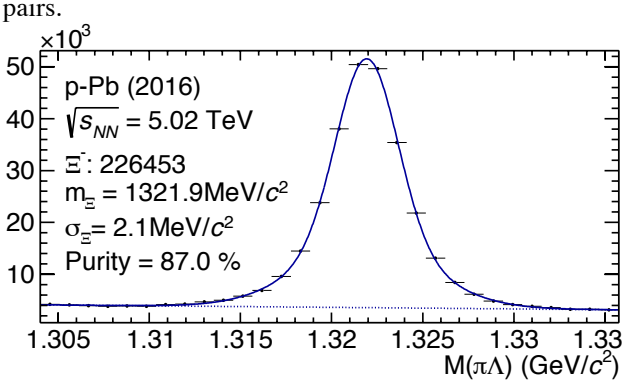

Figure 1: Ξ – Signal reconstructed in the $\Lambda\pi$ channel from p-Pb Data at $\sqrt{s_{NN}}$ =5.02 TeV.

References

[1] HADES Collaboration, Λp interaction studied via Femtoscopy in p+Nb recations at $\sqrt{s_{NN}}$=3.18 GeV, Phys. Rev. C, 94, 025201 (2016)

[2] Michael Annan Lisa and Scott Pratt et al, Femtoscopy in Relativistic Heavy Ion Collisions: Two Decades of Progress, Annual Review of Nuclear and Particle Science, 55, 357-402 (2005)

[3] D.L. Mihaylov, V. Mantovani Sarti et. al, A femtoscopic Correlation Analysis Tool using the Schrödinger equation (CATS), arXiv:1802.08481

[4] Kenji Sasaki, Sinya Aoki et. al, Baryon interactions from lattice QCD with physical masses -- S=−2 sector, arXiv:1702.06241

Experiment collaboration: CERN-ALICE
Accelerator infrastructure: CERN-LHC
Grants: SFB: Sonderforschungsbereich 1258 "Neutrinos und Dunkle Materie in der Astro- und Teilchenphysik (NDM)"
Strategic university co-operation with: TU München

Low-mass dielectron production in pp collisions at $\sqrt{s}$ = 13 TeV with ALICE*

I. Vorobyev[1,2], A.Dashi[1,2], O. Vazquez Doce[1,2], T. Dahms[1,2], for the ALICE collaboration

[1]Excellence Cluster Universe, Technische Universität München, Garching, Germany;
[2]Physik Department, Technische Universität München, Garching, Germany

Electron–positron pairs (dielectrons) are a unique experimental tool to investigate the hot and dense medium created in ultra-relativistic heavy-ion collisions. Such pairs are produced during all stages of the collision and do not interact strongly. Therefore, they carry information about the medium properties and the whole space-time evolution of the system.

Measurements of dielectron production in minimum-bias proton–proton (pp) collisions provide an important vacuum reference for any modifications observed in heavy-ion collisions. Moreover, the measurement of e^+e^- pairs from semileptonic decays of correlated heavy-flavour hadrons in the intermediate-mass region ($1.1 < m_{ee} < 2.9$ GeV/c^2) allow further studies and understandings of the primordial heavy-flavour production. Recent studies of pp collisions with high charged-particle multiplicities showed interesting results similar to the observations previously made in heavy-ion collisions. Measurements of low-mass dielectrons could provide further insight into the underlying physics processes.

The dielectron analysis is performed in the central barrel spectrometer of ALICE [1]. For both multiplicity classes the collision events are triggered on by the V0 detector. Charged particle tracks are reconstructed with the Inner Tracking System (ITS) and the Time Projection Chamber (TPC) in the kinematic range $|\eta_e| < 0.8$ and $p_{T,e} > 0.2$ GeV/c. Specific energy loss in the TPC and the time-of-flight information from the TOF detector are used for the electron identification.

All electron and positron candidates are paired considering the combinations with opposite but also same charge. The combinatorial background is estimated via the geometric mean of same-sign pairs within the same event. Conversions of real photons in the detector material are removed from the raw signal by their orientation relative to the magnetic field. The resulting raw dielectron spectra in high-multiplicity and minimum-bias events are shown in Fig. 1.

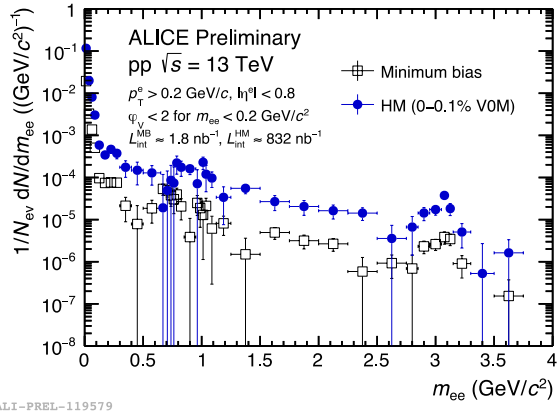

Figure 1: Raw dielectron spectra in minimum-bias (black) and high-multiplicity (blue) events.

The current work focuses on the analysis of approximately 5 times more pp collision data from 2016. The raw dielectron spectra will be corrected for the reconstruction efficiencies using detailed Monte Carlo simulations. The results will be compared to the expectations from all known hadronic sources, i.e. the hadronic cocktail, contributing to the dielectron spectrum in the ALICE central barrel acceptance. For the high-multiplicity cocktail, the light-flavour hadron p_T distributions are adjusted according to the measured modification of charged hadron p_T spectra [2]. The contribution of correlated semileptonic decays of open charm and bottom mesons is estimated with PYTHIA and POWHEG simulations. For the multiplicity dependence, the results on D-meson production as a function of p_T and multiplicity [3] are used to weight the open charm and bottom contributions. In the intermediate mass range the data will be fitted with PYTHIA and POWHEG templates of open charm and bottom production, which will allow us to extract the heavy-flavour cross sections. Finally, assuming the equivalence between the fraction of real direct photons and the fraction of virtual direct photons at zero mass, the former can be extracted from the dielectron spectrum measured at small invariant mass.

* Work supported by Excellence Cluster “Origin and Structure of the Universe”, DFG EClust 153 and BMBF ALICE: “Verbundprojekt 05P2015”

References

[1] ALICE Collaboration, JINST3 (2008) 08002
[2] ALICE Collaboration, Phys. Lett. B 753, 319 (2016)
[3] ALICE Collaboration, JHEP 09, 148 (2015)

 DOI:10.15120/GR-2018-1

Production of electrons from semileptonic heavy-flavour hadron decays in proton-proton and heavy-ion collisions measured with ALICE at the LHC*

C. de Conti[1], A. Dubla[2,3], M. Faggin[5], S. Hornung[2,3], S. P. Rode[4], for the ALICE collaboration

[1]Universidade de Sao Paulo, Brasil; [2]GSI, Darmstadt, Germany; [3]Heidelberg university, Germany; [4]Indian Institute of Technology Indore, India; [5]University of Padova

The transverse momentum (p_T) spectra and the nuclear modification factor (R_{AA}) of electrons from semileptonic heavy-flavour hadron decays is measured in Pb-Pb collisions at $\sqrt{s_{NN}}$ = 5.02 TeV and in Xe-Xe collisions at 5.44 TeV. The modification of the p_T spectra is studied at mid-rapidity (|y| < 0.8) in the p_T interval 0.5-6 GeV/c. The R_{AA} is calculated using the proton-proton (pp) reference cross-section measured in the same p_T interval and at the same center-of-mass energy as for the Pb-Pb measurement. For the Xe-Xe R_{AA} the pp reference was obtained using an interpolation procedure. In addition, the production cross-section was also measured in pp collisions at $\sqrt{s}$ =7 TeV and $\sqrt{s}$ = 13 TeV.

Introduction

In ultra-relativistic heavy-ion collisions at the Large Hadron Collider (LHC) a strongly-interacting matter, characterised by high energy density and temperature, is produced. Under these conditions, the formation of a deconfined state of quarks and gluons, the Quark-Gluon Plasma (QGP), is predicted by Quantum ChromoDynamic (QCD) calculations on the lattice. The production of heavy quarks, i.e. charm (c) and beauty (b) is characterised by a timescale shorter than $1/(2*m_{c,\,b})$, where m is the mass of the quark. This timescale (e.g. ~ 0.08 fm/c for charm) is expected to be smaller than the QGP thermalization time (~ 0.6-1 fm/c). Heavy quarks interact with the QGP and suffer energy loss while propagating through it. The modification of the p_T spectra in heavy-ion collisions with respect to those in pp collisions at the same centre-of-mass energy is quantified by the nuclear modification factor R_{AA}, defined as:

$$R_{AA} = \frac{(dN_{AA}/dp_T)}{(d\sigma_{pp}/dp_T)\cdot\langle T_{AA}\rangle}, \quad (1)$$

where dN_{AA}/dp_T is the measured yield in heavy-ion collisions and $d\sigma_{pp}/dp_T$ is the corresponding cross-section in pp collisions.

* Work supported by GSI, BMBF, DST-DAAD and HGS-HIRe and ISOQUANT.

The average nuclear overlap function, $\langle T_{AA}\rangle$, is estimated via Glauber model calculations and is proportional to the average number of binary nucleon-nucleon collisions in nucleus-nucleus (AA) collisions in a given centrality class.

Low-p_T heavy-flavour measurements are very important to test the binary scaling of the heavy-quark production in heavy-ion collisions. In addition, they allow to extract information about possible influences from the initial state effects, like the modification of the parton distribution functions at the LHC energies. They also carry information about different hadronisation mechanisms, namely the fragmentation in the vacuum and the coalescence in the medium. At high-p_T heavy quarks are sensitive to the medium energy density, through the mechanism of parton energy loss.

Results

The p_T-differential cross section for electrons from heavy-flavour hadron decays at mid-rapidity in pp collisions at $\sqrt{s}$ = 5.02, 7 and 13 TeV using the photonic-electron tagging are shown in the left, middle and right panel of Figure 1, respectively. The statistical uncertainties are shown as vertical bars and the systematic uncertainties as empty boxes. The dashed line indicate the central value of the FONLL calculation [1]. The full systematic band of the model originates from the variation of the factorization and normalization scale as well as the heavy-quark masses and the uncertainty of the parton distribution function (PDF) used. In the lower panels of Figure 1 the ratios of the experimental measurements with the central value of the FONLL calculations are shown. Within the systematic uncertainties of the measurement and the calculation, the theoretical calculation is in good agreement with the data. The measured cross sections are close to the upper edge of the FONLL uncertainty band.

Figure 2 shows the R_{AA} of electrons from heavy-flavour hadron decays at mid-rapidity (|y| < 0.8) as a function of p_T in Pb-Pb collisions at $\sqrt{s_{NN}}$ = 5.02 TeV for the 0-10% centrality class. The new low p_T measurement is shown together with the high p_T results obtained using the TPC+EMCal detectors to identify the electron (orange closed marker) [2].

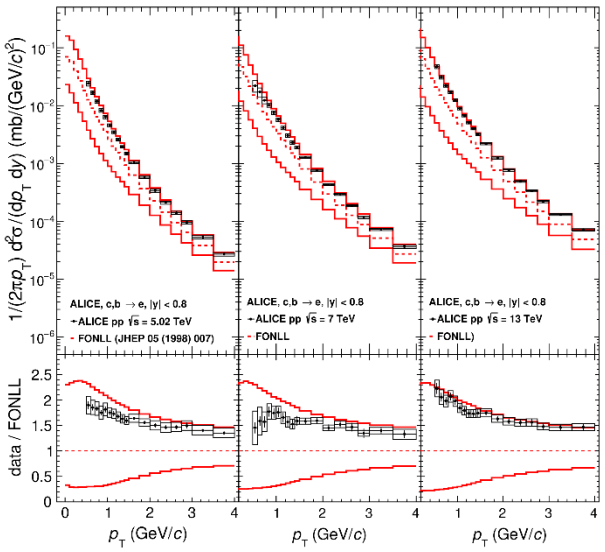

Figure 1: p_T-differential cross section of electrons from heavy-flavour hadron decays at mid rapidity in pp collisions at $\sqrt{s}$ = 5.02 TeV, 7 TeV and 13 TeV compared to pQCD calculations.

The statistical and systematic uncertainties of the spectra in Pb-Pb and pp were propagated as independent uncertainties. The uncertainty on the normalisation (3%) is the uncertainty on $\langle T_{AA} \rangle$ and it is represented by a filled box at R_{AA} = 1. At high p_T, the R_{AA} is below unity, showing a suppression of the yield of electrons from heavy-flavour hadron decays with respect to pp due to the energy loss of heavy quarks in the QCD medium.

For p_T < 1.5 GeV/c, the data is compatible with unity

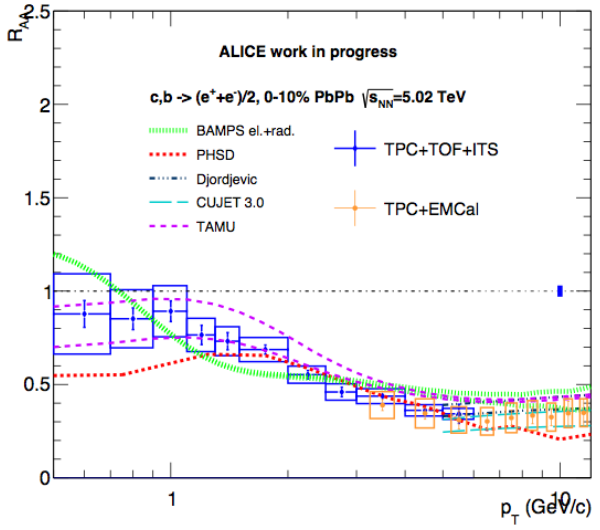

Figure 2: Heavy-flavour hadron decay electron RAA at mid-rapidity as a function of pT in central Pb-Pb collisions at $\sqrt{s_{NN}}$ = 5.02 TeV compared to models [3-6].

within systematic uncertainties. Models which include shadowing, like TAMU [4], predict an R_{AA} smaller than one even at low p_T and are in good agreement with the experimental measurement.

In Figure 3 the R_{AA} of electrons from heavy-flavour hadron decays at mid-rapidity ($|y|$ < 0.8) as a function of p_T in Xe-Xe collisions at $\sqrt{s_{NN}}$ = 5.44 TeV is shown in the 0-20% centrality interval. The measurement is important to further study and constrain the energy loss dependence of the heavy quarks with respect to the size of the colliding nuclei. In addition, the modification of the parton distribution functions using a similar centre-of-mass collision energy but different nuclei can be investigated. Also in this case the uncertainty on the normalisation (9%) is the uncertainty on $\langle T_{AA} \rangle$ and it is represented by a filled box at R_{AA} = 1. When compared with the R_{AA} in Pb-Pb collisions an indication of a smaller suppression in Xe-Xe collision is observed.

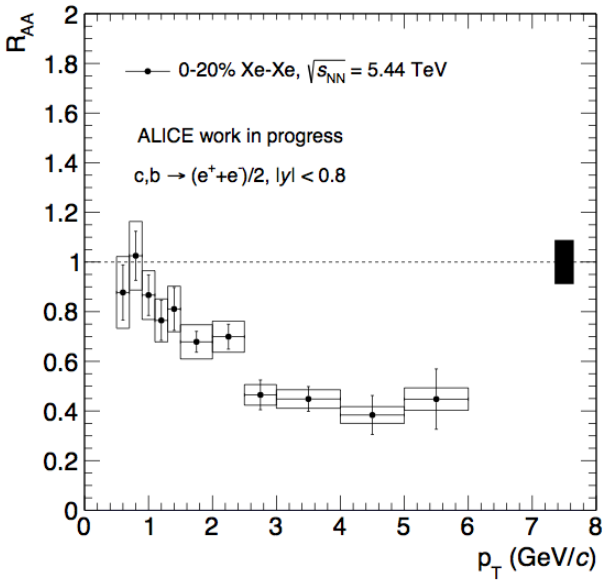

Figure 3: Heavy-flavour hadron decay electron R_{AA} at mid-rapidity as a function of p_T in the 0-20% centrality class in Xe-Xe collisions at $\sqrt{s_{NN}}$ = 5.44 TeV.

References

[1] M. Cacciari et al., JHEP 05 (1998) 007
[2] ALICE Collaboration, Nucl. Phys. A 967 (2017)
[3] J. Uphoff et al., J.Phys.Conf.Ser. 509 (2014) 012077
[4] M. He et al., Phys.Lett. B735 (2014) 445–450
[5] W. Cassing et al., Phys.Rev. C78 (2008) 034919
[6] J. Xu, J. Liao et al. Chin. Phys. Lett. 32 no. 9, (2015)

 DOI:10.15120/GR-2018-1

Quality assurance of GEM-based readout chambers for the Time Projection Chamber of ALICE

L. Kreis[1,2], M. Habib[1,3], A. Harlenderová[1,2], S. Hornung[1,2], J. Hehner[1], S. Masciocchi[1,2], D. Miśkowiec[1], T. Rudzki[1,2], B. Voss[1], the ALICE Collaboration

[1]GSI, Darmstadt, Germany; [2]Ruprecht-Karls-Universität Heidelberg, Germany; [3]Technische Universität Darmstadt, Germany

In the upcoming long shutdown period of the LHC, ALICE will be upgraded to be able to record Pb–Pb collisions at an event rate of 50 kHz. The current readout chambers of the Time Projection Chamber (TPC) are multiwire proportional chambers, which limit the event rate to 3 kHz. A new readout based on gas electron multipliers (GEM) is currently under construction. A stack of four GEMs is used, where two large pitch foils are sandwiched between two standard pitch foils.

These new readout chambers will allow continuous data-taking during LHC Run 3 and 4. The ALICE TPC readout chambers come in two sizes: the inner readout chambers and the outer readout chambers (OROC) with one stack and three GEM stacks, respectively. The TPC upgrade project is distributed between different institutes. GSI is responsible for the framing of GEMs from the largest stack and for the OROC assembly.

After the assembly, several parameters are measured to guarantee a stable operation of the chambers at the LHC, while maintaining the performance of the current setup [1]. The ion backflow (defined as the ratio of the cathode current and the current on the pad plane $IBF = I_{cathode} / I_{pads}$ at an effective gas gain of 2000 has to be below 1%. The local energy resolution measured with an 55Fe source at the same operating point must be below 12%.

The chambers are transferred onto a 2D scanning device. The gas tightness is evaluated by flushing the chamber while monitoring the oxygen content. The voltage settings for an effective gain of 2000 are determined for each GEM stack. These settings are used in the following tests. The energy resolution is measured for each GEM stack at one point with an 55Fe source. The resolution is determined by a Gaussian fit to the spectrum. Gain uniformity and ion backflow are measured with x-ray irradiation at each point using the 2D scanner. A chamber passes the test if the gain uniformity is better than 20%. An example of the ion backflow is shown in Fig. 1.

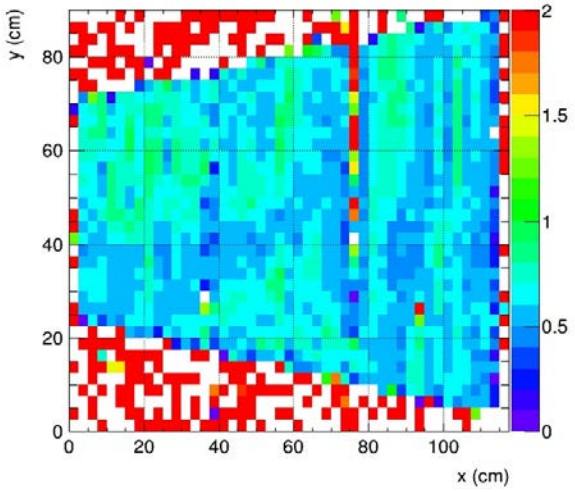

Figure 1: Two-dimensional scan of the ion backflow showing the uniformity of the chamber OROC/6.

Each solder joint of the high voltage connections and the GEM foils is irradiated for 15 minutes to check for possible defects which may cause discharges. After the 2D scans, the chamber load exceeding the anticipated LHC Run 3 and Run 4 conditions is simulated in a shielding box. During this six-hour-long full area irradiation the chamber is monitored for possible discharges. Subsequently the leakage current for each GEM is measured to be able to exclude any possible short circuits. If a chamber passes all the tests, it is moved into a transportation box in which it will be sent to CERN.

The work at the GSI detector lab is progressing well. The first two chambers were already shipped to CERN. The final assembly of the TPC will take place in 2019.

Work supported by BMBF and GSI.

References

[1] The ALICE Collaboration, “Upgrade of the ALICE Time Projection Chamber”, CERN,

October 2013, https://cds.cern.ch/record/1622286

 DOI:10.15120/GR-2018-1

Read-out electronics for the ALICE TPC upgrade

C. Lippmann[1] and the ALICE collaboration

[1]GSI, Darmstadt, Germany

The front-end electronics for the upgrade of the ALICE Time Projection Chamber (TPC) is based on the 32-channel SAMPA ASIC and a radiation-hard data and control link (CERN GBT). The SAMPA ASIC incorporates for each channel a charge-sensitive amplifier, a shaper, and a 10-bit ADC. The TPC uses the SAMPA (5 per Front-End Card, FEC) in direct-serialization mode, where all ADC values are sent via electrical links to the GBTx multiplexer ASIC (2 per FEC) and through the optical read-out links without compression. In this way, the data can be corrected for the Common Mode Effect in the FPGA-based read-out card, the ALICE Common Readout Unit (CRU), with high precision. The Common Mode Effect is a systematic, common baseline shift expected at high occupancies.

Beamtest results

A pre-production Inner Readout Chamber (IROC) has been tested together with 6 prototype versions of the TPC FEC with SAMPA chips of version 'v2' at the CERN Proton Synchrotron with electrons and pions at 1 to 6 GeV/c. Since CRUs were not yet available the Read-Out Receiver Card (RORC) of the current ALICE experiment was fitted with a custom firmware (T-RORC) implementing the 12 bi-directional GBT links necessary for communicating with the 6 FECs.

The SAMPAs on the 6 FECs are synchronised with dedicated control signals. They synchronously sample the detector signals on 960 channels. Triggers from the beam scintillators are received on the T-RORC and open a time window of 0.1 ms length, where the ADC data are stored to disk.

The particle identification achieved at 1 GeV/c is shown in Fig. 1. The separation power is compatible with the value expected at this short track length (63 pad rows). For a full TPC sector the deposited charge information from 152 pad rows will be used, and the separation power will improve accordingly.

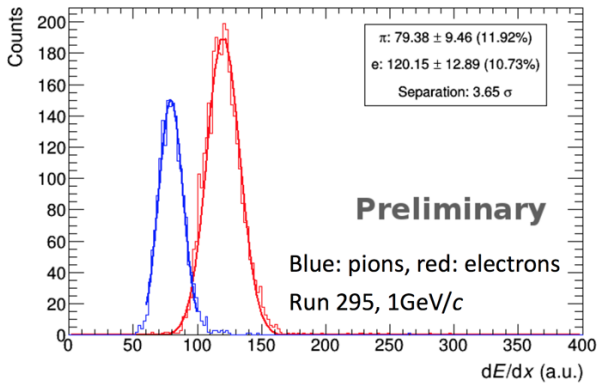

Figure 1: Particle separation power (electrons and pions) measured with a TPC pre-production IROC.

The read-out system was running stable for the full beam time over many days. No issues with synchronisation between the SAMPAs have been seen. During and after the beam test the data decoded, reconstructed and analysed with software based on the official ALICE online-offline package.

Noise results

The TPC FEC connects to the detector via flexible signal cables (in order to decouple the weight from the FEE from the read-out chambers and drift field cage). The Printed Circuit Board (PCB) for the final version is based on rigid flex technology where the flexible cables are realized as one layer of the PCB (see Fig. 2).

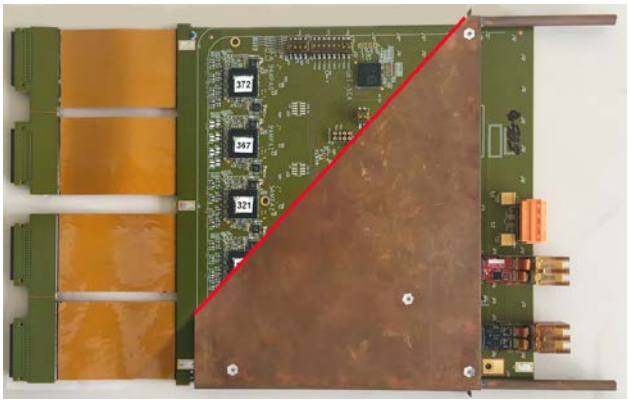

Figure 2: Overlay of 2 images showing a TPC Front-End Card (FEC) with and without its copper cooling envelope. The 4 flexible signal cables, the input protection network and the SAMPA ASICs are visible on the left, the power and optical connectors on the right.

FECs of this revision ('1a') and equipped with the different versions of the SAMPA (v2, v3 and v4) have been tested on the IROC after the beamtest. A noise distribution for 6 FECs is shown in Fig. 3. The mean noise in this particular detector region is 0.93 LSB. The targeted noise value is 1 LSB, corresponding to an equivalent noise charge (ENC) of 670 electrons.

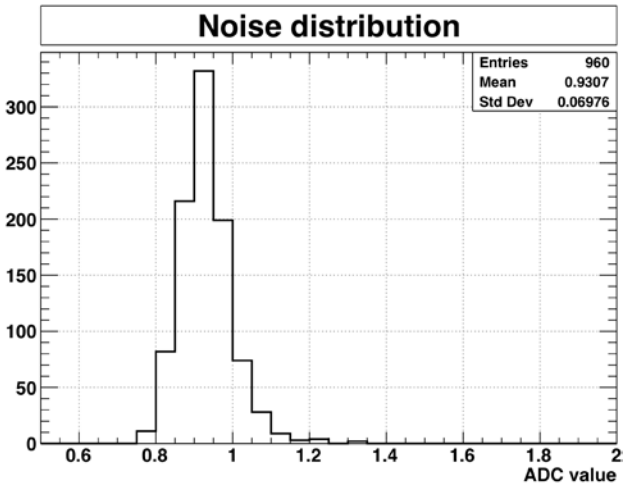

Figure 3: Noise distribution on 960 channels using 6 revision '1a' FECs.

The revision ‘1a’ of the FEC with SAMPA v4 will go into production. The SAMPA production readiness review (PRR) was successfully held on 20 February 2018. The PRR for the TPC FEC is planned for Spring 2018.

*Work supported by BMBF and GSI.

 DOI:10.15120/GR-2018-1

Nuclear modification factors in Xe-Xe collisions measured with ALICE*

J. Gronefeld[1] for the ALICE collaboration
[1]GSI, Darmstadt

The suppression of charged particle yields in heavy-ion collision compared to a superposition of independent nucleon-nucleon collisions at RHIC was one of the first indications of the creation of a deconfined medium[1, 2]. This observation is related to parton energy loss in the hot and dense QCD matter created in the collision of heavy ions, leading to a modification of transverse-momentum (p_T) distributions of the resulting particles, as initially suggested by Bjorken in 1982 [3].

Results from ALICE [4, 5] show that hadron yields at high p_T in central Pb–Pb collisions at LHC are suppressed even stronger than at RHIC, indicating a hotter and denser medium.

The suppression is quantified in terms of the nuclear modification factor:

$$R_{AA} = \frac{dN_{AA}/dp_T}{\langle T_{AA} \rangle \, d\sigma_{pp}/dp_T}$$

Here, dN_{AA}/dp_T represents the p_T-differential charged-particle yield in nucleus-nucleus (AA) collisions, while $d\sigma_{pp}/dp_T$ stands for the p_T-differential cross section in proton-proton (pp) collisions. The average nuclear overlap function $\langle T_{AA} \rangle$ is determined by Glauber Monte-Carlo calculations for each class of centrality.

In absence of medium effects, the nuclear modification factor will be equal to unity, while $R_{AA} < 1$ indicates a suppression of charged-particle yields.

To obtain the primary charged-particle yield as a function of p_T, corrections are made for tracking efficiency and acceptance and for contamination by secondary particles. These correction factros are obtained from Monte-Carlo simulations that are reweighted to account for differences in the particle composition of event generators and the data. In addition the distribution is corrected for p_T resolution .

The charged particle nuclear modification factor for Xe-Xe and Pb-Pb collisions at two different center-of-mass energies is shown as a function of the charged particle multiplicity per unit of rapidity for three ranges in p_T. All systems exhibit a similar trend, showing an increase in suppression for events with a increased charged particle production.

For high charged particle densities we observe the same R_{AA} for all collision systems and for all energies at high p_T where parton energy loss is believed to play a dominant role (lower panel). This shows that a deconfined medium is created in heavy-ion collisions that exceeds a charged particle density of 400 per unit of rapidiy independently of the collision system.

At low p_T (top panel) a energy dependence of the R_{AA} is observed, which is attributed to the inceased particle production with higher collision energy.

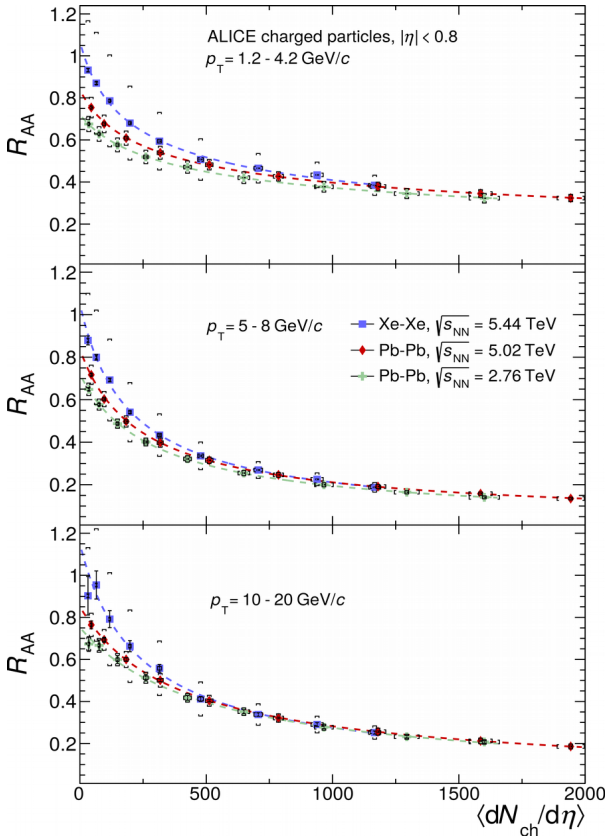

The charged particle R_{AA} as a function of charged particle density.

[1] PHENIX Collaboration, Phys. Rev. Lett. 88, (2002) 022301.
[2] STAR Collaboration, Phys. Rev. Lett. 89, (2002) 202301.
[3] J. Bjorken, Preprint FERMILAB-PUB-82-059-THY (1982).
[4] ALICE Collaboration, Phys. Lett. B 746, (2015).
[5] ALICE Collaboration, arXiv: 1802.09145 (2018).

* Work supported by GSI, TU Darmstadt and HGS-HIRe

Measurement of ^{3}He elliptic flow in Pb-Pb collisions with ALICE at the LHC

A. Caliva[1], the ALICE collaboration

[1]GSI, Darmstadt, Germany

The elliptic flow coefficient (v_2) of (anti-)^{3}He is measured as a function of p_T in Pb-Pb collisions at $\sqrt{s_{NN}}$ = 5.02 TeV for different centrality ranges using the Event Plane (EP) method [1].

This measurement provides an important contribution to the understanding of collectivity effects for loosely bound nuclear systems, complementing the picture obtained from the v_2 of (anti-)deuterons [2] and (anti-)protons [3], and puts additional constraints to the coalescence approach and other hadronization models that describe the elliptic flow of light (anti-)nuclei in heavy-ion collisions.

Analysis strategy

In Pb-Pb collisions with non-zero impact parameter, the hot and dense partonic matter is created with an initial spatial asymmetry with respect to the reaction plane, defined by the impact parameter and the beam direction.

This initial geometrical anisotropy produces a non-uniform azimuthal distribution of particles with respect to the reaction plane, due to the different pressure gradients “in-plane” and “out-of-plane”.

The elliptic flow coefficient (v_2) is defined as the asymmetry between the numbers of particles emitted in-plane and out-of-plane:

$$v_2 = \frac{\pi}{2R_2}\frac{N_{\text{in-plane}}(p_T) - N_{\text{out-of-plane}}(p_T)}{N_{\text{in-plane}}(p_T) + N_{\text{out-of-plane}}(p_T)}$$

The centrality of the collision is determined from the charged particle multiplicity measured by two forward detectors (V0A and V0C).

Pileup rejection is applied to select single Pb-Pb collisions and all events are required to have a reconstructed vertex within 10 cm from the geometric centre of the ALICE experiment in order to ensure a uniform response of the detectors in the central barrel.

All reconstructed tracks are required to fulfil a set of track quality criteria. The ^{3}He candidates are identified by requiring that their specific energy loss dE/dx in the TPC is within 3σ from the expected mean for ^{3}He calculated from the Bethe-Bloch formula, being σ the resolution in the dE/dx measurement.

The contribution from secondary ^{3}He produced by spallation in the detector material is suppressed by selecting tracks with transverse distance-to-closest approach (DCA) to the primary vertex smaller than 0.1 cm.

The systematic uncertainties due to tracking, particle identification, occupancy effects in the TPC, event selection and feed-down from weak decays of hyper-triton, are in the range 6-8%.

Results

The elliptic flow of ^{3}He measured in Pb-Pb collisions at 5.02 TeV, shown in Fig.1, has a clear centrality dependence and a slower rise with p_T compared to other particle species due to the larger mass of ^{3}He [3].

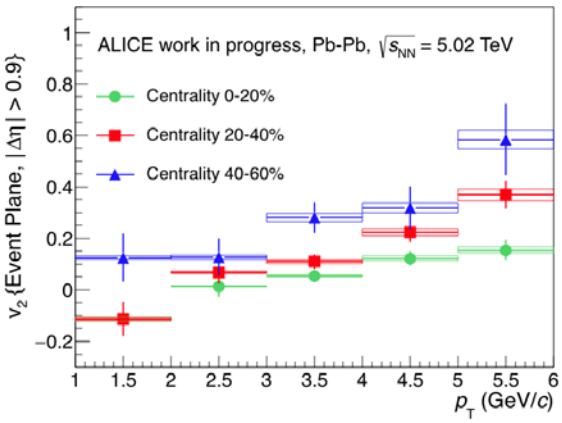

Figure 1: Elliptic flow coefficient (v_2) of ^{3}He as a function of p_T measured in Pb-Pb collisions at $\sqrt{s_{NN}}$ = 5.02 TeV for different centrality classes.

References

[1] A. Bilandzic et al., Phys. Rev. C 83, 014909 (2011).

[2] S. Acharya et al., The ALICE Collaboration, Eur. Phys. J. C77, 658 (2017).

[3] B. Abelev et al., The ALICE Collaboration, JHEP 06, 190 (2015).

Experiment collaboration: CERN-ALICE
Accelerator infrastructure: CERN-LHC

Work supported by GSI

 DOI:10.15120/GR-2018-1

Optimization of the HV scheme for GEM-based detectors

L. Lautner[1,2], P. Gasik[1,2], L. Fabbietti[1,2] and the ALICE TPC collaboration

[1]Physik Department E62, TU München, 85748 Garching, Germany; [2]Exellence Cluster `Origin and Structure of the Universe´, 85748 Garching, Germany

Gas Electron Multiplier (GEM) [1] - based detectors are widely used in many experiments (COMPASS, LHCb, TOTEM) and future upgrades (ALICE, CMS). Electrical discharges that may occur during operation of those detectors can damage them permanently in form of increased leakage currents or electric short circuits that render the detector e ectively blind. Initital discharges, caused by high charge densities obtained in a single GEM hole [2] may trigger a propagated (secondary) discharge between two GEMs in a stack or between the last GEM and the readout anode. The latter is especially dangerous - as the front-end electronics can be severely a ected by high energy released in a discharge event. The behaviour of the electric eld in the gap between GEM foils or a GEM foil and the readout anode after an initial spark cannot explain the appearance of the propagated discharges whose nature is still not fully understood. However, the thorough optimization of the HV scheme in terms of its RC characteristics allows to mitigate (or even avoid) the appearance of these potentially harmful events.

In this report we present our measurements on the in uence of the RC components on the propagated discharge probability. The study has been conducted with a single 10×10 cm^2 GEM foil in Ar-CO_2 (90-10) and Ne-CO_2-N_2 (90-10-5) mounted at a 2 mm distance to the readout anode (induction gap) and a drift gap, between the cathode and the GEM, of 19.5 mm. A mixed (^{239}Pu, ^{241}Am, ^{244}Cm) source is placed on top of the cathode, emitting alpha particles perpendicular to the GEM. The voltage di erence across the GEM was set su ciently high to increase the primary discharge probability.

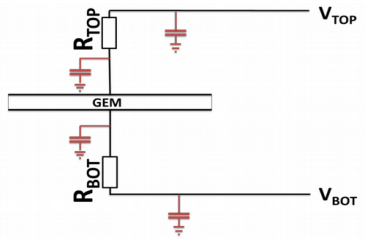

Figure 1: HV scheme of the system with all considered RC elements

Figure 1 presents the RC elements of the HV scheme used in the measurements. Each cable in the system introduces a parasitic capacitance marked in red in the scheme. R_{TOP} and R_{BOT} are the decoupling resistors installed on the top and the bottom side of the GEM, respectively. Particular attention should be paid to R_{BOT} as it has a signi cant in uence on the secondary discharge probability as shown in Fig. 2.

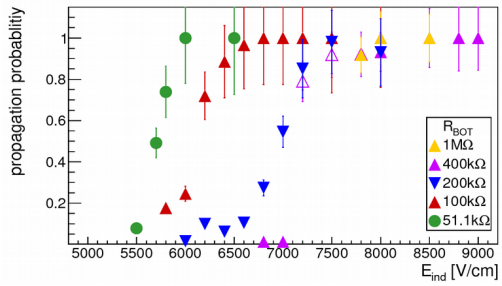

Figure 2: Secondary discharge probability for di erent values of the decoupling resistor R_{BOT} as a function of the induction eld in Ar-CO_2 (90-10)

A large resistance on the GEM bottom electrode increases the potential of that electrode after a primary discharge and thus also the induction eld which should make propagation more likely. In contrary, however, the measured onset of the propagted discharges increases with the increasing value of the induction eld. This points to a development of a current in the induction gap which, as a consequence, induces a current across the R_{BOT} resistor. The latter results in a potential drop (thus the decrease of the induction eld) and quenching of a propagated discharge. Therefore, a clear recommendation for $R_{BOT} > 0$ can be given. In the course of this study, a set of recommendations for the stable operation of GEM detectors has been derived. The Cable length between decoupling resistors and GEM electrodes should be minimized as additional capacitances may keep E_{IND} high after primary discharges. As the cable length between the power supply and the decoupling resistors does not in uence the propagation probability for su ciently large values of R_{BOT} and R_{TOP}, those can be freely choosen. For $R_{BOT,}$ a value greater than 100 kΩ has been proven acceptable. The measurements presented in this report may serve as a baseline for the HV scheme optimization of mulit-GEM based detectors.

References

[1] F. Sauli, NIM A 386 (1997) 531-534

[2] P. Gasik, A. Mathis & L. Fabbietti, NIM A 870 (2017) 116-122

Experiment beamline: none
Experiment collaboration: CERN-ALICE
Experiment proposal: none
Accelerator infrastructure: none
PSP codes: none
Grants: GSI F&E TMLFRG1316 CBM-RICH
Strategic university co-operation with: none

 DOI:10.15120/GR-2018-1

d*E*/d*x* resolution studies of a pre-production read-out chamber with GEMs for the ALICE TPC

T. Klemenz[1], P. Gasik[1], A. Mathis[1], H. Schulte[2], J. Wiechula[2]

[1]Physik Department E62, Technische Universität München, Germany; [2]IKF, Goethe Universität Frankfurt am Main, Germany

The ALICE Collaboration is planning a major upgrade of its central barrel detectors to be able to cope with the increased LHC luminosity beyond 2020 [1]. In order to record at an increased interaction rate of up to 50 kHz in Pb-Pb collisions, the TPC will be operated in an ungated mode with continuous read-out [2]. This demands for a replacement of the currently employed gated Multi-Wire Proportional Chambers by GEM-based (Gas Electron Multiplier) read-out chambers without compromising the performance, in particular in terms of particle identification capabilities via the measurement of the specific energy loss. A stack of 4 GEMs, where two large pitch foils are sandwiched between two standard pitch foils, has proven to meet the requirements when powered with a proper High voltage (HV) configuration. These are an ion back flow (IB) < 1% and an energy resolution for a ^{55}Fe source ($\sigma(^{55}\mathrm{Fe})$) < 12%. The increase in interaction rate and the requirements of a continuous read-out not only demand for significant modifications of the read-out chambers, but also the front-end cards and the corresponding software framework.

To validate the performance of a 4-GEM Inner Read-Out Chamber (IROC) from the pre-production phase of the project, the dE/dx resolution was evaluated with a beam of electrons and pions at the Proton Synchrotron at CERN. The detector was equipped with the newly developed front-end electronics based on the SAMPA ASICs [3], sampling the signal with 5 MHz. Throughout the measurements, 11 HV configurations, corresponding to different values of the local energy resolution and IB, were used to power the IROC. The online and offline data analysis was conducted with O^2, the new software framework for reconstruction, simulation and analysis in ALICE.

For the data analysis, only events with single tracks were selected in order to make use of the particle identification provided by a threshold Cherenkov counter as a reference. Local gain variations in the GEM stack and channel-by-channel variations of the front-end electronics may cause variations of the gain. These were measured and corrected for on a pad-by-pad level. With a width of 6.3% these gain variations are very well within the specifications of < 10%. At 1 GeV/c, a dE/dx resolution for pions (11.92%) and electrons (10.73%) as well as the corresponding separation power (3.65 σ), defined as

$$S_{AB} = \frac{\left|\langle dE/dx\rangle_A - \langle dE/dx\rangle_B\right|}{0.5\left(\sigma(dE/dx)_A + \sigma(dE/dx)_B\right)} \quad (1)$$

for two particle species A and B, is obtained.

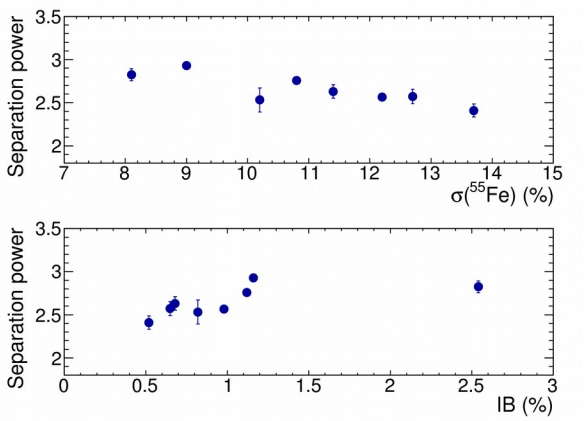

Figure 1: Separation power of electrons and pions as a function of ^{55}Fe resolution (top) and ion back flow (bottom) at a beam momentum of 2 GeV/c

In Fig. 1 the separation power as a function of the ^{55}Fe resolution (top) and the ion back flow (bottom) is shown. The data points represent different HV configurations. One can see that the separation power has only a shallow dependency on those parameters and therefore the separation power does not set any tight constraints on the choice of the final HV configuration for the IROC.

The new read-out system for the TPC upgrade has been tested at the CERN Proton Synchrotron. The read-out chamber, front-end electronics and software framework all work as intended. Currently, the project is in the final production phase. All read-out chambers are scheduled to be assembled until 2019, when the LS2 is supposed to start. The installation and commissioning of the read-out chambers will last until the end of 2020.

References

[1] B.Abelev et al. [ALICE Collaboration], "Upgrade of the ALICE Experiment: Letter of Intent", CERN-LHCC-2012-012 (2012), https://cds.cern.ch/record/1475243

[2] B.Abelev et al. [ALICE Collaboration], "Technical Design Report for the Upgrade of the ALICE Time Projection Chamber", CERN-LHCC-2013-020 (2014), https://cds.cern.ch/record/1622286

[3] S.H.I. Barboza et al., SAMPA chip: a new ASIC for the ALICE TPC and MCH upgrades, 2016 JINST 11 C02088.

Grants: Excellenzcluster Universe, Origin and Structure of the Universe DFG EClust 153; BMBF ALICE: „Verbundprojekt 05P2015"

Systematic studies of correlations between different order flow harmonics in Pb-Pb collisions at $\sqrt{s_{NN}}$ = 2.76 TeV

A. Bilandzic[1,2], L. Fabbietti[1,2], and the ALICE Collaboration

[1]Physik Department E62, Technische Universität München, 85748 Garching, Germany; [2]Excellence Cluster 'Origin and Structure of the Universe', 85748 Garching, Germany

Systematic studies, comprising the centrality dependence of correlations between the higher order harmonics (the quadrangular v_4 and pentagonal v_5 flow) and the lower order harmonics (the elliptic v_2 and triangular v_3 flow), as well as their transverse momentum dependences, have been recently measured by the ALICE Collaboration, using new flow observables dubbed Symmetric Cumulants. These results provide further constraints on the properties of quark-gluon plasma produced in ultra-relativistic heavy-ion collisions.

Introduction

The main emphasis of the ultrarelativistic heavy-ion collision programs at the Relativistic Heavy Ion Collider (RHIC) and the Large Hadron Collider (LHC) is to study the deconfined phase of strongly interacting nuclear matter, the quark-gluon plasma (QGP). Difference in pressure gradients and the interactions among matter constituents produced in the spatially anisotropic overlap region of the two colliding nuclei result in anisotropic transverse flow in the momentum space. The large values of measured flow harmonics demonstrated that the shear viscosity to the entropy density ratio (η/s) of the QGP in heavy-ion collisions at RHIC and LHC energies is close to a universal lower bound 1/4π [1].

New constraints on η/s of QGP and on initial conditions in heavy-ion collisions

The newly developed flow observables, Symmetric Cumulants (SC), have provided the first experimental constraints on the temperature dependence of η/s of the QGP produced in heavy-ion collisions [2,3]. In these measurements only the centrality dependence of few lower order SC observables have been reported. The next step in this direction came with the recent measurement of centrality dependence of higher order SC observables and of their transverse momentum dependence [4].

The comparisons to theoretical models show that all the models with large η/s, regardless of the initial conditions, fail to describe the centrality dependence of higher order correlations. Based on the tested model parameters, the data favor small η/s values and the initial conditions obtained from the AMPT model [4].

When it comes to the differential measurements, it was found that SC observables exhibit moderate p_T dependence in midcentral collisions. This might be an indication of possible viscous corrections to the equilibrium distribution at hadronic freeze-out [4].

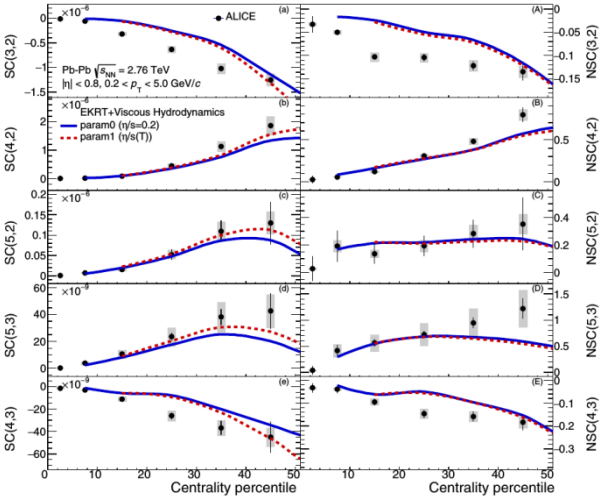

Figure 1: The centrality dependence of SC (left) and normalized SC observables (right) in Pb-Pb collisions at $\sqrt{s_{NN}}$ = 2.76 TeV. Results are compared to the event-by-event EKRT+viscous hydrodynamic calculations [5]. The lines are hydrodynamic predictions with two different parametrizations for temperature dependence of η/s.

The calculations for the two sets of parameters which describe the lower order harmonic correlations best are compared to the data in Fig. 1.

Together with the measurements of individual harmonics, these new results for SC observables can be used to further optimize model parameters and put better constraints on the initial conditions and the transport properties of nuclear matter in ultrarelativistic heavy-ion collisions.

References

[1] P. Kovtun, D. T. Son, A. O. Starinets, Phys. Rev. Lett. 94 (2005) 111601.
[2] A. Bilandzic et al, Phys. Rev. C 89, 064904 (2014).
[3] ALICE Collaboration, Phys. Rev. Lett. 117, 182301 (2016).
[4] ALICE Collaboration, Phys. Rev. C 97, 024906 (2018).
[5] H. Niemi, K. J. Eskola, and R. Paatelainen, Phys. Rev. C 93, 024907 (2016).

 DOI:10.15120/GR-2018-1

Correction for secondary particles contamination in the charged particle yield measurement in Xe-Xe collisions by ALICE*

M. Habib for the ALICE collaboration
TU Darmstadt and GSI

Introduction

During the LHC operation in 2017 with Xe beams the ALICE experiment has recorded a sample of Xe-Xe collisions with a energy (per nucleon pair, $\sqrt{s_{NN}}$) of 5.44 TeV. A measurement of the primary charged particle transverse momentum (p_T) yield for this collision system is ongoing [1]. The measurement requires precise knowledge about the contamination by particles originating from interaction with the detector material or secondary decays with a lifetime $\tau > 1$ cm/c.

This contamination is usually determined from Monte Carlo (MC) simulations. However, most of the models under predicts the production of secondaries from weak decays. To correct for this phenomena a data driven method based on template fits to the distance to closest approach (DCA), defined as the smallest distance between particle trajectory and the collision vertex, is applied.

Method

Using a MC sample we construct DCA templates for primaries, secondaries originating from decays and interaction with the detector material. The DCA distributions generated with MC have a well known and distinguishable shapes which are shown in the Fig. 1 (upper panel).

A linear combination of the templates can describe the reconstructed data while it gives access to the composition of the measured data sample. However non-physical results were observed showing a lager contribution of secondaries from material than from decay products, which originates due to the fit procedure. To overcome this problem, we assume the relative amount of secondaries form material to be well described in MC and redo the template fit fixing its fraction to the MC prediction. The fit result still describes the data while showing the expected trend. The scaled MC DCA distributions and the ratio of the fit to the measurement are shown in the Fig.1.

Systematic Uncertainty

The ratio deviates from unity by less than 5 %, which is used to assign a corresponding systematic uncertainty on the fit quality.

A second systematic uncertainty is estimated from the fit with two templates only distinguishing between secondaries and primaries. The comparison to the standard method leads to an additional relative uncertainty of roughly 10 % on the reweighting factor.

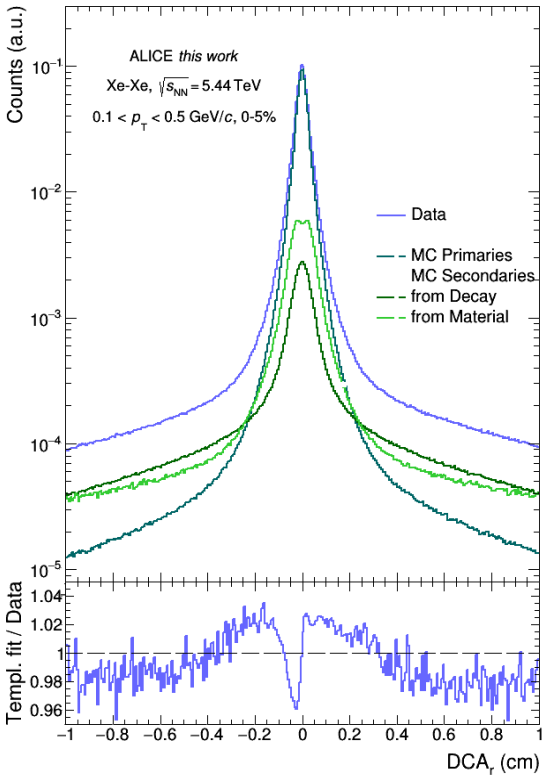

Figure 1: DCA distribution for data and three different MC templates (primaries, secondaries from decay and material) and the ratio of the fit to data.

Result

The fit results show that the secondary particles in the MC are underestimated by 20 - 60 %.

A corresponding reweighting factor is introduced to rescale the secondaries contribution for the primary charged particle yield measurement.

This data driven correction has a significant effect in the small p_T (< 1 GeV) region, while overall having a relative small uncertainty below 3 %.

References

[1] J. Gronefeld, GSI Scientific Report 2017, contribution 112

* Work supported by GSI, TU Darmstadt and HGS-HIRe

Low-mass dielectron production in Pb-Pb collisions at $\sqrt{s_{NN}} = 5.02$ TeV with ALICE

C. Klein[1] and the ALICE Collaboration

[1]IKF, Goethe Universität, Frankfurt, Germany

The ALICE experiment at the CERN-LHC was designed to understand the properties of the strongly interacting quark-gluon plasma (QGP) produced in ultrarelativistic heavy-ion collisions. The production of electron-positron pairs (dielectrons) demonstrated to probe the QGP. Dielectrons only interact electromagnetically and are therefore not affected by the strong force in the hot and dense QGP matter. They are produced in all stages of the collision and therefore give access to the complete spacetime evolution of the system. Whereas proton-lead collisions help to disentangle cold- from hot-medium effects, the dielectron measurement in proton-proton collisions serves as a baseline. With dielectron measurements in lead-lead collisions one can extract directly the temperature of the QGP and can investigate in-medium modifications of the ρ-meson which are associated to a predicted chiral-symmetry restoration [1].

The data set in this study was recorded in 2015 during LHC Run 2 and consists of approximately 84 million events in the centrality class of 0-80% measured in the ALICE central barrel at a center of mass energy of $\sqrt{s_{NN}}$ = 5.02 TeV. Electron and positron identification is based on their specific energy loss in the Inner Tracking System (ITS) and in the Time Projection Chamber (TPC). Additionally, the Time Of Flight (TOF) detector helps to reject heavier hadrons. This identification scheme results in a high electron identification efficiency while rejecting most of the hadronic contamination.

To extract dielectron spectra, in every event electrons and positrons are paired forming the so-called unlike-sign spectrum (ULS). The ULS consists of the dielectron signal and additional correlated and combinatorial background. To estimate this background, in each event like-sign pairs are created to form the like-sign spectrum (LS). The dielectron signal is then obtained by subtracting LS from ULS.

Due to a very low signal to background ratio, efficient background rejection is crucial. The major contribution to the combinatorial background originates from real-photon conversions in the detector material and in the beam pipe around the collision vertex. Real-photon conversions dominate at very low invariant masses m_{ee} < 0.02 GeV/c² of the signal spectrum, see Fig. 1.

Since photons have zero mass, the electron and positron from a photon conversion are emitted in the same direction. This property is used in two different ways. The first conversion rejection method is exploiting the fact that dielectrons with zero opening angle are very close to each other in the detector. Those two tracks are not distinguishable in a given silicon layer of the ITS: they share an ITS cluster. Selecting only tracks with zero shared clusters in the ITS leads to a reduction of conversion dielectrons by a factor of 98.5% while keeping 68% of the dielectron signal.

The second method takes advantage of the pair orientation of conversion dielectrons ϕ_V relative to the magnetic field which is given only by the magnetic field of the ALICE solenoid magnet. This property allows to separate them from dielectrons from hadronic decays where the pair orientation is random. While charge-ordered conversion pairs show a peak at higher ϕ_V, signal pairs have no angular correlation. Remaining conversion pairs can be rejected by choosing only pairs with $\phi_V < 2$ and correcting for the cut. These two conversion rejection methods, higher statistics and better understanding of the detector lead to an improved performance of the Pb-Pb dielectron analysis compared to the Run 2 analysis at $\sqrt{s_{NN}}$ = 2.76 TeV [2].

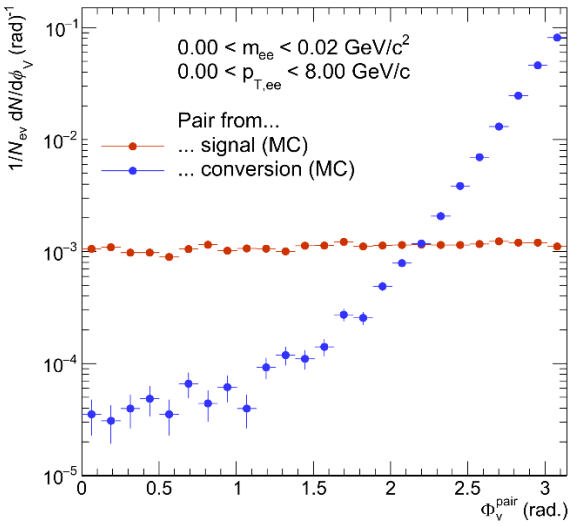

Figure 1: Dielectron signal pairs (red) and conversion pairs (blue) at very low mass m_{ee} < 0.02 GeV/c². Selecting tracks with zero shared ITS clusters reduces the conversion contribution by 98.5% while keeping 68% of the total signal. A subsequent selection on pairs with $\phi_V < 2$ reduces remaining contribution by conversions pairs.

References

[1] Rapp, Chanfrey, Wambach. (1995). Medium Modifications of the Rho Meson at CERN/SPS Energies. Phys.Rev.Lett. 76 (1996) 368-371

[2] Calivà, Alberto. (2017). Measurement of dielectrons in pp, p–Pb and Pb–Pb collisions with ALICE at the LHC. Journal of Physics: Conference Series. 779. 012052.10.1088/1742-6596/779/1/012052

Work supported by: BMBF and Helmholtz Association

 DOI:10.15120/GR-2018-1

Proton-proton reference spectrum at √s = 5.44 TeV

E. Perez Lezama[1] for the ALICE collaboration

[1]GSI, Darmstadt, Germany

Particle production at high energies is often described as a result of the interplay of perturbative (hard) and non-perturbative (soft) QCD processes. Therefore, the measurements of transverse momentum spectra in pp collisions are important to provide a baseline for calculations in perturbative QCD and constraints for a better tuning of models and event generators. In addition, they constitute a valuable reference to study nuclear effects in nucleus-nucleus and proton-nucleus collisions, in particular allowing one to measure the nuclear modification factors.

In order to calculate the nuclear modification factor, a pp reference for the same collision energy is required. Since the Xe–Xe data was taken at $\sqrt{s_{NN}}$ = 5.44 TeV, and there is no pp measurement available at this energy, we construct the pp reference using measured data at √s = 2.76 TeV, √s = 5.02 TeV [2] and √s = 7 TeV. We have implemented two different methods:

- Scaling the √s = 5.02 TeV pp spectrum up using the PYTHIA 8 Monash tune event generator, as shown in equation 1.
- Interpolation between the data at √s = 5.02 TeV and √s = 7 TeV assuming a power law behaviour as a a function of √s .

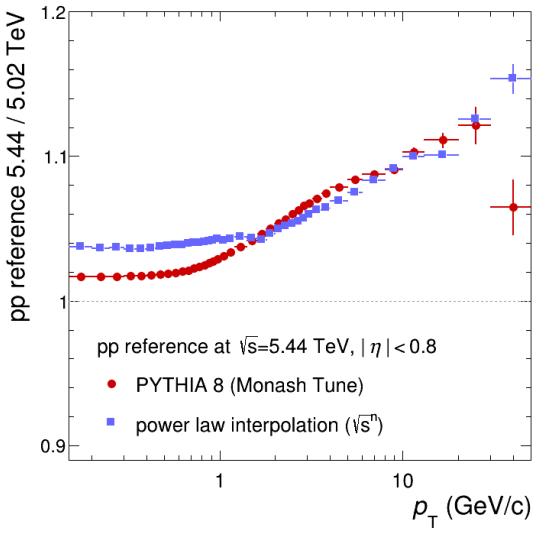

Figure 1: Ratio of generated p_T-differential cross section in pp at √s = 5.44 TeV to the measured one at √s = 5.02 TeV.

The ratio of the pp reference spectra at √s = 5.44 TeV and √s = 5.02 TeV from the power-law extrapolation is shown in figure 1 together with results obtained with the alternative method. The systematic uncertainty of the pp reference at √s = 5.44 TeV has two contributions which are added quadratically. For each p_T interval, we take the systematic uncertainty of the pp references at √s = 5.02 TeV and √s = 7 TeV and interpolate them by a power-law fit to √s = 5.44 TeV. Figure 2 shows the interpolated reference spectrum compared to the reference constructed using PYTHIA-scaling.

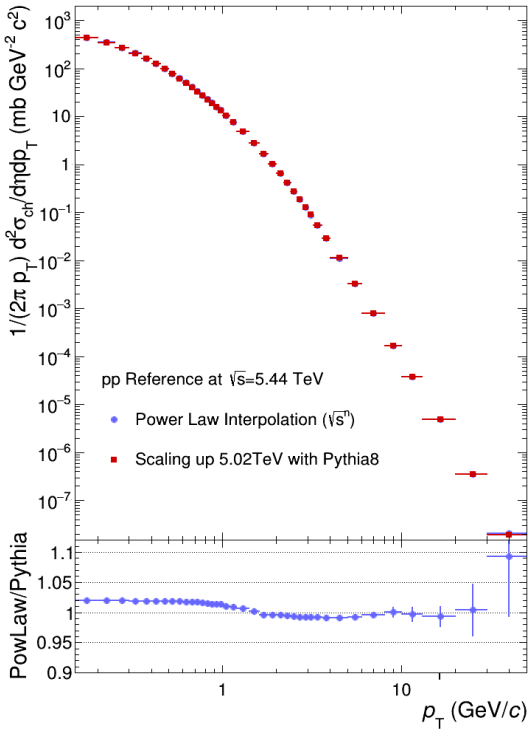

$$\frac{d\sigma}{d\eta dp_T} = \frac{\left(\frac{d\sigma}{d\eta dp_T}\right)^{Measured}_{\sqrt{s}=5.02\,TeV} \times \left(\frac{d\sigma}{d\eta dp_T}\right)^{MC}_{\sqrt{s}=5.44\,TeV}}{\left(\frac{d\sigma}{d\eta dp_T}\right)^{MC}_{\sqrt{s}=5.44\,TeV}} \quad (1)$$

Figure 2: p_T-differential cross section in pp at √s = 5.44 TeV and the measured one at √s = 5.02 TeV. Bottom panel shows the ratio of the two cross sections.

References

[1] arXiv:1802.09145
[2] Eur. Phys. J. C 73 (2013) 2662

Work supported by GSI and HGS-HIRe.

Production of antiparticles in p-Pb collisions at 5.02 TeV with ALICE

L.Córdova[1], B.Hohlweger[1], L.Fabbietti[1,2], for the ALICE collaboration

[1]Technische Universität München, Physik Department E62, Garching Germany; [2]Excellence Cluster `Origin and Structure of the Universe`, Garching, Germany

Under the assumption that dark matter particles can annihilate to form standard model particles, the indirect search for dark matter looks for these annihilation products. Cosmic-ray particles and antiparticles can often be challenging to detect due to a high background originating from the high-energy cosmic ray propagation through the interstellar medium. Low-energy antideuterons, however, have an ultra-low astrophysical background. The predicted flux of antideuterons originating from the annihilation of various viable dark matter candidates exceeds the background flux by more than two orders of magnitude in the kinetic energy range below 0.25 GeV/n. For that reason, low-energy antideuterons could be a unique probe for indirect searches for dark matter [1].

Hence, for the indirect dark matter search it is important to understand how antideuterons interact with matter. The ALICE detector allows to identify and track antideuterons from its creation in the collision or from decays. Since the ALICE Transition Radiation Detector (TRD) has a high material budget, the interaction probability of antideuterons with this detector can be investigated by analyzing the products with the next detector layer, the ALICE Time Of Flight detector (TOF). The basic principal of the measurement is shown in Figure 1.

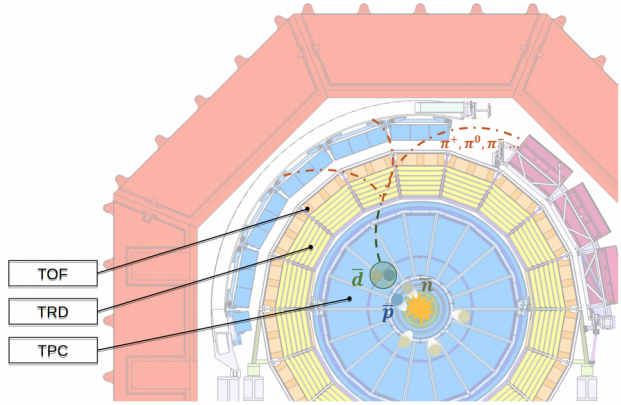

Figure 1: Cross section of the ALICE detector. Schematic representation of an antideuteron that interacts with the TRD material and produces a pion shower, which can be analyzed with the TOF.

In order to have a baseline in the antideuteron analysis, beside (anti-)deuterons, also (anti-)protons are identified in a first step.

During the analysis, a kink at the momentum region p ~ 1.0 GeV/c was found in the (anti-) proton spectrum. By looking at the mass hypothesis for the energy loss correction in the ALICE Time Projection Chamber the source of this irregularities was found. In the region p ~ 1.0 GeV/c an electron mass was assumed to correct protons and this led to a wrong energy loss correction. The correction was obtained with a fit to the data and implemented to correct the momentum track-by-track.

In a next step the track cuts implemented in the analysis need to be optimized in order to measure the production and extract the absorption cross sections of protons, deuterons and their corresponding antiparticles. Especially the Monte Carlo data of (anti-) deuteron needs further investigation.

The Monte Carlo productions with injected nuclei, which are necessary for the (anti-)deuteron analysis, have an entirely different statistical background than the data and cannot be applied as templates for the yield of primaries and secondaries. At the moment, when calculating the purity of (anti-) deuterons, we get a result of almost 100% in the whole momentum range, which means that there are too many nuclei injected. This is why the yields of the Monte Carlo data first need to be rescaled according to a fit that best describes the experimental sample. Further, it must be considered that scattering data for (anti-) deuterons is very limited but required as an input for the simulation in GEANT for the propagation of (anti-) deuterons through the detector and the resulting detector signals[2].

Finally, the analysis can focus on the conversions of antiparticles when interacting with the TRD material. Since the lower limit of the energy range of identified (anti-) deuterons is given by the surrounding magnetic field, for low energetic (anti-) deuterons an analysis with a lower magnetic field could be done in the future.

References

[1] T. Aramaki, S. Boggs et al. Review of the theoretical and experimental status of dark matter identification with cosmic-ray antideuterons, Physics Reports, 618, 1-37 (2016).

[2] ALICE Collaboration. Production of light nuclei and anti-nuclei in pp and pb-pb collisions at lhc energies, Phys. Rev. C 93, 024917 (2015).

 DOI:10.15120/GR-2018-1

Neutral pion and ηmeson production in p-Pb and Pb-Pb collisions at the LHC*

A. Marin[1], F. Bock[2], P. González-Zamora[3], Y. Kharlov[4], L. Leardini[5], A. Morreale[6], T. Okubo[7], A. Passfeld[8], D. Peresunko[9], K. Reygers[5], M. Sas[10], J. Stachel[5], for the ALICE collaboration

[1]GSI Helmholtzzentrum für Schwerionenforschung GmbH, Darmstadt, Germany; [2]CERN, Geneva, Switzerland, [3]Benemérita Universidad Autónoma de Puebla, Puebla, Mexico, [4]NRC "Kurchatov institute"-IHEP, Protvino, Russia, [5]Physikalisches Institut, Ruprecht-Karls-Universität Heidelberg, Heidelberg, Germany, [6]SUBATECH, IMT Atlantique, Université de Nantes, CNRS-IN2P3, Nantes, France, [7]Hiroshima University, Hiroshima, Japan, [8]Institut für Kernphysik, Westfälische-Wilhelms-Universität-Münster, Münster, Germany, [9]NRC "Kurchatov Institute", Moscow, Russia [10]Institute for Subatomic Physics of Utrecht University, Utrecht, The Netherlands

Neutral pion and η meson production has been measured in p-Pb collisions at $\sqrt{s_{NN}}$ = 5.02 TeV [1] and Pb-Pb collisions $\sqrt{s_{NN}}$ = 2.76 TeV [2] with the ALICE experiment at the CERN LHC. The measured η/π^0 ratio deviates from m_T scaling for p_T < 3 GeV/c in both systems. At high p_T, a large suppression of the same magnitude for π^0 and η meson production is observed in central Pb-Pb collisions with respect to the scaled pp reference, while the π^0 and η R_{pPb} ratios are consistent with unity above a p_T of 2 GeV/c. These results support the interpretation that high p_T particle suppression in Pb-Pb collisions is due to parton energy loss in the hot QCD medium.

Results

The measurement of neutral pions and η mesons in a broad p_T range in Pb-Pb collisions can provide information on the energy loss mechanisms in the hot QCD medium. Their measurement in p-Pb collisions is needed to disentangle initial and final-state effects.

Photons are reconstructed in ALICE using two complementary techniques: the photon conversion method (PCM), and electromagnetic calorimeters (PHOS and EMCal). Neutral mesons are reconstructed in the two-photon decay channel and additionally in the Dalitz decay channel for the p-Pb system. Neutral pions and η mesons are identified as peaks at their corresponding rest mass in two-photon invariant mass distributions. The invariant differential yields are measured independently in each method and then combined using the Best Linear Unbiased Estimate.

The invariant yields of π^0, and, for the first time at the LHC, of η mesons have been measured for central and semi-central Pb-Pb collisions at $\sqrt{s_{NN}}$ = 2.76 TeV, as well as for non-single diffractive (NSD) p-Pb collisions at $\sqrt{s_{NN}}$ = 5.02 TeV up to 20 GeV/c, and compared to different theoretical model predictions [1, 2]. The measured η/π^0 ratio in p-Pb (Fig. 1) and Pb-Pb collisions reaches a plateau value for p_T > 3 GeV/c of 0.483±0.015*stat*±0.015*sys* and 0.457±0.013*stat*±0.018*sys*, respectively. For p_T < 3 GeV a deviation from m_T scaling is observed in both collisions systems. Decay of heavier resonances into π^0 and presence of radial flow even for the p-Pb system are among the possible explanations. The large radial flow in central Pb-Pb collisions gives rise to the enhancement of the η/π^0 ratio at p_T ~ 2-4 GeV/c, as similarly observed for $K^{\pm}/\pi^{\pm}$. The nuclear modification factor of π^0 or η in Pb-Pb collisions quantifies particle production suppression at high p_T in heavy-ion collisions. For π^0 and η mesons a large suppression factor of ~ 8-9 is observed at p_T = 7 GeV/c in central 0-10% Pb-Pb collisions (Fig. 2), with increasing trend at higher p_T. The π^0 suppression is stronger than the one observed at lower center-of-mass energies. The π^0 and η R_{pPb} are consistent with unity for p_T > 2 GeV/c in p-Pb collisions. These results support the interpretation that π^0 and η meson high p_T suppression in central Pb-Pb collisions is due to parton energy loss in the hot QCD medium.

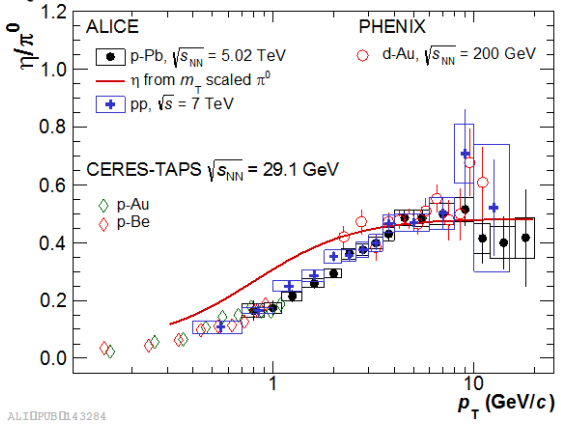

Figure 1: η/π^0 ratio measured in p-Pb collisions compared to m_T scaling and to existing measurements.

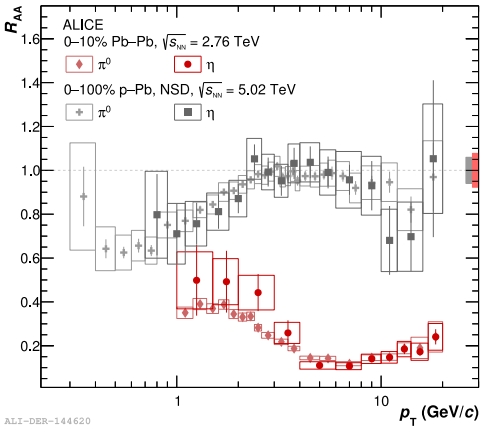

Figure 2: Measured π^0 and η meson R_{AA} in 0-10% central Pb-Pb collisions and in NSD p-Pb collisions.

References

[1] ALICE Collaboration, S. Acharya *et al.*, "Neutral pion and η meson production in p-Pb collisions at $\sqrt{s_{NN}}$ = 5.02 TeV ", arXiv: 1801.07051.

[2] ALICE Collaboration, S. Acharya *et al.*, "Neutral pion and η meson production at mid-rapidity in Pb-

Pb collisions at $\sqrt{s_{NN}}$ = 2.76 TeV", arXiv: 1803.05490.

*Work supported by BMBF, GSI, and University of Heidelberg

 DOI:10.15120/GR-2018-1

Inclusive and non-prompt J/ψ production in Pb-Pb collisions at $\sqrt{s_{NN}}$ = 5.02 TeV measured at mid-rapidity with ALICE

R.T.Jimenez Bustamante[1,2], L.Layer[1,2], D.Weiser[2], S.Masciocchi[1,2], A.Andronic[1,3], I.Arsene[4], M.Köhler[2],

and the ALICE collaboration

[1]GSI, Darmstadt; [2]Universität Heidelberg,[3] Universität Münster; [4]University of Oslo

Introduction

Quarkonium and open heavy-flavor production plays a crucial role as a probe of the hot deconfined medium created in heavy ion collisions. The suppression of charmonium production induced by the color screening of quarks was proposed more than 30 years ago as a probe of the formation of the Quark Gluon Plasma (QGP) [1]. At LHC collision energies, the average number of charm-anticharm quark pairs per event exceeds the average number of charm-anticharm quark pairs per event at RHIC by one order of magnitude. Two different approaches [2,3] suggested new production mechanisms playing a role at LHC collision energies, leading to a charmonium enhancement in the most central A-A collisions. The inclusive J/ψ nuclear modification factor R_{AA} measured by ALICE [4,5] at $\sqrt{s_{NN}}$ = 2.76 TeV, showed a striking enhancement in central collisions compared to the measurements at lower energies [6,7], supporting the models including (re)generation. The transport and comovers models assume the creation of the charmonium states due to continuous dissociation and regeneration throughout the lifetime of the medium [8,9,10]. On the other hand the statistical hadronization model [11] assumes creation of charmonium at the phase boundary. Due to the increase of the initial number of charm-anticharm pairs relative to the total number of quarks, an increase of the R_{AA} with the collision energy is predicted by the models. The statistics gathered by ALICE during LHC Run 2 measurement at $\sqrt{s_{NN}}$ = 5.02 TeV provides essential information for the suppression and regeneration picture.

The determination of the non-prompt J/ψ fraction gives access to the physics of B-hadrons. Since the mass of heavy quarks is large compared to the temperature of the medium, they are produced in the early stage of the collision and thus experience the entire space-time evolution of the system [12]. While there is a strong experimental indication for a thermalization of charm quarks in the medium, beauty quarks are not expected to fully thermalize, since their lifetime is larger than the lifetime of the plasma [13]. Therefore they carry information starting form the beginning of the collision. Experimentally at RHIC and at the LHC a strong suppression of the nuclear modification factor R_{AA} has been observed [12]. From a theoretical point of view, the large masses of the heavy quarks make the computation of the transport coefficients, which characterize transport properties of the medium, feasible directly from first principle QCD calculations [13]. Measurements of the nuclear modification factor R_{AA} and the flow coefficient v_2 of heavy-flavour hadrons are an essential observable to constrain phenomenological models that build a bridge between experiment and first principle QCD calculations.

Inclusive J/ψ production

The ALICE experiment [14] allows to measure J/ψ mesons at mid-rapidity (|y| < 0.8) in the dielectron decay channel. Two main detectors are used for the electron reconstruction. The Inner Tracking System (ITS), consisting of six layers of silicon detectors located around the interaction point, is used for tracking, vertex determination and triggering. The Time Projection Chamber (TPC) is the main tracking detector and is also used for particle identification via the measurement of the specific energy loss in the detector gas (dE/dx). The electrons are identified using the TPC information, and the invariant mass distribution is constructed using opposite sign pairs.

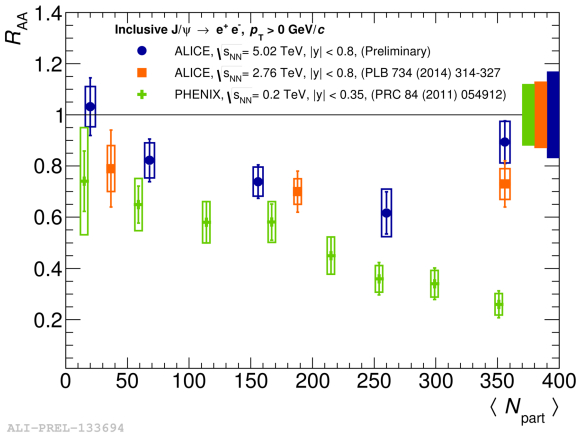

Figure 1: Nuclear modification factor of inclusive J/ψ as a function of centrality at different energies.

Work supported by: GSI, CONACYT, University of Heidelberg

The analysis of the inclusive and non-prompt J/ψ production presented here is based on 75 million minimum bias events in Pb-Pb collisions at $\sqrt{s_{NN}}$ = 5.02 TeV. This allows to measure the inclusive J/ψ production in 5 different centrality classes: 0-10%, 10-20%, 20-40%, 40-60% and 60-90%.

Figure 1 shows the inclusive R_{AA} at $\sqrt{s_{NN}}$ = 5.02 TeV as a function of centrality compared to the ALICE measurement at $\sqrt{s_{NN}}$ = 2.76 TeV at mid-rapidity [7]. The centrality dependence is similar at the two energies. However, a slight increase is observed in the most central collisions. Within the uncertainties the results at both energies are compatible. The measurement by PHENIX at $\sqrt{s_{NN}}$ = 0.2 TeV [9] clearly shows a stronger suppression of the R_{AA} values in central collisions compared to ALICE measurements.

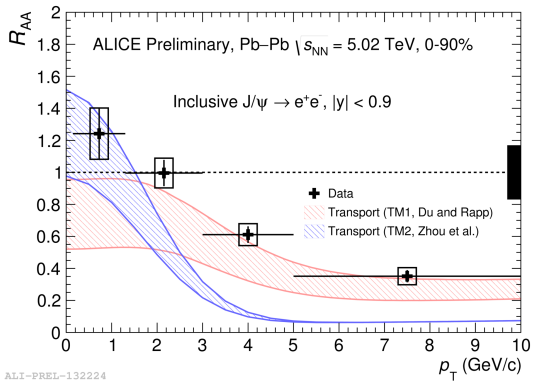

Figure 2: Nuclear modification factor of inclusive J/ψ as a function of transverse momentum.

The inclusive R_{AA} at $\sqrt{s_{NN}}$ = 5.02 TeV is also measured as a function of transverse momentum in the centrality classes 0-90%, 0-20%, 20-40% and 40-90%. In figure 2 the results for the 0-90% centrality class is shown. The increase of the R_{AA} towards low momentum is consistent with the (re)generation scenario and in agreement within uncertainties with the model calculations.

Non-prompt J/ψ production

The non-prompt J/ψ fraction coming from the decay of B-hadrons is determined by decomposing the inclusive J/ψ yield into its prompt and non-prompt components via a 2-dimensional log-likelihood fit to the invariant mass and the pseudo-proper decay length of the J/ψ. The distribution of the pseudo-proper decay length of the non-prompt J/ψ mimics the proper decay length of B-hadrons and thus can be used as a discriminative variable. The same selections as for the inclusive J/ψ analysis are applied. Additionally, machine learning techniques are used to calculate a variable based on the PID and kinematics of the electron candidates in order to enhance the signal-to-background ratio and the significance of the measurement. Figure 3 shows the results for the nuclear modification factor R_{AA} at $\sqrt{s_{NN}}$ = 5.02 TeV for the non-prompt J/ψ. The results are shown together with the results of CMS at $\sqrt{s_{NN}}$ = 2.76 TeV at mid-rapidity [15] and various models are overlaid [16,17,18]. The measurement of ALICE extends the measurement of CMS towards lower transverse momentum. A strong suppression of the nuclear modification factor is observed for intermediate and high transverse momenta. Qualitatively, the models are in agreement with the measurement.

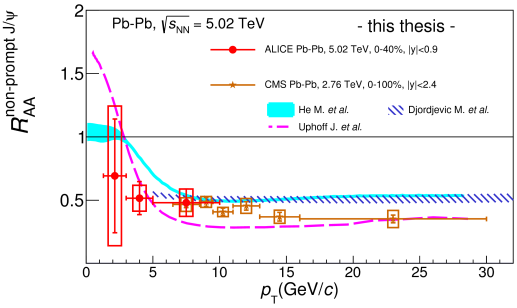

Figure 3: Nuclear modification factor of non-prompt J/ψ as a function of transverse momentum.

References

[1] T.Matsui, H.Satz, Phys Lett B.178 (1986) 416
[2] P. Braun-Munzinger, J. Stachel, Phys. Lett. B 490, (2000) 196–202
[3] R. L. Thews, M. Schroedter, J. Rafelski, Phys. Rev. C 63, (2001) 054905.
[4] ALICE Coll., Phys.Rev.Lett. 109 (2012) 072301
[5] ALICE Coll., Phys. Lett. B 734 (2014) 314–327.
[6] NA 50 Coll., Eur. Phys. J. C 39, 335 (2005)
[7] PHENIX Coll.Phys. Rev. C 84, 054912 (2011).
[8] X Zhao, R. Rapp, Nucl. Phys. A 859 (2011) 114–125.
[9] K. Zhou et al, Phys. Rev. C 89 5, 459 (2014) 054
[10] E.G. Ferreiro, Phys. Lett. B 731 (2014) 57–63
[11] A.Andronic, P. Braun-Munzinger, J. Stachel, Phys. Lett. B 652 (2007) 259-261
[12] A. Andronic and others, Eur. Phys. J. C76 (2016)
[13] Aarts, G. and others, Eur. Phys. J. A53 (2017)
[14] ALICE Coll., Int. J. Mod. Phys. A 29 (2014) 1430044
[15] CMS Coll., Eur. Phys. J. C77 (2017)
[16] Djordjevic, Magdalena and Djordjevic, Marko, Phys. Lett. B734 (2014)
[17] Uphoff and others, Phys. Lett. B717 (2012)
[18] He and others, Phys. Lett. B735 (2014)

Work supported by: GSI, CONACYT, University of Heidelberg

 DOI:10.15120/GR-2018-1

Stability tests of ALICE TPC GEM chambers at the LHC

C. Garabatos[1], K. Schweda[1], Robert Münzer[2], Renato Negrao[3], and Rainer Renfordt[2]

[1]GSI, Darmstadt, Germany; [2]Goethe University, Frankfurt, Germany; [3]University of São Paulo, Brazil

The current multi-wire proportional chambers of the ALICE TPC are replaced by new chambers composed of quadruple stacks of GEMs as detectors for the forthcoming LHC Run 3, in 2020.

The production of these 80 (72 plus spares) detectors is ongoing. As ultimate test for the stability of these micro-pattern devices against discharges under the harsh condition of the LHC, a subset of the final detectors are sequentially operated in the ALICE cavern at the LHC itself.

Sets of two detectors (one Inner and one Outer Readout Chamber) are placed close to the LHC beam pipe at about 10 m from the interaction point at the ALICE cavern, where particle densities are about one order of magnitude higher than those expected in the TPC chambers in Run 3 with 50 kHz Pb-Pb collision rate. Figure 1 shows one OROC under the beam pipe at the ALICE experiment.

The detectors are included in the TPC gas circuit and are thus operated with the same gas mixture. They are powered with a HV system which includes the final, cascaded power supplies especially designed for GEM operation, protection resistor networks close to the detector, and a set of high precision, high bandwidth picoammeters. A custom-made Labview application allows for a safe operation of the HV system, including automatic ramping according to the LHC modes, such that the HV is on only when there is no beam or stable beams. The voltages and currents are thus monitored and recorded, potential current excursions analysed, and a tripping mechanism is put is place.

All pads of each readout plane are connected together into a digital oscilloscope, located in the cavern, which is remotely controlled and readout. Thus, the operator can control and monitor the detectors from the surface, since there is no access to the cavern while beams are on the machine.

The HV powering scheme is a crucial aspect for the safe operation of these detectors, since the voltage in each electrode of the GEM stack is closely coupled to the voltages in the neighbouring electrodes. Thus, if a spark in a given place leads to an overvoltage between any two electrodes, further sparking may result into irreversible damage of the GEM foils.

Operation of first prototypes in this manner showed instabilities and damage due precisely to the sub-optimal HV configuration strategy. Further improvements – adequate choice of protection resistor networks, cascading scheme, tripping mechanism, decoupling resistors – lead to success.

Final production chambers were thus exposed to the LHC conditions at forward rapidity under nominal gas and HV conditions without any trips for several weeks of operation. Minor discharges were recorded during this period. Operation included special ALICE tests where the particle rates expected in Run 3 were reproduced in the experiment, which resulted in about one order of magnitude higher doses in the forward location of the Upgrade GEM detectors.

Plans for 2018 are to periodically install in the ALICE cavern two sets of detectors with four readout chambers in total – two inner readout chambers and two outer ones-, operate them for several weeks, and then replace them during technical stops or other suitable opportunities, in order to qualify a meaningful subset of the full production.

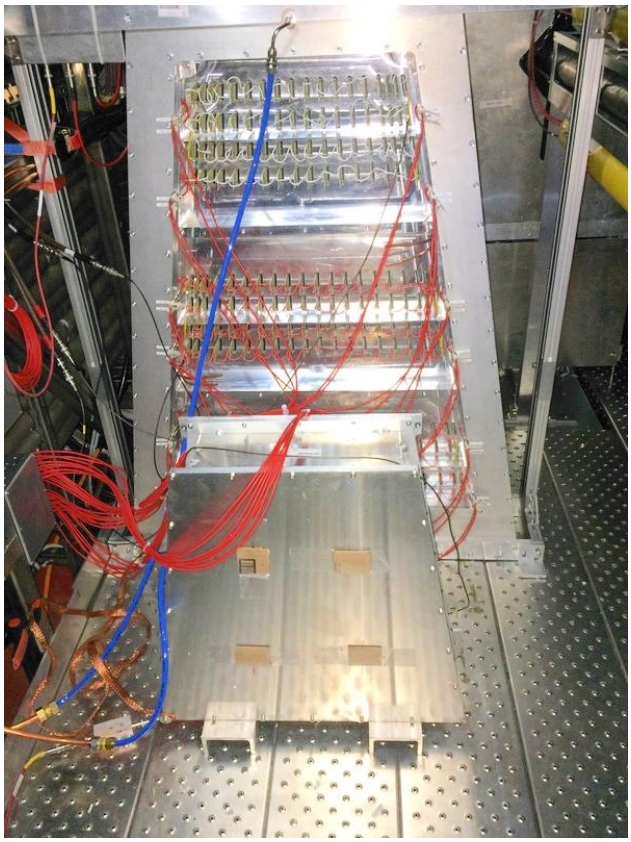

Figure 1: Set of two chambers placed close to the LHC beam pipe in the ALICE cavern ready to be operated with beams.

Experiment collaboration: CERN-ALICE
PSP codes: none
Strategic university co-operation with: Frankfurt-M / Heidelberg / Munich / Bonn / Budapest / Bucharest / Helsinki / New Haven / Oakridge / Detroit

*Work supported by BMBF, GSI.

Report by the GSI-ALICE group

K. Schweda[1], for the ALICE collaboration

[1]GSI, Darmstadt, Germany

ALICE is currently engaged in the Run-2 period of the LHC operation at CERN that started in 2015. Collisions of lead nuclei (Pb) at the highest energy ever reached in the laboratory were recorded in 2015, and a second Pb-Pb run will take place at the end of 2018. During the heavy-ion period in autumn 2016, proton-lead collisions were recorded which do not only provide a reference for the Pb-Pb system but are also interesting in their own right. Collisions were recorded at two collision energies: a first period was devoted to 5.02 TeV per nucleon pair to match the energy of the Pb-Pb run and to increase the statistics of the p-Pb data sample recorded in 2013 with a new minimum bias data sample. Collisions at the highest reachable energy of 8 TeV were recorded in a second period at high interaction rate, with triggers from the muon system, the calorimeters and the transition radiation detector.

The LHC produced for the first time collisions of xenon nuclei at a center-of-mass energy of 5.44 TeV during a pilot run with 6 hours of stable beams in October 2017. The remaining time was dedicated to proton-proton collisions at 13 TeV in order to collect a high-statistics data sample with a reach up to highest transverse momenta. A high-multiplicity trigger enables the study of features of events that resemble aspects typical of heavy-ion collisions.

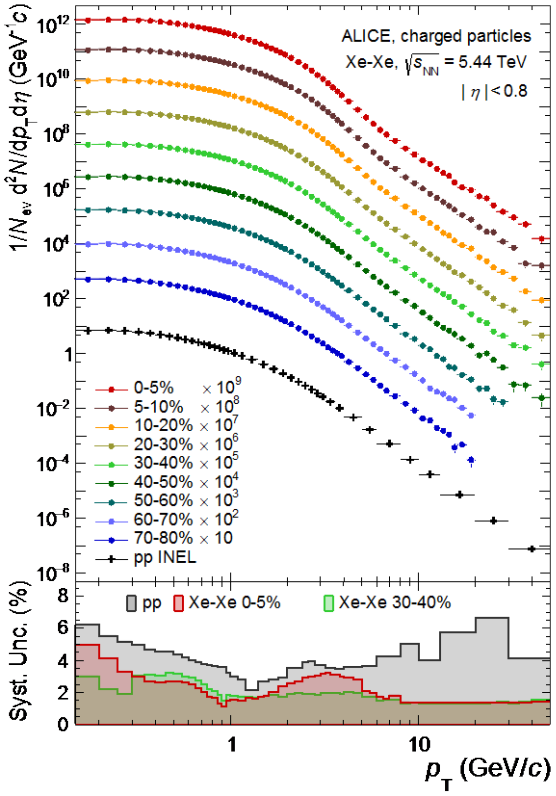

Figure 1: Transverse momentum spectra of charged particles in Xe-Xe collisions at 5.44 TeV together with an interpolated pp reference spectrum (top panel) and systematic uncertainties (bottom panel).

Until April 2018, ALICE has published 198 peer reviewed scientific papers, with an average of 93 citations each.

The GSI ALICE group is deeply involved in Run-2, starting from the responsibility to continuously operate the Time-Projection-Chamber (TPC) and the participation in the mandatory shifts to operate the experiment at CERN, up to the calibration and analysis of the recorded data and the publication of the results.

The GSI ALICE group is engaged in the analysis of data from all collisions systems and, recently, made public several results of high scientific impact. All relevant results are discussed individually in contributions to this GSI Scientific Report. Here, a brief overview is given.

Transverse momentum spectra and the nuclear modification factor of electrons from semileptonic heavy-flavour hadron decays were measured in Pb-Pb collisions at 5.02 TeV, in Xe-Xe collisions at 5.44 TeV, and in pp collisions at 7 and 13 TeV. At high momenta, the nuclear modification factor is below unity, exhibiting a substantial suppression of the yield of electrons from heavy-flavour hadron decays with respect to pp collisions due to the energy loss of heavy quarks in the QCD medium. Models including shadowing of parton distributions predict a nuclear modification factor below unity even at low momentum and are in better agreement with the data than models without shadowing.

Inclusive and non-prompt production of J/ψ and its centrality dependence was measured in Pb-Pb collisions at 5.02 TeV. Non-prompt J/ ψ production originates from the decay of B mesons. Thus both measurements give access to transport coefficients of heavy quarks in the QCD medium. The inclusive measurement confirms the observation in Pb-Pb collisions at 2.76 TeV of a reduced suppression in central collisions when compared to lower energies.

The Xe-Xe data allow for studying the dependence of particle production on the collision system size where xenon neatly bridges the gap between existing data from pp, p-Pb and Pb-Pb collisions with atomic mass numbers of A=129 for xenon, and A=208 for lead. Figure 1 shows the transverse momentum spectra of charged particles in Xe-Xe collisions at 5.44 TeV in nine centrality classes together with an interpolated pp reference spectrum (top panel) and systematic uncertainties (bottom panel).

 DOI:10.15120/GR-2018-1

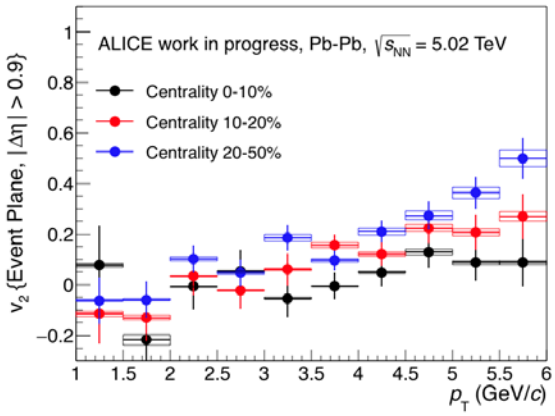

Figure 2: Elliptic flow coefficient (v2) of 3He in Pb-Pb collisions at 5.02 TeV.

The elliptic flow coefficient (v2) of (anti-)3He was measured versus transverse momentum in Pb-Pb collisions at 5.02 TeV for different centrality ranges using the Event Plane method, see Fig. 2. This measurement decisively adds to the picture obtained from the v2 of (anti-) deuterons and (anti-)protons and poses a serious challenge to the coalescence approach and other hadronization models that describe the elliptic flow of light anti-nuclei in heavy-ion collisions.

The GSI ALICE group is centrally involved in the preparation of the experiment upgrades, to be completed until the end of 2020. These upgrades will allow ALICE to fully exploit the improved performance of the LHC in Run-3, when Pb nuclei will collide with a rate of 50 kHz.

The construction of new readout chambers for the ALICE TPC, equipped with Gas Electron Multiplier (GEM) foils is at full swing.

A pre-production GEM-based Inner Readout Chamber (IROC) has been tested together with 6 prototype versions of the TPC front-end card based on SAMPA version ‘v2’ at the CERN Proton Synchrotron with electrons and pions at 1 to 6 GeV/c.

The measured noise and separation power in particle identification meet the design specifications. Groups of two detectors, i.e. one Inner and one Outer Readout Chamber (OROC), are placed close to the LHC beam pipe at about 10 m from the interaction point in the ALICE cavern, where particle densities are about one order of magnitude higher than those expected in the TPC chambers in Run-3 at a 50 kHz Pb-Pb collision rate. Figure 3 shows one OROC being positioned below the beam pipe at the ALICE experiment.

Final production chambers were thus exposed to the LHC conditions at forward rapidity under nominal gas and high voltage conditions without any trips during several weeks of operation. However, minor discharges were observed.

Plans for 2018 are to periodically install in the ALICE cavern sets of four readout chambers – two inner readout chambers and two outer ones-, operate them for several weeks, and then replace them during technical stops or other suitable opportunities, in order to qualify a meaningful sub-set of the full production for the final installation for Run-3 operations at the LHC.

*Work supported by BMBF, GSI.

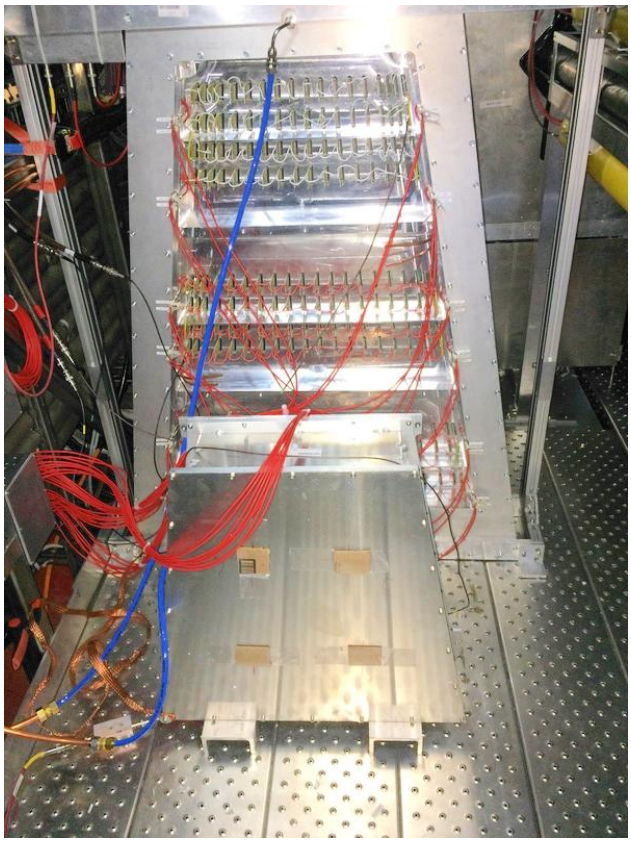

Figure 3: Four chambers (two inner and two outer readout chambers) placed close to the LHC beam pipe in the ALICE cavern ready to be operated with beams.

CATS - the modern tool for femtoscopy studies

V. Mantovani Sarti[1], D.L. Mihaylov[1] and L.Fabbietti[1,2]

[1]Physics Department E62, TUM, Garching, Germany; [2]Excellence Cluster Universe, Garching, Germany

Femtoscopy relates the correlation function $C(k)$ between particle pairs to their emission source $S(r,k)$ and the wave function $\Psi(r,k)$. The latter is obtained by solving the Schrödinger equation (SE) for an interaction potential $V(r)$.

Investigating small collision systems, such as proton-proton, has the advantage of probing the inner part of the interaction potential. However, modelling the correlation function for small sources requires an exact determination of the wave function, which is not provided by the common femtoscopic tools developed for investigating correlations in heavy-ion collisions. For this reason, we have developed a new "Correlation Analysis Tool using the Schrödinger equation" (CATS) [1] capable of modelling $C(k)$ exactly using a numerical solution to the SE.

CATS was used to fit the ALICE experimental results for p-p and p-Λ correlations in pp collisions at $\sqrt{s} = 7TeV$. The source was assumed to be Gaussian and the size was extracted from a combined fit of the p-p and the p-Λ correlations. Both systems show the presence of a linear baseline, which is not reproduced by transport models. Thus, the fit is performed by multiplying C(k) with a linear function. The result is show in fig. 1.

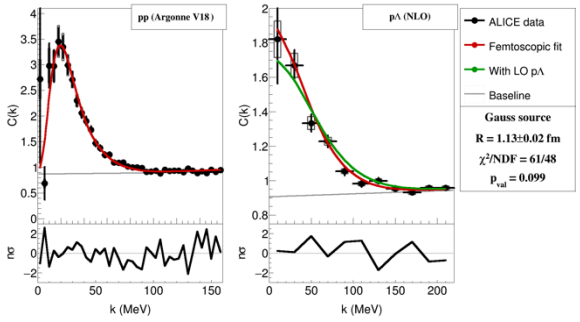

Figure 1: The ALICE preliminary, pp at $\sqrt{s} = 7TeV$ [2] was fitted using CATS to model the p-p correlation function. The p-Λ interaction was evaluated with the Lednický model [3] using the scattering parameters of a next to leading order (NLO) chiral effective theory calculation [4].

For more exotic pairs, such as hyperon-hyperon or hyperon-nucleon in the $S = -2$ sector, the correlation function $C(k)$ permits to gain access to the underlying strong interaction, which so far has not been fully constrained by scattering or hypernuclei data. We expect to be able to use the ALICE pp data at $\sqrt{s} = 13TeV$ to get an insight into the Λ-Λ and p-Ξ⁻ correlations (fig. 2). For this purpose, we established collaborations with theory groups working on chiral effective field theory and lattice calculations, allowing us to probe the most modern potentials for different particle species and make predictions about the feasibility to study those pairs experimentally.

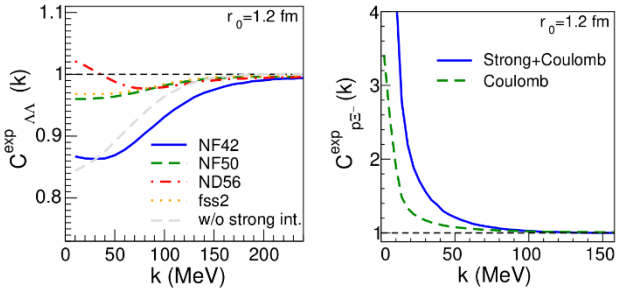

Figure 2: The predicted experimental correlation function for Λ-Λ (left) and p-Ξ⁻ (right), including momentum resolution and feed-down effects expected in pp collisions at LHC energies.

In the left panel of Fig. 2 we compare the Λ-Λ correlation functions for different attractive (NF50, ND56 and fss2) potentials and one potential (NF42) which allows for a bound state [5]. The binding potential (NF42) is well separated from the attractive ones, which implies that a high statistics experimental data sample can differentiate between those cases. For the p-Ξ⁻ (right) we use a preliminary lattice local potential from the HAL QCD collaboration [6]. We see a significant modification of $C(k)$ due to the strong interaction, which should be possible to detect experimentally.

To get better constraints on the investigated interaction potentials, we are working on a CATS based analysis framework capable of performing global fits over all available femtoscopic data.

The work on CATS and the complementary studies are in preparation for publication and currently to be found on arXiv [1].

This work is supported by SFB1258.

References

[1] D. L. Mihaylov, V. M. Sarti, O. W. Arnold, L. Fabbietti, B. Hohlweger and A. M. Mathis, arXiv:1802.08481 [hep-ph].

[2] O.Arnold [for the ALICE collaboration], poster at the QM2017 conference.

[3] R. Lednicky and V. L. Lyuboshits, Sov. J. Nucl. Phys. 35 (1982) 770 [Yad. Fiz. 35 (1981) 1316].

[4] J. Haidenbauer, S. Petschauer, N. Kaiser, U.-G. Meissner, A. Nogga and W. Weise, Nucl. Phys. A 915 (2013) 24 doi:10.1016/j.nuclphysa.2013.06.008 [arXiv:1304.5339 [nucl-th]].

[5] A. Ohnishi, K. Morita, T. Furumoto, JPS Conf. Proc. 17 (2017) 031003 doi:10.7566/JPSCP.17.031003 [arXiv:1512.08444 [nucl-th]].

[6] T. Hatsuda, K. Morita, A. Ohnishi and K. Sasaki, Nucl. Phys. A 967 (2017) 856 doi:10.1016/j.nuclphysa.2017.04.041 [arXiv:1704.05225 [nucl-th]].

 DOI:10.15120/GR-2018-1